STENT GRAFT UPDATE

Jafar Vossoughi
Nicholas Kipshidze
John W. Karanian (Eds)

Medical
and
Engineering
Publishers, Inc.

STENT GRAFT UPDATE

Applied Cardiovascular Medicine & Science
Series

Series Editors:

Jafar Vossoughi, PhD
Biomed Research Foundation
Washington, DC

Nicholas Kipshidze, MD, PhD
Lenox Hill Heart and Vascular Institute
Lenox Hill Hospital, New York, NY

John W Karanian, PhD
Center for Devices and Radiological Health
US Food and Drug Administration, Rockville, MD

STENT GRAFT UPDATE

Edited by

Jafar Vossoughi, PhD
Biomed Research Foundation
Washington, DC

Nicholas Kipshidze, MD, PhD
Lenox Hill Hospital
New York, NY

John W Karanian, PhD
US Food and Drug Administration
Rockville, MD

Medical
and
Engineering
Publishers, Inc

First published in the United States of America by
Medical and Engineering Publishers, Inc
PO Box 11834
Washington, DC 20008
USA
(http://www.erols.com/medengrgpubinc/)

Library of Congress Cataloging-in-Publication Data

Stent Graft Update
Edited by Jafar Vossoughi, Nicholas Kipshidze, John W Karanian. First edition
Includes bibliographical references and index
2000

LC #: 00-107409
ISBN #: 1-930636-00-8

Printed in the United States of America.

Printed on acid-free paper.

Contents

Part III: Biologic Response

Part IV: Animal Modeling

Part V: Clinical Perspectives

List of Contributors

Dorothy B Abel
Office of Device Evaluation and
Radiological Health
Food and Drug Administration
9200 Corporate Blvd
Rockville, MD 20850

Holly G Alexander, BA
Advanced Tissue Sciences, Inc
10933 North Torrey Pines Road
La Jolla, CA 92037

Steven Archuleta, BA
Center for Devices and
Radiological Health
Food and Drug Administration
12725 Twinbrook Parkway
Rockville, MD 20852

Robert E Bair, PhD, PE
NSF Industry/University
Cooperative Research Center
for Biosurfaces
State University of New York at
Buffalo
110 Parker Hall
Buffalo, NY 14214-3007

Ivan Bakhutashuili, MD, PhD
Medical College of Wisconsin
9200 West Wisconsin Ave.
Milwaukee, WI 53226

Redmond P Burke, MD
Division of Cardiovascular
Surgery
Miami Children's Hospital
33200 SW 60 Court, Suite 102
Miami, FL 33155-4069

Carlos Donayre, MD
Division of Vascular Surgery
Harbor-UCLA Medical Center
1000 West Carson Street
Torrance, CA 90509

Andrew Farb, MD
Department of Cardiovascular
Pathology
Armed Forces Institute of
Pathology
Washington, DC 20306-6000

Victor J Ferrans, MD, PhD
Pathology Section
National Heart, Lung and Blood
Institute
National Institutes of Health
Bethesda, MD 20205

Lois A Fiala, MD
Department of Surgery
Uniformed Services University
of the Health Services
4301 Jones Bridge Road
Bethesda, MD 20814

Michael R Fino, BS
Advanced Tissue Sciences, Inc
10933 North Torrey Pines Road
La Jolla, CA 92037

Kenneth L Gage
University of Pittsburgh
Center for Biotechnology and
Bioengineering
Room 407
300 Technology Drive
Pittsburgh, PA 15219

David Gillespie, MD
Department of Surgery
Uniformed Services University
of the Health Services
4301 Jones Bridge Road
Bethesda, MD 20814

Dionne A Graham, MS
Advanced Tissue Sciences, Inc
10933 North Torrey Pines Road
La Jolla, CA 92037

Neal Hadro, MD
Department of Surgery
Uniformed Services University
of the Health Services
4301 Jones Bridge Road
Bethesda, MD 20814

Michael Hallisey, MD
Connecticut Vascular Institute
University of Connecticut
School of Medicine, Suite 911
85 Seymour Street
Hartford, CT 06106

E M Hausmann, DMD, PhD
School of Dental Medicine
State University of New York at
Buffalo
Department of Oral Biology
365 Squire Hall
Buffalo, NY 14214-3008

Stephen L Hilbert, MD, PhD
Center for Devices and
Radiological Health
Food and Drug Administration
12725 Twinbrook Parkway
Rockville, MD 20852

Ned H C Hwang, PhD
Medical Engineering Division
National Health Research Inst
128 Yen-Chiu-Yea Road
Taipei 11529, Taiwan, ROC

Elizabeth D Jacobson, PhD
Deputy Director for Science
Office of the Commissioner
Food and Drug Administration
5600 Fishers Lane
Rockville, MD 20852

John W Karanian, PhD
Office of Device Evaluation and
Laboratory of Large Animal
Research
Center for Devices and
Radiological Health
Food and Drug Administration
Rockville, MD 20850

Nicholas Kipshidze, MD, PhD
Lenox Hill Heart and Vascular
Institute
Lenox Hill Hospital
130 East 77th Street
New York, NY 10021

Frank Kolodgie, MD
Department of Cardiovascular
Pathology
Armed Forces Inst of Pathology
Washington, DC 20306-6000

George E Kopchok, BS
Division of Vascular Surgery
Harbor-UCLA Medical Center
1000 West Carson Street
Torrance, CA 90509

Lee K Landeen, MS
Advanced Tissue Sciences, Inc
10933 North Torrey Pines Road
La Jolla, CA 92037

Ann A Lee, PhD
Advanced Tissue Sciences, Inc
10933 North Torrey Pines Road
La Jolla, CA 92037

Anne E Myer, PhD
NSF Industry/University
Cooperative Research Center
for Biosurfaces
State University of New York at
Buffalo
110 Parker Hall
Buffalo, NY 14214-3007

Thomas J McCarthy, DVM
Baxter Healthcare Corporation
17221 Red Hill Ave, M/S 44
Irvine, CA 92614

Gail K Naughton, PhD
Advanced Tissue Sciences, Inc
10933 North Torrey Pines Road
La Jolla, CA 92037

Takao Ohki, MD
Division of Vascular Surgery
Albert Einstein College of
Medicine
Montefiore Medical Center
111 East 210th Street
New York, NY 10467

Anthony Ratcliffe, PhD
Advanced Tissue Sciences, Inc
10933 North Tarrey Pines Road
La Jolla, CA 92037

Narendra K Simha, PhD
Department of Mechanical
Engineering
PO Box 248294
University of Miami
Coral Gables, FL 33124

Harry Sahota, MD
Good Samaritan Hospital
9810 Park Street
Bellflower, CA 90706

Frank J Veith, MD
Division of Vascular Surgery
Albert Einstein College of
Medicine
Montefiore Medical Center
111 East 210th Street
New York, NY 10467

Anthony C Venbrux, MD
Radiology and Surgery
Cardiovascular and
International Radiology Lab
The Johns Hopkins Medical
Institutions
600 N Wolfe St, Blalock 544
Baltimore, MD 21287

Renu Virmani, MD
Department of Cardiovascular
Pathology
Armed Forces Institute of
Pathology
Washington, DC 20306-6000

Jafar Vossoughi, PhD
Biomed Research Foundation
4401-A Connecticut Ave, NW
PMB 327
Washington, DC 20008-2322

William R Wagner, PhD
University of Pittsburgh
Center for Biotechnology and
Bioengineering
Room 407
300 Technology Drive
Pittsburgh, PA 15219

Irwin Walot, MD
Division of Radiology
Harbor-UCLA Medical Center
1000 West Carson Street
Torrance, CA 90509

Jeffrey A White, MS
Division of Cardiovascular
Surgery
Miami Children's Hospital
33200 SW 60 Court, Suite 102
Miami, FL 33155-4069

Rodney A White, MD
Division of Vascular Surgery
Harbor-UCLA Medical Center
1000 West Carson Street
Torrance, CA 90509

Ray Workman, MD
Department of Surgery
Uniformed Services University
of the Health Services
4301 Jones Bridge Road
Bethesda, MD 20814

Diane Wray-Cahen, PhD
Center for Devices and
Radiological Health
FDA, OST DLS/ HSB
Laboratory of Large Animal
Research
8401 Muirkirk Road
Laurel, MD 20708

Kenneth Wrigh, PhD
Department of Diagnostic
Radiology-057
University of Texas
MD Anderson Cancer Center
1515 Holcombe Blvd
Houston, TX 77030

Zu-Xi Yu, MD, PhD
Center for Devices and
Radiological Health
Food and Drug Administration
12725 Twinbrook Parkway
Rockville, MD 20852

Joan Zeltinger, PhD
Advanced Tissue Sciences, Inc
10933 North Torrey Pines Road
La Jolla, CA 92037

ACKNOWLEDGEMENTS

We are pleased to acknowledge the excellent contributions of the authors of the chapters. Editorial assistance of Theresa Conway, Daniel Shimko, and Elizabeth Browning is greatly acknowledged.

We are also grateful to the FDA Center for Veterinary Medicine, Office of Research for providing meeting space for the Workshop. This book was generated from the lectures given at the Stent Graft Workshop took place at the FDA - CVM.

Without our industrial sponsors, the Workshop and this book could not have been possible. The editors and the authors are, therefore, indebted to:

Advanced Tissue Sciences, Inc
Baxter Healthcare Corporation
Bio-Vascular, Inc
Boston Scientific Corporation
WL Gore & Associates

DISCLAIMER

The opinions presented in this book are the opinions of the individual authors and are not to be construed as conveying either an official endorsement or criticism by any of the editors and the industrial sponsors including the US Department of Health and Human Services and the Food and Drug Administration.

Every effort has been made to ensure the accuracy of the information presented in this book. However, due to the constant and rapid development in medical technology, editors, authors, nor the publisher can accept any legal or other responsibilities for the errors, accuracy and omissions that may have occurred at the time of publication.

PREFACE

This book is the first in a series of books and monographs planned to be published in the general area of "Applied Cardiovascular Medicine and Science."

The book contains chapters that are based on talks given at the "Stent Graft Workshop" held recently at the FDA – Center for Veterinary Medicine, Laurel, Maryland. The workshop was organized by the three editors and its purpose was to bring together professional, manufacturing, and regulatory communities to discuss the latest developments related to stent grafts. In particular, the objectives of the meeting were to: 1) foster communication between the professional, manufacturing, and regulatory communities; and 2) generate a preclinical/clinical stent graft update which summarizes current device safety and performance.

Jafar Vossoughi
vossoughi@msn.com
Nicholas Kipshidze
nkipshdze@compuserve.com
John W Karanian
Jwk@cdrh.fda.gov

Part I

INTRODUCTION, STANDARDS, AND HISTORY

Chapter 1

INTRODUCTORY COMMENTS

Elizabeth D Jacobson, PhD

Greetings on behalf of the FDA's Center for Devices and Radiological Health (CDRH). The contributions to this workshop on stent grafts are outstanding and represent both the preclinical and clinical cutting edge in this area of research. Since I do not want to take too much time from the program, my introductory comments will be brief.

There is great interest in this topic, given the significance of the therapeutic values of these devices. One of the concerns that both FDA and its critics have, when faced with a fast-moving technology, is that FDA will end up being a bottleneck as companies submit premarket approval applications for products. There are at least three ways to vaccinate against this:

- By early, vigorous and open discussions of the scientific and engineering issues,
- By early consultation between FDA and industry when a product is envisioned,
- By the use of consensus standards whenever possible.

Elizabeth Jacobson, PhD (corresponding author), Deputy Director for Science, Office of the Commissioner, Food and Drug Administration, 5600 Fishers Lane, Rockville, MD 20852
Stent Graft Update, Edited by J Vossoughi, N Kipshidze, JW Karanian

(http://www.erols.com/medengrgpubinc/)

The need for open scientific discussion is obviously bringing coals to Newcastle for this group. We need critical dialogue leading to both a clear understanding of the critical scientific issues and of the critical questions needing resolution for premarket applications.

This dialogue should take place between the professional, manufacturer and regulatory communities. Early discussion and agreement on what is scientifically necessary save false steps. Dialogue needs to happen at the earliest stages of product development and continue through the developmental lifetime of the product. We at the agency are committed to early and rapid decisions. A few years ago, 75% of applications for Investigational Device Exemptions (IDE's) were turned down on the first round. Today, 75% are accepted. This was not by accident. The Center has worked hard to get questions resolved early through discussions with sponsors. Further, Congress has codified in the newest FDA law, the Food and Drug Administration Modernization Act of 1997 (FDAMA), the need for pre-IDE discussions.

We really did not need Congress to tell us that this was a good idea, we were already doing it. Moving prevalent technology, such as stent grafts, safely and expeditiously through preclinical and clinical trials is a good example of the system working.

The proceedings of this Stent Grafts Workshop will be an excellent representation of the current status of this technology. This publication will serve as a touchstone for current information on the safety and effectiveness of these devices.

I know that our professional and industry colleagues would like to obtain information itemizing what needs to get done to obtain quick approval, and probably are justifiably dissatisfied with the lack of guidance in this area.

However, when a field is moving rapidly, it is difficult to generate good guidance. We hope the proceedings from this workshop can assist in this regard and serve as the basis for guidance and for consensus standards.

As some of you may know, FDAMA has given us the ability to recognize consensus standards in order to streamline the review process. To date, we have recognized nearly 400 standards and are very interested

in receiving manufacturer declarations of conformance to those standards. When such a declaration is made, manufacturers do not need to submit the data showing conformance to the agency, but need only keep it on file. This makes for a less bulky application and more expedient review time -- something to keep in mind for stent grafts. These proceedings also address the details of stent graft standards development to date.

Chapter 2

STANDARDS FOR ENDOVASCULAR DEVICES

Dorothy B Abel

Standards for medical devices are intended to promote consistent and comprehensive evaluations of the devices within the scope of the standard. Webster defines a standard as "an accepted measure of comparison for quantitative or qualitative value: Criterion." For medical devices, this generally translates into the compilation and recognition of accepted requirements and methods.

Endovascular devices, particularly endovascular grafts, pose difficulties in writing standards because the requirements and testing methods have not yet been established for these devices. This is primarily due to the novelty and diversity of this product area with respect to both the device designs and their clinical application. These limitations have not only affected the development of standards, but also restricted the scope of workshops and seminars devoted to these

Keywords: *Standards, medical devices, endovascular devices, ISO initiatives, Association for the Advancement of Medical Instrumentation*

Dorothy B Abel (corresponding author), Office of Device Evaluation and Radiological Health, US Food and Drug Administration (HFZ-450), 9200 Corporate Blvd, Rockville, MD 20850.

The views and opinions expressed here are those of the author and do not necessarily reflect those of the US Food and Drug administration, US Department of Health and Human Services, and the Public Health Service.

Stent Graft Update, Edited by J Vossoughi, N Kipshidze, JW Karanian

products. Such meetings are certainly valuable, however, the information presented should be considered within the context of the mature of the technology. Although useful insight is provided by experts in the various means of interest, it is important to keep in mind that consensus has not yet been achieved. In addition, with respect to endovascular grafts, the Food and Drug Administration (FDA) has not specified, nor recognized, any specific testing requirements.

ISO INITIATIVES FOR ENDOVASCULAR DEVICES

The vascular prostheses working group of the International Organization of Standardization (ISO) is working on the standardization of endovascular devices. The group had intended to work on developing standards for endovascular *grafts*. The work was expanded to cover endovascular *devices*, as members of the committee who also participate in the ongoing efforts of the European Community lobbied to expand the scope to be consistent with their projects. As a result, the ISO committee is now responsible for standardizing endovascular grafts, bare stents, vena cava filters, venous stents and TIPS stents. The delivery systems for these devices are also currently being included in this work item.

As it is premature to write a standard for these devices, the committee decided to write a technical report first[1]. A Technical Report type 2 format was chosen due to the fact hat these endovascular devices are still under technical development. With the relatively recent development of some of these devices, acceptable standardized *in vitro* tests and long term results of clinical trials are not yet available. This technical report aims to insure that manufacturers will address all aspects of design evaluation that relate to the safety of the product. This report will essentially become the rationale for the requirements that will be included in a future standard(s) for these devices. It will also be valuable in standardizing the terminology for these devices. Since this is a unique approach toward developing a standard, the contents of the report are described.

The critical components of the technical report are found in the Annexes. Annex A of the ISO technical report contains a table intended to provide a logical method for identifying a set of tests to assess endovascular device performance. This table is titled the "Attributes Table." Annex B includes a list of the Bench Tests identified in the Attributes Table, with a description for the purpose of each test, and

[1] Committee draft ISO/CD ISO/DTR 15539-1998

Annex C includes definitions for the Reportable Accessory Devices, and Annex E contains a bibliography.

Table 1 explains the headings for the Attributes Table. This information is included in the introduction to Annex A of the report.

TABLE 1
EXPLANATION OF ATTRIBUTES TABLE

Column Number	Title	Explanation	Context
1	Device/ Procedure Related Attributes	Individual design goals	The device should have an adequate ____(Column 1).
2	Problem(s)	Difficulties that may be encountered that could result in not meeting the individual design goal.	If the device does not have an adequate __(Column 1), there could be a problem with __(Column 2).
3	Reportable Clinical Events	Complications or failures that may be observed with clinical use if the problems occur.	If there is a problem with (Column 2), __(Column 3) could occur and should be documented.
4	Bench Tests	A list of tests, exclusive of animal and clinical studies, that may be conducted to validate and verify the individual design goal.	The following tests may be conducted to evaluate the adequacy of the ____(Column 1): ____(Column 4).
5	Animal Studies	Specified aims of animal studies to validate and verify the individual design goal	In order to evaluate the adequacy of the __ Column 1) an *in vivo* environment, the animal study should __(Column 5)

TABLE 1 CONTINUED			
6	Clinical Studies	Specific aims of clinical studies to verify the individual design goal	In order to evaluate the adequacy of the __ (column 1) in a clinical environment, the clinical study should __(Column 6)
7	Information Supplied by the Manufacturer	Information to be supplied by the manu-facturer to minimize the potential for failures to occur	To minimize the risk of __ (Column 2) or __ (Column 3), __(Column 7) should be provided by the manufacturer.

The exercise of completing the rows of the Attributes Tables was done for about 20 attributes for the delivery system and implant, with understandably fewer attributes for the accessory devices. By systematically identifying the design goals, the potential problems that could be encountered, and the clinical events, appropriate tests and information that need to be supplied by the manufacturer were identified.

An example of a row in the Attributes Table in Annex A, for the attribute *fixation effectiveness* follows:

The problems that could be encountered if there is not adequate fixation effectiveness include incomplete apposition to the vessel wall and excessive or inadequate radial force. These problems could lead to a list of clinical events, such as attachment site leak and prosthesis migration. The list of bench tests, such as radial force and crush resistance, may be conducted to evaluate the adequacy of the fixation effectiveness for the device. The specific aims of the animal studies to evaluate the adequacy of the fixation effectiveness should include: to assess position, integrity and functionality, to conduct appropriate histological and pathological investigation of explants, and to evaluate the previously identified reportable clinical events. The specific aims of the clinical studies to evaluate the adequacy of the fixation effectiveness should be the same as those for the animal studies, with the addition of the aim to monitor lesion morphology. The information to be supplied by the manufacturer should include directions regarding restrictions and requirements to

assure proper fixation, for example anatomical restrictions and sizing recommendations. This example is presented here in columnar form.

TABLE 2

EXCERPT FROM ATTRIBUTE TABLE

Device/Procedure Related Attributes	Fixation Effectiveness
Problem(s)	-Incomplete apposition to vessel wall -Excessive or inadequate radial force
Reportable Clinical Events	-Attachment site leak -Prosthesis migration -Lumen obstruction -Vascular trauma -Trauma to adjacent structures -Branch vessel Occlusion -Aneurysm enlargement -Aneurysm rupture
Bench Tests	-Radial force -Crush resistance -Recoil -Local Compression -Conformability to vessel wall -Migration Resistance -Simulated use
Animal Studies	-Assess position, integrity and functionality -Appropriate histological and pathological investigation of explants -Evaluate reportable clinical events
Clinical Studies	-Assess position, integrity and functionality -Monitor lesion morphology -Appropriate histological and pathological investigation of explants -Evaluate reportable clinical events
Information Supplied by the Manufacturer	N/A

The applicable rows from the table in Annex B that explain the purpose of each listed bench test are as follows:

TABLE 3

EXCERPT FROM BENCH TESTS TABLE

Conformability to Vessel Wall	Evaluate device conformity to vessel wall.
Crush Resistance	Record the minimum force at which permanent deformation occurs.
Local Compression	Evaluate the elastic deformation of the device in response to localized pressure.
Migration Resistance	Ability of device to remain stationary under simulated use.
Radial Force (Hoop Strength)	Evaluate the change in diameter of a self-expanding device as a function of radially applied pressure.
Recoil	Quantify the amount of elastic recoil and correlate this to recommended sizing. This information should be made available by the manufacturer.
Simulated Use	A model, which simulates the intended use of conditions and allows the evaluation of the applicable performance parameters

Finally, the applicable rows from the Table in Annex C which define the reportable clinical events are as follows:

TABLE 4

EXCERPT FROM REPORTABLE EVENTS TABLE

Aneurysm Enlargement	Any enlargement of the diameter or volume of the aneurysm sac greater than documented measurement error, as determined by contrast enhanced CT or other appropriate modality
Aneurysm Rupture	The rupture of the native aneurysm sac
Attachment Site Leak	Blood flow into the aneurysm sac arising at or from the attachment site occurring at any time after endovascular repair as determined by contrast CT scan, ultrasound,

TABLE 4 CONTINUED	
	angiography or direct observation at surgery or autopsy
Branch Vessel Occlusion	Clinically significant, unplanned exclusion of a major branch vessel
Lumen Obstruction	Unintentional obstruction of flow through the vascular lumen due to twisting or kinking of the prosthesis, oversizing, failure of the device to fully open, or any other cause
Prosthesis Migration	Longitudinal movement of all or part of a stent or attachment system for a distance of greater than 1 cm relative to anatomical landmarks determined prior to discharge
Trauma to Adjacent Structures	Injury to adjacent structures associated with vascular trauma (see definition below)
Vascular Trauma	Injuries to vessels as a result of an endovascular procedure, including dissections or perforations. The specific site and source of the injury as well as the clinical sequelae should be reported. All required surgical or interventional procedures required to repair the injury should also be reported.

This example demonstrates the logic used to develop the ISO report and the level of information captured in the report. Clearly this report cannot be used as a laundry list for testing to be completed on an endovascular device, but rather, may be used as a template in completing the exercise of identifying the appropriate testing for each individual device.

STATUS AND SUMMARY

The Technical Report was distributed to the member countries of ISO for comment and these comments were discussed at a meeting in London in October. After resolving the comments, the document will be modified as appropriate and distributed for comment and vote. Hopefully, the report will be published within a year.

This report, particularly the Attributes Tables, will form the basis for the requirements of a future standard for these devices. The strategy for developing the standard is the same as that used for stents.

devices) will need to be discussed at future meetings of the working group.

Anyone interested in participating in this effort should call Joe Lewelling of the Association for the Advancement of Medical Instrumentation (AAMI), the secretariat to ISO for this committee, at (703) 525-4890, extension 206.

Chapter 3

HISTORICAL DEVELOPMENT OF STENT GRAFTS

Jafar Vossoughi, PhD

Stent grafts are used for the endovascular treatment of abdominal aortic aneurysms (AAA), arteriovenous fistulas (AVF), arterial false aneurysms (FA), treatment of dissecting aneurysms (DA), and the thoracic aneurysms (TA).

The use of a stent graft for the treatment of AAA is more important now than it was years ago because the diagnosis of AAA has been seen more frequently during the last two decades [17]. This is perhaps related to the aging population, the extensive use of modern computerized tomographic scanning, and the ultrasonography of different pathologies. For the past four decades, it has appeared that the most appropriate method to prevent AAA rupture has been the replacement with a synthetic graft [2, 15, 16, 21, 25, 26]. In this chapter a brief development of stents and stent grafts is presented.

Insertion of tubular structures into the blood vessels of animals is not a new technique. The first such attempt was made by Alexis Carrel in

Keywords: *History, stent, stent graft, angioplasty, interventional*

Jafar Vossoughi, PhD (corresponding author), Biomed Research Foundation, 4401-A Connecticut Ave, NW, PMB 327, Washington, DC 20008-2322

Stent Graft Update, Edited by J Vossoughi, N Kipshidze, JW Karanian

1912, when he is credited with inserting a glass tube into an animal's blood vessel [3]. It appears that no one attempted to follow up the prophetic vision of Carrel for many years. More than a half century later, in 1964, Charles Dotter inserted a set of telescopic coaxial tubes with gradually increasing diameter into diseased peripheral vessels using a blunt dissection technique [6]. His goal of catheter intra-aortic insertion of scaffolds is actually the beginning of the concept of practical stenting. His original thinking was that permanent scaffolding would counteract the problem of elastic recoil. He also thought that natural process of fibrosis and re-intimalization would take place once a splint created an adequate false lumen. His initial attempt using Silastic® tubes, however, failed due to thrombosis and migration [7]. Later, replacement of the material with uncoated stainless steel or nickel titanium alloy wire coils appeared more promising [9]. Continued potency of the open coil construction was attributed to the rapid formation of a new firmly anchored lining surface.

The term "stent" has been derived from the splint used by a London dentist, (Charles Stent living in nineteenth century), to stabilize skin grafts [32, chapter 1]. The percutaneous implantation of nitinol coil stents in dogs was first reported in 1983 by Cragg, et al [4]. All the stents implanted in canine aortas remained potent until recovery at four weeks without even an anticoagulation agent. At the same time, Maass, et al [14] experimented with the self-expanding stainless steel coil stents. They reported problems such as migration, tilting and thrombosis of the simple spiral design which resulted in geometric modification. A lesson learned from spiral design was the double helix construct, which proved to be much more stable with no sign of thrombosis.

In 1985, Caesar Gianturco used a spring-loaded stainless steel zigzag stent in short segments of large vessels in which migration of some of the stents was observed [31, 32]. The first implantation of a similarly designed stent in humans took place in 1985 in Kiev by Volados and associates [32]. For more details and historic overview of Volandos' work see Chapter 18 of this book by Kipshidze, et al. Surprisingly, this first human implantation of a stent was not acknowledged even inside the Soviet block until four years later. Palmaz, et al were the first to use balloon expandable stents using the Palmaz stainless steel slotted tube design also in 1985 [22]. Due to the strict regulatory rules in the US, this stent was not used in clinical practice for an additional two years. Another balloon expandable stent, the Gianturco's interdigitating coil design, was tested in animals more or less during the same period [30]. The stent implantation was rapidly spreading with the introduction of

self-expanding mesh stent "wall stent ™." The self-expanding mesh stent on a delivery catheter was the first stent used in clinical practice by Sigwart, et al. The clinical landmark showing the value of stenting occurred in 1986 during a live demonstration at the Royal Brompton Hospital, London, UK by Ulrich Sigwart and his surgical group through an emergency procedure of a multiple stent placement in the totally occluded LAD of a 50 year old female patient with complications in LAD and RCA. She remained asymptomatic over at least ten years. This demonstration was a conclusive proof that in the most complicated intravascular procedures, the intravascular scaffolding can be a viable procedure [32].

Over two decades of clinical experience with stents have greatly advanced the technology and eliminated most of the undesired complications. Stents are now being used in aortas, carotid arteries, coronary arteries, femoral arteries, iliac arteries, renal arteries, and non-cardiovascular applications such as bile ducts, bronchi, trachea, esophagus, and urinary tract [5, 10, 11, 20, 27-29, 37].

Stent grafts are the latest generation of the endovascular devices that utilize the advantages of stent technology in combination with those of vascular grafts.

Stent Grafts: How the Technology Developed

Charles Dotter, who is credited for the original work on endoluminal treatment of vascular disease, extended his invention to involve endovascular grafting [1, 7, 8, 32, 33]. Soon others expanded the concept and a variety of endoluminal grafts were produced [12]. Using the experience gathered from simple stents, stainless steel and nitinol were used in these early acute experiments [12]. For the grafts' coatings, polyurethane and porous nylon fabrics were the materials of choice [18].

Endoluminal treatment of vascular disease was initiated by Charles Dotter who took Seldinger's idea of diagnosis and extended and applied it to treatment. In transformation from diagnosis to treatment, the concept of intraluminal intervention in vascular disease called "transluminal angioplasty" came to be a new therapeutic discipline [1, 8].

In 1977, Parodi attempted to exclude aortic aneurysms by endovascular techniques. He combined the endovascular stent developed by Julio Palmaz with a thin-walled Dacron prosthesis developed by Hector Barone, into an aortic graft termed "stent-graft" which had the advantage

that it could be placed into the human aorta from a remote site [23, 24]. Such a revolutionary method also had its own problems, ie, the precise sizing of the aneurysm and its neck, and problems associated with the distal anchoring of the stent graft [13]. Despite many related problems, all five ill patients receiving stent grafts from Parodi survived [23]. Other complications recognized early were wound infection and groin hematoma. Also, some technical problems related to graft irregularities at anchoring sites, kinks in graft body and limbs, and pre-graft leaks at the proximal and distal anastomosis were recognized and resulted in an unsuccessful outcome of this new procedure.

Also in 1976, Parodi initiated the use of stents in place of sutures to secure the proximal and distal ends of fabric graft which created a leak tight seal [26]. The operative mortality of the technique is now better that 5% with the median survival of about 10 years [19].

The technique rapidly underwent a variety of improvements by many interventionalists and vascular surgeons who incorporated advances in MRI, CT, and endovascular ultrasound [13, 23]. With the introduction of the new graft materials, improved delivery system, and advanced instrumentation, use of the stent graft is being increased. Although there are still problems related to stent grafts, many problems associated with failure of proximal or distal anchoring and the production of distal embolization are now well under control. The challenges remaining are technological and medical in nature and are being addressed by researchers and clinicians on a continual basis. Most of the difficult problems, however, are related to complicated patients.

There is still great risk of wound infection and hematoma, in particular groin hematoma. Since one-size-does-not-fit-all, there are still problems related to graft irregularities at the anchoring sites and graft kinks. Another potential problem is related to the perigraft leak at the proximal and distal anastomasis. Reconstruction and prosthetic graft replacement at the curved vessels and branches remain challenging surgical procedures. Improvements in instrumentation and anchoring mechanisms will certainly eliminate many of the failures of proximal and distal anchoring and production of distal embolization [1].

Vascular response to endovascular implants can be improved by better stent graft design and by introduction of more appropriate materials to improve neointimal hyperplasia, inflammation, and thrombosis. Intelligent alteration in prosthetic graft design parallel with pharmacological therapy will certainly improve the long-term clinical

outcome. Additionally, incorporation of tissue and genetic engineering will certainly help modulate neointimal proliferation and subacute thrombosis. New technologies are also needed to treat long segment diseased vessels for which endovascular grafts are the most suitable treatment modality. For discussion on biomechanics related problems see Chapter 4.

REFERENCES

1. Bergan, JJ. Stent Grafts: An Introduction. In: Sigwart, U (Editor). **Endoluminal Stenting**. WB Saunders Company Ltd, London, 1996, 443-436
2. Brown, OW, LH Hollier, PC Pairolero, et al. Abdominal Aortic Aneurysms and Coronary Artery Disease: A Reassessment. Arch Surg 1981; 116:1484-1488
3. Carrel, A. Results of the Permanent Intubation of the Thoracic Aorta. Surg Gyn Obst 1912; 15:245-248
4. Cragg, A, G Lund, J Rysavy, et al. Nonsurgical Placement of Arterial Endoprostheses: A New Technique Using Nitinol Wire. Radiology 1983; 147:261-263
5. Cremer, M, J Deviere, J-M Dumonceau. Esophageal Stents. In: Sigwart, U (Editor). **Endoluminal Stenting**. WB Saunders Company Ltd, London, 1996
6. Dotter CT, MP Judkins. Transluminal Treatment of Atherosclerotic Obstruction: Description of a New. Technique and Preliminary Report of its Application. Circulation 1964; 30:654-660
7. Dotter, CT. Transluminally-Placed Coiled Endarterial Tube Grafts. Invest Radiology 1969; 4:329-332
8. Dotter, CT, J Rosch. Transluminal Angioplasty: The Catheter Treatment of Peripheral Arterial Obstruction. In: Dale, WA (Editor). **Management of Arterial Occlusive Disease**. YearBook Medical Publishers, Chicago, 1971, 257-267
9. Dotter, CT, RW Buschmann, MK McKinney, et al. Transluminal Expandable Nitinol Stent Grafting: Preliminary Report. Radiology1983; 147:259-260
10. Goldstraw, P, G Ladas. Bronchial Stenting. In: Sigwart, U (Editor). **Endoluminal Stenting**. WB Saunders Company Ltd, London, 1996
11. LaBerge, JM. Biliary Stenting. In: Sigwart, U (Editor). **Endoluminal Stenting**. WB Saunders Company Ltd, London, 1996
12. Lawrence, DD, C Charnsaugavej, KC Wright, C Gianturco, S Wallace. Percutaneous Vascular Graft Experimental Evaluation. Radiology 1987; 163:357-360

13. Lumsden, AB, RC Allen, EL Chaikof. Ruptured Abdominal Aneurysm Following Stent Graft Placement. Am J Surg, 1995, 170: 174-178
14. Maass, D, D Demierre, D Deaton, et al. Transluminal Implantation of Self-adjusting Expandable Prostheses: Principles, Techniques, and Results. Prog Artif Org 1983, 27:979-987
15. Marin, ML, FJ Veith. Clinical Applications of Endovascular Grafts in Aortailiac Occlusive Disease and Vascular Trauma. Cardvsc Surgery 1995; 3:115-120
16. Marin, ML, FJ Veith, RJ Lyon, et al. Endovascular Bypass for the Treatment of Aortailiac Occlusive Disease. In: Sigwart, U (Editor). **Endoluminal Stenting**. WB Saunders Company Ltd, London, 1996
17. Melton, NJ, LK Bickerstaff, LH Hollier, et al. Changing Incidnece of Abdominal Aortic Aneurysms: a Population-based Study. Am J Epidem 1984; 120:379-386
18. Mirich, D, KC Wright, S Wallace, et al. Percutaneously Placed Endovascular Grafts for Aortic Aneurysm: Feasibility Study. Radiology 1989;170:1033-1037
19. Nevelsteen, A, L Wouters, R Suy. Aortofemoral Dacron Reconstruction for Aortoiliac Occlusive Disease: A 25-Year Survey. Eur J Vasc Surg 1991; 5:179-186
20. Oesterling, JE, BA Kletscher. Stenting of te Prostate with UroLume™ Prosthesis. In: Sigwart, U (Editor). **Endoluminal Stenting**. WB Saunders Company Ltd, London, 1996
21. Ohki, T, FJ Veith, ML Marin, et al. Endovascular Approaches for traumatic Arterial Lesions. Sem Vasc Surg, 1997; 10: 272-285
22. Palmaz, JC, RR Sibbitt, FO Tio, et al. Expandable Intraluminal Vascular Graft: a Feasibility Study. Surgery 1986; 99:199-205
23. Parodi, JC, JC Palmaz, JD Barone. Trasnfemoral Intraluminal Graft Implantation for Abdominal Aortic Aneurysms. Ann Vasc Surg 1991; 5:491-499
24. Parodi, JC, FJ Criado, HD Barone, et al. Endoluminal Aortic Aneurysm Repair Using a Balloon-Expandable Stent Graft Device: A Progress Report. Ann Vasc Surg 1994; 8523-529
25. Parodi, JC, ML Marin, FJ Veith. Transfemaral Endovascual Stented Grafts Repair of an Abdominal Aortic Aneurysm. Arch Surg 1995; 130:549-552
26. Parodi, JC. Endovascular Stent Grafts for Aortic Aneurysms, Arteriovenous Fistulas and False Aneurysms. In: Sigwart, U (Editor). **Endoluminal Stenting**. WB Saunders Company Ltd, London, 1996
27. Pauer, W. Stenting of the Ureter. In: Sigwart, U (Editor). **Endoluminal Stenting**. WB Saunders Company Ltd, London, 1996

28. Press, SM, GH Badlani. Uretral Stents. In: Smith, AD **(Editor), Smith's Textbook of Endourology**, WB Saunders, Philadelphia. 1995
29. Press, SM, GH Badlani. Urethral Strinctures Treated with the UroLume™ Stent. In: Sigwart, U (Editor). **Endoluminal Stenting.** WB Saunders Company Ltd, London, 1996
30. Roubin, GS, KA Robinson, SB King, et al. Early and Late Results of Intracoronary Arterial Stenting After Coronary Angioplasty in Dogs. Circulation 1987; 76:891-897
31. Serruys, PW, BH Straus, KJ Beatt, MD Bertrand, J Puel, AF Rickards, B Meier, JJ Goy, P Vogt, L Kappenberger, U Sigwart. Angiographic Follow-Up After Placement of a Self-Expanding Coronary Artery Stent. N Engl J Med 1991; 324:13-17
32. Sigwart, U (Editor). **Endoluminal Stenting**. WB Saunders Company Ltd, London, 1996
33. Szilagyi, DE, JP Elliott, RF Smith, et al. A 30-year Survey of the Reconstructive Surgical Treament of Aortoiliac Occlusive Disease. J Vasc Surg 1986; 3:421-436
34. Taylor, PR. Vascular Stents and Stent Grafts: A Vascular Surgeon's View. Carvsc Intervnt Radiol 1997; 20:1-4
35. Wright, KC, S Wallace, C Charnsangave, et al. Percutaneous Endovascular Stents: An Experimental Evaluation. Radiol 1985; 156:69-72
36. Yao, JST, WH Pearce, (Editors). **Techniques in Vascular and Endovascular Surgery**. Appleton and Lange, 1998
37. Yochia, D. The use of Urethral Stents for the Treatment of Urethral Stintures. Ann D'Urologie 1993; 27:245-252

Part II

BIOMECHANICS AND TISSUE ENGINEERING

Chapter 4

STENT GRAFT BIOMECHANICS

Jafar Vossoughi, PhD

Percutaneous angioplasty and many other catheter-based techniques are all based on the pioneering work of Charles Dotter (see Chapter 3 for an historic overview). Originally, the terminology of endovascular graft was used as a vascular conduit that is placed within the vascular system. It is most widely used as an arterial graft inserted into the vascular tube through a remote access site guided by the arterial lumen. Such procedure is conducted minimally invasively and under fluoroscopy. To hold the device in place, a variety of techniques such as balloon-expandable or self-expanding fixation methods are used [33, 38, 63].

STENT GRAFT

Stent graft is a blend of a prosthetic thin-walled Dacron knitted graft and the intravascular balloon-expandable stent. It is a single device possessing the flexible homeostatic sealing properties of a graft and the efficient anchoring mechanism of the stent [63]. Therefore, it is more technologically sophisticated than a vascular graft or stent alone.

Keywords: *Biomechanics compliance mismatch, flow, shear stress, residual stress, geometry, stiffness, rigidity*

Jafar Vossoughi, PhD (corresponding author), Biomed Research Foundation, 4401-A Connecticut Ave, NW, PMB 327, Washington, DC 20008-2322

Stent Graft Update, Edited by J Vossoughi, N Kipshidze, JW Karanian

STENT GRAFT BIOMECHANICS

Since the stent graft is a single device composed of two other devices, *ie*, graft and stent, the biomechanical problems associated with the stent graft are the combined biomechanical problems of stents and grafts as well as other mechanical problems particular to stent graft alone. In the following pages a variety of biomechanical problems associated with stent grafts will be briefly discussed. Although mostly relevant, biomechanical problems related to grafts or stents alone will not be discussed. The literature dealing with graft biomechanics and stent biomechanics alone is very rich and the reader may consult limited references listed at the end of this chapter [26, 42, 54, 68]. This includes mostly the problems associated with graft and stent materials, biocompatibility, degradation, etc.

HEMODYNAMICS AND ENDOVASCULAR PROSTHESES

Similar to any other biological entity, blood vessels have their own natural mechanism with specific homeostasis that tend to maintain all hemodynamic parameters at steady state level (within the specific limits and conditions) [10, 21]. This is accomplished by coordinated efforts of complex physiologic processes. The activities of all organ systems are integrated by automatic adjustments of a variety of parameters within narrow limits that take action once the system parameters and conditions are excited, altered, or otherwise disturbed by any stimuli within or outside of the organism or its surroundings. In more applied terms, (both medical and biomechanical), it is said that the biological organ or tissue undergoes "remodeling." This remodeling must certainly have an organized biochemical basis that may be reflected in pathological, biomechanical, and even geometric alterations that can be measured. It is the biomechanical and geometric remodeling that are pertinent to the subject of this chapter and are the only remodeling modalities that are briefly discussed here.

ALTERATION IN BLOOD PRESSURE

It is well documented that an alteration in natural blood pressure accompanies biomechanical and geometric remodeling of the vessel wall [13, 18-20, 22, 47, 48, 58]. It is important to note that such remodeling takes place fairly quickly resulting in gross changes in elasticity

(compliance, etc) and wall thickening in the arteries [13, 14, 18-20, 29, 35, 47, 48, 58, 62]. If the disturbances are acute or at lower intensities, such as small increases in blood pressure, the system will bring everything back to the natural homeostatic levels. The remodeling occurs once such a limit is exceeded or the disturbance is maintained chronically.

Once the biological system (such as an artery) is invaded, such as by intervention or permanent placement of stent, graft, valve, etc, some local alterations are imposed on the host artery. After such invasion, a chain of local and systematic biological events takes place. Those that could not be tolerated by the natural defense and the homeostatic mechanism of the system may result in local or systemic biological alterations, some of which can be detrimental locally or systemically. In the following sections, the responses of the vessel to a few such alterations believed to be important are briefly discussed.

BLOOD FLOW DISTURBANCE

The cardiovascular system is designed in a way that blood can flow through the arteries continuously and for life without creating any chronic problem. There are, however, many instances in which the initiation of some disease are attributed to blood flow (such as artherogenesis around the bends and branches) [4, 5, 7, 9, 15, 23, 24, 31, 39, 40, 44-46, 50, 56]. It is shown by many investigators using numerical methods and/or experiments that local flow disturbances are involved in atherogenesis, in particular, around the entrance of the daughter branches and at the vicinity of the bifurcations [2, 8, 34, 45, 46]. Most of the frequently encountered atherosclerotic lesions are seen in these locations. Many factors may be attributed to the formation of atherosclerotic lesions, among which are the flow separation, turbulence, variation in local shear stress, etc [11, 12, 16, 27, 28, 34, 36, 37]. Some of the major biomechanical changes are expected to be encountered by a natural function of the endothelial cells [7]. In many instances, it is demonstrated that the endothelial cell barrier protects the vessel wall against disease such as atherosclerosis. It is also postulated that the initiation of atherosclerosis has to do (at least partially) with the de-endothelialization process. This can happen in each external intervention (catheterization, ballooning, implantation, surgery, etc).

Local flow patterns are disturbed at the anastomasis. Intimal hyperplasia, considered to be the major cause of late vascular graft failure, is frequently seen in regions near anastomoses [6, 17, 30, 49, 51, 56, 59]. Although this is an art, surgical improvements will certainly reduce the graft failure. The case of stent grafts is similar: a better anchoring mechanism causing minimal flow disturbance can reduce stent graft failure rate. The trade off here, of course is, to also have no leak.

MECHANICAL PROPERTY MISMATCH

The host vessel has its own natural mechanical properties. Bypass surgery or implantation of stent grafts (or vascular synthetic grafts or stents) contributes to the compliance mismatch. It is believed that most of the mechanical failures of the grafts, as well as portions of the host vessel adjacent to the anastomasis, are caused by compliance mismatch [1, 25, 32, 41, 55, 57, 59, 64, 65, 66].

It appears that in most cases, the inclusions of the synthetic graft or stent increases the rigidity and stiffness of the host vessel that compromises the graft or stent hemorheology and may make the graft or stent more thrombogenic. Since the compliance of the individual vessels change considerably along the arterial tree, it appears that there may be no simple solution to this problem; not to mention there is a large compliance variation among the various available stents and grafts.

SMALL VERSUS LARGE CALIBER VESSELS

Surgery of large vessels (aorta, iliac, carotid, and femoral arteries) is usually successful. It appears that the type of graft material, the geometry, and some of the other problems (such as those related to anastomosis) are not considered to be the significant problems for large arteries. However, for small vessels, such as coronaries and lower extremity and peripheral arteries, these problems are detrimental. Again, it is logical to conclude that biomechanical factors are even more crucial for small arteries. For example, small arteries are under low blood flow, whereas large arteries experience high blood flow.

Most of the early failures of grafts (and more so for small diameter grafts) are associated with thrombosis, (within thirty days of implantation) [17]. Although many other factors, such as chemical

properties and surface characteristics of the graft, may be responsible for such early failures, it is believed that the effect of blood flow rate on thrombosis formation is very important [3, 4, 7, 15, 43]. Sauvage, et al [53] proposed the concept of "thrombotic threshold velocity" in describing the dependence of the accumulation of thrombus on blood velocity.

VASCULAR RESIDUAL STRESS AND STRAIN

It has been shown that arteries are residually stressed in vivo [60, 61]. It has also been shown that vascular residual stress is an important biological parameter that is highly sensitive and responds to minute external changes (such as changes in blood pressure) and the formation of atherosclerosis [13, 14, 19, 20, 35, 47, 48, 58]. Biomechanicians also believe that vascular residual stress is an important factor in natural growth, development, and remodeling of the vessel wall [13, 18, 19, 20, 22, 47, 48, 58]. Once the stent graft (or graft or stent alone) is implanted, the *natural remodeling mechanism* (vascular residual stress) is absent and thus the remodeling process in coping with the intervention is weakened. For example, residual stress reduces the actual stress level on the intimal surface of the wall [13, 18, 22, 47, 48, 58] and once a stent graft is implanted, such a stress reduction mechanism is no longer available.

ALTERATION OF SHEAR STRESS

Most of the failures in engineering materials and structures are due to excessive shear stress. Materials and structures are usually tolerant to higher levels of normal stress but fail under significantly lower levels of shear stress. It is natural to expect that biological materials and organs such as blood vessels also follow a similar trend.

We have already discussed the role of local blood flow characteristics and their importance in stent graft failure. Alteration in the local blood flow is usually associated with alteration of shear stress on the wall of vessels. Analogous to engineering materials and structures, alteration of shear stress can be a major factor in the failure of stent grafts. In studying fluid dynamics of a stented vessel by using numerical simulation, Xu, et al [67] have demonstrated that each time blood flow encounters a stent wire, the shear stress drastically changes. The result

also is dependent on the spacing between stent wires (and most probably configuration). Immediately before and after each stent wire, the fluid velocities are very low, and the flow is almost stagnant. At these sites, the wall shear stresses are significantly altered. This is considered an important biomechanical risk factor that predisposes the patient to lesion development and thrombosis formation. A more intelligent stent (stent graft) design may reduce the device failure.

CONCLUDING REMARKS

Stent grafts, (as well as grafts or stents alone), must satisfy highly demanding hemodynamic requirements. Ideal stent grafts should be biocompatible (ie, nontoxic, noncarcinogenic, biodurable, noninflamatory, and biostable), and hemocompatible (impervious to blood, infection resistant, and acutely thromboresistant). Many of these requirements are related to materials and have already been resolved to a degree. What are not yet resolved are the non-material biomechancial considerations. The ideal stent graft should have axial and circumferential compliance comparable to those of the host vessel. Similarly, the geometric mismatch should also be reduced or eliminated if at all possible.

REFERENCES

1. Abbott, WM, J Megerman, JE Hasson, et al. Effect of Compliance Mismatch on Vascular Graft Patency. J Vasc Surg 1987; 5:376-382
2. Anayiotos, AS, SA Jones, DP Giddens, et al. Shear Stress at a Compliant Model of the Human Carotid Bifurcation. J Biomech Eng
3. Baird, RN, WM Abbott. Pulsatile Blood Flow in Arterial 1994; 116:98-106 Grafts. Lancet 1976; 2:948-950
4. Bassiouny, HS, S White, S Glasgov, et al. Anastomotic Intimal Hyperplasia: Mechanical Injury of Flow Induced. J Vasc Surg, 1992; 15:708-717
5. Berry, JL, JE Moore Jr, VS Newman, WD Routh. In Vitro Flow Visualization in Stented Arterial Segments. J Vasc Inv 1997;3:63-68
6. Cantelmo, NL, WC Quist, FW Lo Gerfo. Quantitative Analysis of Anastomic Intimal Hyperplasia in Paired Dacron and PTFE Grafts. J Cardiovasc Surg 1989; 30:910-915
7. Davies, PF, KA Barbee, R Lal, et al. Endothelial Surface Dynamics in Flow Signal Transduction. Ann NY Acad Sci 1995; 748:86-103

8. Delfino, A, JE Moore Jr, N Steriopulos, et al. Wall Stresses in the Cardiod Bifurcation: Effects of Non-homogeneity and Correlation with Intimal Thickness. J Vasc Inv 1998; 4:61-71
9. Deng, X, M King, R Guidoin. Localization of Artherosclerosis in Arterial Junctions. Modelling the Release Rate of Low Density Lipoprotein and its Breakdown Products Accumulated in Blood Vessel Walls. ASAIO Journal 1993; 39:M489-M495
10. Fabregues, S, K Baijens, R Riev, P Bergeron. Hemodynamics of Endovascular Prostheses. J Biomech 1998; 31:45-54
11. Friedman, MH, GM Hutchins, CB Bargeron. Correlation Between Intimal Thickness and Fluid Shear in Human Arteries. Artherosclerosis 1981;39:425-436
12. Friedman, MH, DL Fry. Arterial Permeability Dynamics and Vascular Disease. Artherosclerosis 1993;104:189-194
13. Fung, YC. **Biomechanics: Motion, Flow, Stress, and Growth.** Springer-Verlag, New York, 1990
14. Fung, YC, SQ Liu. Changes of Zero-Stress State of Rat Pulmonary Arteries in Hypoxic Hypertension. J Appl Physiol 1991; 70:2455-2470
15. Giddens, DP, CK Zarins, S Glasgov. The Role of Fluid Mechanics in the Localization and Detection of Artherosclerosis. J Biomech Eng 1993; 115:588-594
16. Goodall, AH. Role of Shear Stress and Turbulence on Platelets in Blood Conduits and on Endothelial Cells in Arterial Conduits. In: Sigwart, U (Editor). **Endovascular Stenting**. WB Saunders Company, Ltd, London, 1996
17. Guidoin, R, X Deng, Y Marois. Failure Models and Performance of Synthetic, Autologous, and Endovascular Grafts. ASAIO J 1997;43: 239-241.
18. Hayashi, K, A Kamiya, K Ono (Editors). **Biomechanics, Functional Adaptaion and Remodeling.** Springer-Verlag, Tokyo, 1996
19. Hong, MK, J Vossoughi, GS Mintz, et al. Altered Compliance and Residual Strain Precede Angiographically Detectable Early Arthersclerosis in Low-Density Lipoprotein Receptor Deficiency. Arterioscler Thromb Vasc Biol 1997; 17:2209-2217
20. Hong, MK, J Vossoughi, CC Haudenschild, et al. Vascular Effects of Diet-Induced Hypercalcemia After Balloon Artery Injury in Giant Flemish Rabbits. Am Heart J 1995; 130:758-764
21. How, TV. RA Black, PL Harris. Hemodynamic Consequences of Intravascular Stent Development. In: Sigwart, U (Editor).

Endovascular Stenting. WB Saunders Company, Ltd, London, 1996

22. Humphrey, JD. Mechanics of Arterial Wall: Review and Directions. Critical Reviews in Biomedical Engineering 1995; 23:1-162
23. Ishibashi, H, M Sunamura, T Karino. Flow Paterns and Preferred Sites of Intimal Thickening in the End-to-End Anastomosed Vessels. Surgery 1995; 117:409-420
24. Karino, T, HL Goldsmith. Aggregation of Human Platelets in an Annular Vortex Distal to a Tubular Expansion. Microvasc Res 1979; 17: 217-237
25. Kinley, CE, AE Marble. Compliance: A Continuing Problem with Vascular Grafts. J Cardiovasc Surg 1980; 21:163-170
26. Kowligi, RR, TJ Edwin, C Banas, RW Calcote. Vascular Grafts: Materials, Methods, and Clinical Applications. In: Wise, DL, et al (Editors). **Encyclopedic Handbook of Biomaterials and Bioengineering**, Part B, Vol 2.. Marcel Dekker, Inc, NY, 1995: 979-1009
27. Ku, DN, DP Giddens, CK Zarins, S Glagov. Pulsatile Flow and Artherosclerosis in the Human Carotid Bifurcation: Positive Correlation Between Plaque Location and Low and Oscillation Shear Stress. Artherosclerosis 1985; 5:293-302
28. Lieber, BB, DP Giddens. Post-stenotic Core Flow Behavior in Pulsatile Flow and its Effects on Wall Shear Stress. J Biomech 1990; 26:597-605
29. Liu, SQ, YC Fung. Relationship Between Hypertension, Hypertrophy, and Opening Angle of Zero-Stress State of Arteries Following Aortic Constriction. J Biomech Eng 1989; 111:325-335
30. Logerfo, FW, WC Quist, MD Nowak, et al. Downstream Anastomotic Hyperplasia: A Mechanism of Failure in Dacron Arterial Grafts. Ann Surg 1983; 197:479-483
31. Lou, Z, WJ Yang. A Computer Simulation of the Blood Flow at the Aortic Bifurcation. Biomed Mat Eng 1991; 1:173-193
32. Lyman, DJ, FJ Fazzio, H Voorhees, G Robinson. Compliance as a Factor Effecting the Patency of a Copolyurethane Vascular Graft. J Biomed Mat Res 1978; 12:337-345
33. Marin, ML, FJ Veith, TF Panetta, et al. Transluminally Placed Endovascular Stened Graft Repair for Arterial Trauma. J Vasc Surg 1994; 19:466-473

34. Mark, FF, CB Bergeron, OJ Deters, MH Friedman. Variations in Geometry and Shear Rate Distributions in Casts of Human Aortic Bifurcation. J Biomech 1989; 22:577-582
35. Matsumoto, T, K Hayashi. Stress and Strain Distribution in Hypertensive and Normotensive Rat Aorta Considering Residual Strain. J Biomech Eng 1996; 118:62-73
36. Moore, JE, DN Ku, CK Zarins, S Glasgov. Pulsatile Flow Visualization in the Abdominal Aorta Under Differing Physiologic Conditions: Implications for the Increased Susceptibility to Artherosclerosis. J Biomech Eng 1992; 114:391-397
37. Moore, JE Jr, C Xu, S Glagov, et al. Fluid Wall Shear Stress Measurements in a Model of the Human Abdominal Aorta: Oscillatory Behavior and the Relationship to Artherosclerosis. Artherosclerosis 1994;110:225-240
38. Moore, WS, CL Vescera. Repair of Abdominal Aortic Aneurysm by Transfemoral Endovascular Graft Placement. Ann Surg 1994; 220: 331-341
39. Morinaga, K, K Okadome, M Kuroki, et al. Effect of Wall Shear Stress on Intimal Thickening of Arterially Transplanted Autogeneous Veins in Dogs. J Vasc Surg 1985; 2:430-433
40. Nazemi, M, C Kleinsteuer, JP Archie. Pulsatile Two-dimensional Flow and Plaque Formation in a Carotid Artery Bifurcation. J Biomech Eng 1990; 23:1031-1037
41. Okuhn, SP, DP Connelly, N Calakos, et al. Does Compliance Mismatch Alone Case Neointimal Hyperplasia? J Vasc Surg 1989; 9: 35-45
42. Palmaz, JC. Review of Polymeric Graft Materials for Endovascular Applications. J Vasc Intv Rad 1998; 9:7-13
43. Parikh, S, C Rogers, ER Edelman. Endovascular Stents: Experimental Data. In: Sigwart, U (Editor). **Endovascular Stenting**. WB Saunders Company, Ltd, London, 1996
44. Peacock, J, S Hankins, T Jones, R Lutz. Flow Instability Induced by Coronary Artery Stents. Assessment with an In Vivo Pulse Duplicator. J Biomech 1995; 28:17-26
45. Perktold, K, M Resch. Numerical Flow Studies in Human Carotid Atery Bifurcations: Basic Discussion of the Geometric Factor in Artherogenesis. J Biomech Eng 1990; 12:111-123
46. Perkhold, K, RO Peter, M Resch, G Langs. Pulsatile Non-Newtonian Blood Flow in Three-Dimensional Carotid Bifurcation Models: A

Numerical Study of Phenomena Under Different Bifurcation Angles. J Biomech Eng 1991; 13:507-515
47. Rachev, A, N Stergiopulos, JJ Meister. A Model for Geometric and Mechanical Adaptation of Arteries to Sustained Hypertension. J Biomech Eng 1998; 120:9-17
48. Rachev, A, N Stergiopulos, JJ Meister. Theoretical Study of Dynamics of Arterial Wall Remodeling in Response to Changes in Blood Pressure. J Biomech 1996; 29:635-642
49. Rhee, K, J Tarbell. A Study of the Wall Shear Rate Distribution Near the End-to-End Anastomosis of a Rigid Graft and a Compliant Artery. J Biomech 1994; 27:329-338
50. Rieu, R, R Pelissier. In Vitro Study of Physiological Type Flow in a Bifurcated Vascular Prosthesis. J Biomech 1991; 24:923-933
51. Rodgers, VGJ, MF Teodori, HS Borovetz. Experimental Determination of Mechanical Shear Stress About an Anastomotic Junction. J Biomech 1987; 20:795-803
52. Rogers, C, E Edelman. Endovascular Stent Design Dictates Experimental Restenosis and Thrombosis. Circulation 1995; 91: 2995-3001
53. Sauvage, LR, MW Walker, K Berger, et al. Current Arterial Prostheses: Experimemtal Evaluation by Implantation in the Carotid and Circumflex Coronary Arteries of the Dog. Arc Surg, 1979; 114:687-691
54. Schrader, SC, R Beyar. Evaluation of the Compressive Mechanical Properties of Endoluminal Metal Stents. Cath Cardvsc Diag 1998; 44:179-187
55. Seifert, KB, D Albo, Jr, H Knowlton, DJ Lyman. Effect of Elasticity of Prosthetic Wall on Patency of Small Diameter Arterial Prostheses. Surg Forum 1979; 30:206-208
56. Staalsen, NH, M Ulrich, WY Kim, et al. In Vivo Analysis and Three-Dimensional Visualization of Blood Flow Patterns at Vascular End-to-End Anastomoses. Eur J Vasc Surg 1995; 10:168-181
57. Stewart, SFC, DJ Lyman. Efects of Vascular Graft/Natural Artery Compliance Mismatch on Pulsatile Flow. J Biomech 1992; 25:297-310
58. Taber, LA. Biomechanics of Growth, Remodeling, and Morphogenesis. Appl Mech Rev 1995; 48:487-545
59. Trubel, W, H Schima, A Moritz, et al. Compliance Mismatch and Formation of Distal Anastomatic Intimal Hyperplasia in Externally

Stiffened and Lume-Adapted Venous Grafts. Eur J Vasc Endv Surg 1995; 10:415-423

60. Vaishnav, RN, J Vossoughi. Estimation of Residual Strain in Aortic Segments. In: Hall, CW (Editor). **Biomedical Engineering II, Recent Developments**, Pergamon Press, 1983, 330-333
61. Vaishnav, RN, J Vossoughi. Residual Stress and Strain in Aortic Segments. J Biomech 1987; 20:235-239
62. Vaishnav, RN, J Vossoughi, DJ Patel, et al. Effect of Hypertension on Elasticity and Geometry of Aortic Tissue from Dogs. ASME J Biomech Engr 1990; 112:70-74
63. Veith , FJ, ML Marin. The Present Status of Endoluminal Stented Grafts for the Treatment of Aneurysms, Traumatic Injuries, and Arterial Occlusions. Card Surg 1996; 4:3-7
64. Walden, R, GJ L'Italien, J Megerman, WM Abbott. Matched Elastic Properties and Successful Arterial Grafting. Archs Surg 1980; 115: 1166-1169
65. Wang, LC, GX Guo, R Tu, NHC Hwang. Graft Compliance and Anastomotic Flow Patterns. Trans ASAIO 1990; 36:90-94
66. White, R, L Goldberg, F Hirose, et al. Effect of Healing on Small Internal Diameter Arterial Graft Compliance. Biomat Med Dev Artif Organs, 1983; 11:21-29
67. Xu, XY, MW Collins. Fluid Dynamics in Stents. In: Sigwart, U (Editor) **Endovascular Stenting**. WB Saunders Company, Ltd, London, 1996
68. Zdrahala, RJ. Small Caliber Vascular Grafts. Part I: State of the Art. J Biomat Appl 1996; 10:309-329

Chapter 5

BIOMECHANICAL AND BIOCHEMICAL PATHS TO DYSTROPHIC MINERALIZATION OF STENTED CARDIOVASCULAR TISSUES

Jeffrey A White, MS, Robert E Baier, PhD, PE, Anne E Meyer, PhD, Redmond P Burke, MD, Ernest M Hausmann, DMD, PhD

A cursory review of the U.S. Patent literature for the 6-month period preceding the Stent Graft Update Workshop [54] that generated this report, revealed 93 just-issued patents on stents, endoluminal grafts, and intraluminal grafts [53]. The pace of technology is rapid, indeed, in this aggressive interventional technique, but the basic biophysical factors underlying structure and function of the stented devices—especially in their tissue contact relationships—have not been adequately revealed to judge them both safe and effective. It is emblematic that, just 3 days after the Workshop closed, the Food and Drug Administration issued a postmarket safety notification about a "premounted stent system" having caused a patient death, 26 related patient injuries, and was undergoing a total market withdrawal by the manufacturer [28].

Keywords: *Mineralization, accelerated testing, valves, pericardium, calcium, phosphorus, bioprosthetics, grafts*

Robert E Baier, PhD, PE (corresponding author), NSF Industry/ University Cooperative Research Center for Biosurfaces, State University of New York at Buffalo, 110 Parker Hall, Buffalo, NY, 14214-3007
Stent Graft Update, Edited by J Vossoughi, N Kipshidze, JW Karanian

Although the stents and stent grafts most widely considered are for patients with symptomatic ischemic disease and/or aneurysmal lesions in cardiovascular sites, there is a growing use of stents in other locations as well, notably to prevent stroke or, more generally, "brain attacks." There are now over 700,000 such brain attacks per year in the US, with 200,000 deaths, one-quarter of which are aneurysm-related rather than directly thromboembolic. These cases, too, are being considered for stenting with device/material combinations having received only a minimum of attention from the "biocompatibility" perspective. Stenting of carotid arteries to forestall the embolic causes of brain attack is also advancing rapidly, again without broad consideration of the risk factors for subsequent closure due to mineralization and embrittlement. Stented tissue, already injured, may present similar qualities to those which promote mineralization in stented zones of glutaraldehyde-tanned bioprosthetic heart valve tissues. What are the prerequisites for this process? Lipid uptake, pulsatility, compliance mismatch, and biomaterials selection may all contribute. Having already noted and reported dystrophic calcification in the original bovine heterografts [6], resistance to that process in glutaraldehyde-preserved neonatal vessel grafts [2, 5, 8], the criticality of compliance matching when vascular surface properties are compromised [23, 32], the investment of mesh tubes with scar tissues that can display different surface properties [3], the catastrophic mineralization from blood that occurs on pulsing elastomers [40], and the selective triggering of mineralization that can occur with materials that differentially denature fibrinogen [51], we examined the process and identity [11] of mineralization occurring in accelerated dynamic tests of stented (heart valve) bioprosthetic tissues.

Calcium-containing minerals are found in a number of different compositions and crystalline phases in nature. The mature phase of naturally occurring calcium-phosphate mineral in the human body is calcium hydroxyapatite -- $Ca_{10}[PO_4]_6[OH]_2$. The formation of calcium hydroxyapatite is necessary in the maturation of bones and teeth.

Mineralization of soft tissue and prosthetic implants has been noted in or around a number of implants, including total hip arthroplasties, vascular grafts, ventricular assist devices, and intrauterine devices and contact lenses [43]. The deposition of calcium-containing apatite mineral seen in association with cardiovascular implants and biomaterials is a leading cause of failure of contemporary bioprosthetic heart valves, polymeric heart valves, and experimental mechanical blood pumps [41].

The accumulation of pathologic calcium-phosphate mineral deposits on cardiovascular implants is a relatively common phenomenon in both biological implants treated with cross-linking agents such as glutaraldehyde, and in necrotic, injured or altered tissue. Thus, it is probable that there are valuable lessons to be learned from the behavior of glutaraldehyde-preserved stent-mounted aortic valve bioprostheses, as implanted in several hundred thousand patients since 1971, that frequently failed with tears or stiffening resulting from calcification. Clinically important calcification of glutaraldehyde-preserved porcine valves implanted in adults generally becomes important after 4-5 years of function; the failure rate as a result of primary tissue degeneration is approximately 20-25% at 7-10 years postoperatively [41]. Mineralization *in vivo* occurs intrinsic and extrinsic to the surfaces of the bioprosthetic tissues and contributes to the ultimate degradation and tissue failure of implants. Most often, calcific deposits in bioprosthetic valves predominate at the cuspal commissures and basal attachments, which have been identified as the sites of greatest dynamic mechanical activity [43] (Figure 1). Two different mechanisms may be involved: stress of the injured (tanned) tissue exceeding some critical limit [18, 48], adjacent to the stent, or lipid expression from tissue disintegration at the flailing edges.

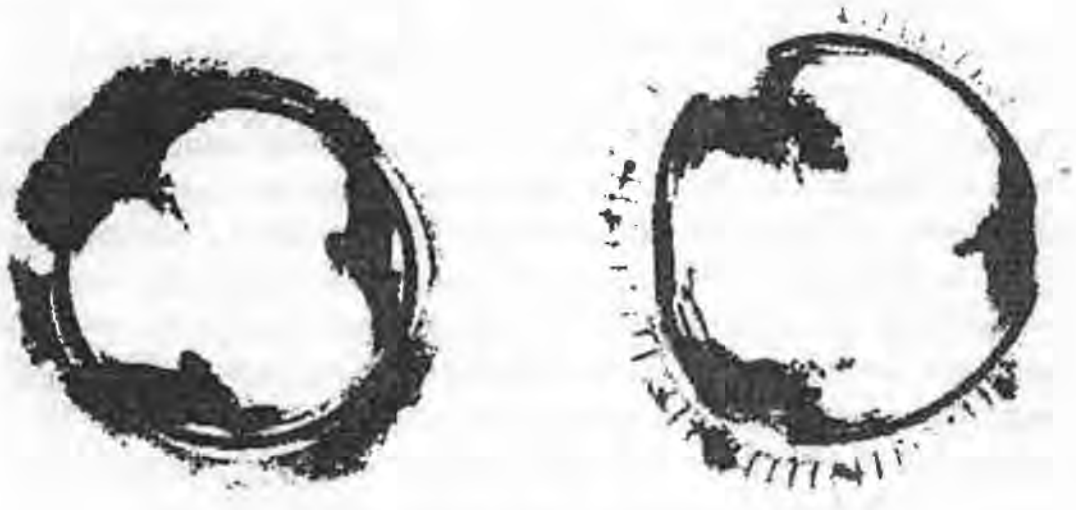

FIGURE 1

X-ray negative of two valves demonstrating localization of mineral deposits around the cuspal commissures and basal attachments

Since the advent of implantable heart valve prostheses in the 1950's, many techniques have been developed to assess and prevent dystrophic calcium-phosphate mineral deposits upon glutaraldehyde-fixed bioprosthetic tissues. Techniques used to assess calcified mineral formed in or on bioprosthetic heart valves and biomaterials *in vivo* include clinical evaluation of recovered replacement valves from adult operative survivors [42], autopsy after cardiac valve replacement [47], subcutaneous implantation of glutaraldehyde-preserved porcine aortic valve leaflets in rats [30], and orthotopic valve replacements in calves [46]. Numerous static [9, 10, 16, 25, 27, 35] and dynamic [12, 18, 34] *in vitro* mineralization methods also have been used to study the mineralization process. Strategies to prevent mineral deposits on bioprosthetic tissue include local controlled-release of diphosphonate [31], Ca++ diphosphonate pretreatment [26], Al+++ preincubation [55], and treatment with anticoagulant warfarin-sodium [40]. Nevertheless, there still is a general lack of understanding of the localization and growth of calcium-phosphate minerals upon a wide range of biomaterials and bioprosthetic implants.

Current data on mineralization of glutaraldehyde-fixed bioprosthetic tissues have been obtained mainly after autopsy or after extensive animal testing. Unfortunately, these studies are difficult, expensive, time-consuming, and necessitate loss of life. Still, these experiments have been instrumental in predicting the relative resistance or vulnerability of various implants to mineralization. *In vitro* mineralization studies thus far have been moderately successful in producing calcified mineral deposits on glutaraldehyde-fixed bioprosthetic tissues in significant quantities and have partially reproduced clinically relevant mineralization patterns [12, 34]. Improved *in vitro* models to mimic and accelerate *in vivo* mineralization are required. This investigation evaluated the efficacies of more aggressive *in vitro* approaches to elucidate the process of biological mineralization in vessel grafts and bioprosthetic valves; the goal of these techniques is to predict the potential for and the pattern of mineralization on dynamically tested glutaraldehyde-fixed bioprosthetic tissues.

MATERIALS

The three bioprosthetic materials employed in this investigation were (1) glutaraldehyde-fixed bovine pericardium, (2) Hancock porcine bioprosthetic heart valves, and (3) glutaraldehyde-fixed human umbilical cord

vein grafts. The samples were given experimental designations for convenience and are summarized below.

Eight glutaraldehyde-fixed bovine pericardium samples were cut from two randomly selected 4" by 4" sheets (supplied by BioVascular Inc, St Paul, MN) and stored in phosphate-buffered saline with 1% benzyl alcohol. Four of the eight samples, measuring 2" by 2," were tested under dynamic/flexing conditions, each with a control measuring 0.25" by 0.75", simultaneously tested in the same calcification solution under static/unflexed conditions. The dynamic/flexed specimens were labeled HSVT1D, HSVT2D, HSVT3D, and HSVT4D. The static/unflexed specimens were labelled HSVT1S, HSVT2S, HSVT3S, and HSVT4S, respectively. Each dynamic sample was tested with its static counterpart sample under accelerated conditions in the same high speed valve tester (manufactured by Columbia Laboratories, Buffalo, NY).

Two Hancock porcine bioprosthetic heart valves (supplied by Medtronic, Inc, Irvine, CA), measuring 21mm and 25mm in diameter, were selected at random from a group of four valves stored in 2.5% glutaraldehyde. The 21mm valve was arbitrarily selected as the dynamic/flexed specimen and labeled HV01. The 25mm valve was selected as the static/unflexed specimen and labeled HV02. The dynamic valve was tested simultaneously alongside its static counterpart valve under mock physiologic conditions in the same pulse duplicator (manufactured by Columbia Laboratories, Buffalo, NY).

One glutaraldehyde-preserved umbilical cord vein graft sample was selected at random from a group of three grafts stored in 50% ethyl alcohol (Dardik Biograft, supplied by Meadox Medicals, Inc, Oakland, NJ). The eight inch long graft was cut into a 7 inch segment and 1 inch segment, each having the same inner diameter of 4mm. The long segment was selected as the dynamic/flexed specimen and labeled B1D, and the short segment was selected as the static/unflexed specimen and labeled B1S. The dynamic sample was tested simultaneously alongside its static counterpart sample under accelerated conditions in a previously described pulsatile flow system [7].

The experimental solution used in this study was chemically engineered to be supersaturated with respect to calcium and phosphate and was selected for its peculiar property of being on the "edge" of precipitation.

The solution was used with each sample and in every testing modality and was shown to remain stable (precipitate free) throughout all experiments. The relative saturation of hydroxyapatite and Gibbs' Free Energy for the solution were calculated at 31.3 and –8.96 KJ/mol, respectively [36]. The relative concentrations of ions in this solution are shown in Table 1.

TABLE 1

Concentration of Ions in Test Solution

	(mM)
Ca^{2+}	4.0
PO_4^{3-}	2.4
Na^{+}	145.0
OH^{-}	19.9

The three testing apparatuses employed in this investigation, (1) a high speed valve tester, (2) pulse duplicator, and (3) pulsatile flow system, were selected for different purposes.

A high speed valve tester (HSVT) is commonly used to evaluate the fatigue resistance of prosthetic heart valves at accelerated cycling rates. In this investigation, the HSVT was used to test the mineralization potential of glutaraldehyde-fixed bovine pericardium samples at various cycling rates up to 16 Hz. The HSVT comprises a direct current (DC) engine with a maximum output of 20 Hz. The engine drives a rigid polymeric lever arm connected to a flexible polymeric diaphragm. The diaphragm oscillates back and forth producing an alternating flow causing the tissue to be flexed back and forth with each cycle. The main chambers of the HSVT are constructed from machined polymethylmethacrylate (PMMA) held together by stainless steel screws. Flexible polyvinylchloride (PVC) tubing was used to connect the compliance chamber with the rest of the system (Figure 2).

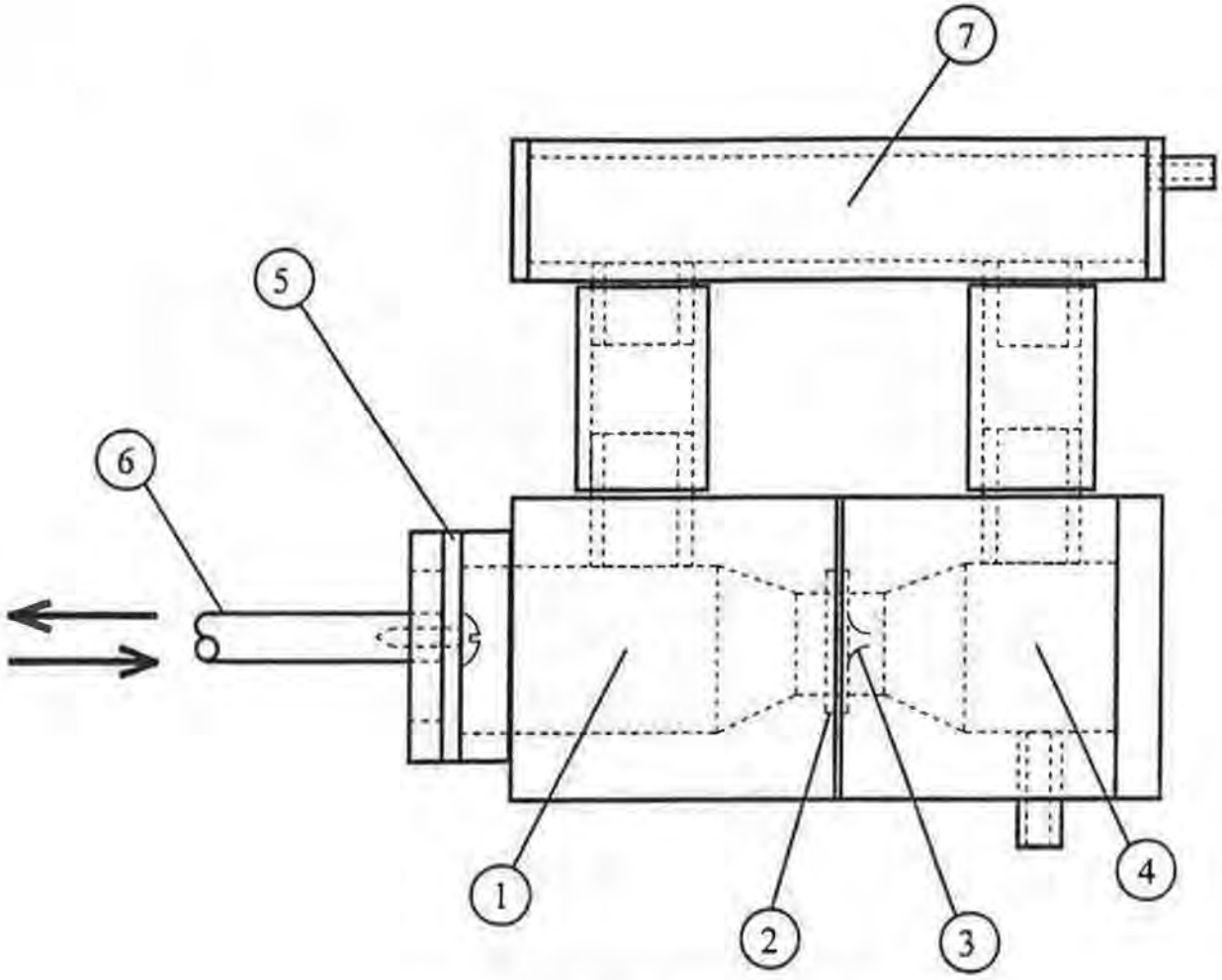

FIGURE 2

Drawing of high speed valve tester and list of parts

1. Flow Entrance Chamber
2. Valve Mount
3. Pericardium Sample
4. Flow Exit Chamber
5. Flexible Diaphragm
6. Drive Shaft
7. Compliance Chamber

A pulse duplicator (PD) is commonly used to test the "safety" and "efficacy" of various prosthetic heart valve designs at physiologic pressures and flows. In this investigation, the PD was used to test the mineralization potential of the porcine bioprosthetic heart valves at simulated physiologic conditions. The PD comprises a 1/40 hp DC variable speed engine connected to a piston which circulates the solution throughout the system. The PD is constructed from silicone-glued PMMA boxes and flexible PVC tubing (Figure 3).

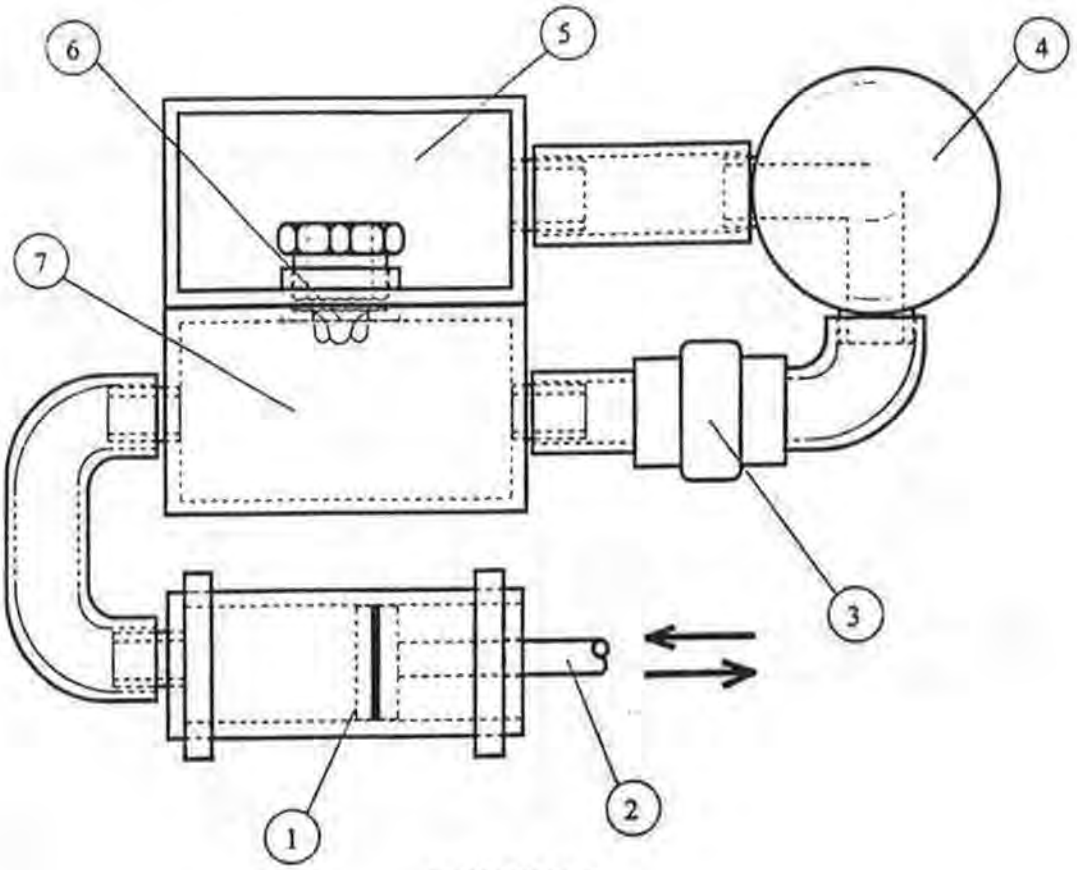

FIGURE 3

Drawing of Pulse Duplicator and List of Parts

1. Piston
2. Drive Shaft
3. One-way Valve
4. Compliance Chamber
5. Flow Entrance Chamber
6. Valve
7. Flow Exit Chamber

A pulsatile flow system (PFS) is commonly used to test the fatigue resistance of intravascular stents and vascular grafts. In this investigation, a pulsatile flow system was used to flex glutaraldehyde-fixed human umbilical cord vein graft samples by way of a propagating pressure pulse in the pumped mineralization solution. The PFS was also used to test the mineralization potential of the human umbilical cord vein graft specimens at an accelerated pulse rate. The system comprises a Masterflex roller occluder pump (Cole Parmer Instrument Co, Vernon Hills, IL) connected in series with a flow chamber containing the umbilical cord vein graft samples. Masterflex silicone tubing was used to connect the pump with the inflow and outflow sections of the chamber.

METHODS

Before each experiment, the high speed valve tester was disassembled and cleaned with 2.5% glutaraldehyde solution. The dynamic test samples, HSVT1D-4D, were further prepared by cutting 1.3 cm perpendicular slits, in a "crosshair" like pattern, at the center of each tissue specimen. No alterations were made to the static/unflexed tissue samples. Referring to Figure 2, before the mineralization solution was added to the tester, the static sample was placed on the bottom of chamber 4 and the dynamic sample was confined between plastic washers at section 2. Chambers 1 and 4 were clamped together by stainless steel screws and 800mL of mineralization solution was added to the tester. Samples were cycled at the rates described in Table 2 for a total of 1 million cycles. (Cycling rates were not selected for any particular reason other than to span the 20 Hz capability of the HSVT.) Static and dynamic samples were checked before and after testing by x-ray photography, multiple-attenuated internal reflection infrared (MAIR-IR) spectroscopy, scanning electron microscopy (SEM), and energy dispersive x-ray (ED Xray) analysis. The temperature of the test solution remained constant at 25 ± 2°C throughout all experiments.

TABLE 2

Cycling Rates for HSVT samples

SAMPLE	CYCLING RATE (HZ)	TIME TO REACH 1 MILLION CYCLES (HOURS:MIN)
HSVT1D	4	69:27
HSVT2D	8	34:43
HSVT3D	12	23:09
HSVT4D	16	17:22

The pulse duplicator also was disassembled and disinfected with 2.5% glutaraldehyde solution before testing of heart valves. During re-assembly, sample HV01 was clamped into the tester at section 6 and sample HV02 was placed at the bottom of chamber 5, as shown in Figure 3. Five liters of mineralization solution were added to the tester, and the motor was adjusted to a speed of 1 Hz and a stroke volume of 50 ml. The

samples were tested for a total of 1 million cycles, corresponding to a run time of 277 hours and 46 minutes. Static and dynamic samples were checked before and after testing by x-ray photography, digital subtraction radiography, scanning electron microscopy, and energy-dispersive x-ray analysis. The following 5 steps were used to perform digital subtraction radiography on the heart valve samples:

1. X-rays were taken with a dental x-ray machine of the valves in solution at baseline and at the end of the experiment.
2. The x-ray tube and heart valve were maintained in an identical position for each pair of x-rays taken at baseline and at the end.
3. Pairs of film images were captured with a CCD camera and the digital images were aligned and subtracted at a resolution of 512 x 480 pixels.
4. Gamma correction was used to reduce the amount of noise created in the subtraction from a mismatch in x-ray developing intensities of the film [33].
5. Specific locations of mineralization, which occurred during the experiment, were false-color-highlighted and these areas superimposed back onto the original x-ray.

The pulsatile flow apparatus was similarly disassembled, cleaned and disinfected with 2.5% glutaraldehyde solution. Sample BID was connected to the inside of the flow chamber, and sample B1S was placed at the bottom of the flow chamber. The tester was filled with mineralization solution, and the pump was adjusted to a flow rate of 200 mL/min with an approximate pulse rate of 200 pulses/min., and an arterial wave form [7]. Samples were cycled for 196 hours and 15 minutes. These grafts typically ultrafilter less than 500 ml of solution per day into an external saline solution under the test conditions used [7]. Static and dynamic samples were checked before and after testing by x-ray photography, scanning electron microscopy, energy-dispersive x-ray analysis, and internal-reflection infrared spectroscopy.

RESULTS

Visual inspection of the bovine pericardial tissue after experimentation revealed the presence of large white patches of deposits on the surfaces of samples HSVT3D and HSVT4D. Collection of this material on sample HSVT3D was primarily located around the rim of the pericardium at the point of fixation to the high speed valve tester as well as at the inner

periphery of the retaining washer (Figure 2, item 2). Close examination of this rim by SEM and EDXray analysis revealed the presence of a calcium-rich ring with calcium-phosphorus-containing mineral growth on top (Figure 4a). Large uniform flat plates of calcium-phosphorus mineral also were discovered between the washer and the pericardium sample of HSVT3D (Figure 4b). Sample HSVT4D mineralized in a similar pattern except that the mineral appeared to occupy a much larger surface area with mineral deposits extended further down toward the center of the sample. SEM and EDXray analysis confirmed the presence of calcium- and phosphorus-containing mineral on the surface of sample HSVT4D as well. No significant amount or localization of calcium or phosphorus was detected on samples HSVT1D and HSVT2D.

The static/unflexed samples of HSVT1-4S also were inspected for mineral deposits. Interestingly, a modest increase in the amount of apparent mineral deposition on the surface was also noticed with an increase in the cycling rate of the high speed valve tester. These mineral deposits were randomly distributed on the surface of the pericardium without any apparent localization. The amounts of mineralization on the surfaces of the static specimens, however, were significantly less than on their dynamically stressed counterparts.

The surface topography, away from any mineral deposits, of samples HSVT1-4D was also compared by SEM, revealing elevated levels of surface damage with increased cycling rates. The higher the cycling rate, the more disordered and elongated the surface structure of the pericardium became. Figure 5 shows electron micrographs of the surfaces of samples HSVT1D and HSVT4D. Sample HSVT1D was cycled at 4 Hz while sample HSVT4D was cycled at 16 Hz.

In order to characterize the type of calcium-phosphorus mineral present on the surface of the samples, SEM and EDXray were carried out on two different forms of hydroxyapatite (HA) controls: human dentin (supplied by Procter & Gamble, Cincinnati, OH) and Macrosorb C Dentin was selected since, as a naturally mineralized collagenous scaffold, it would be instructive to learn whether the mineral deposits detected by SEM and EDXray on the surfaces of the collagenous pericardium specimens are

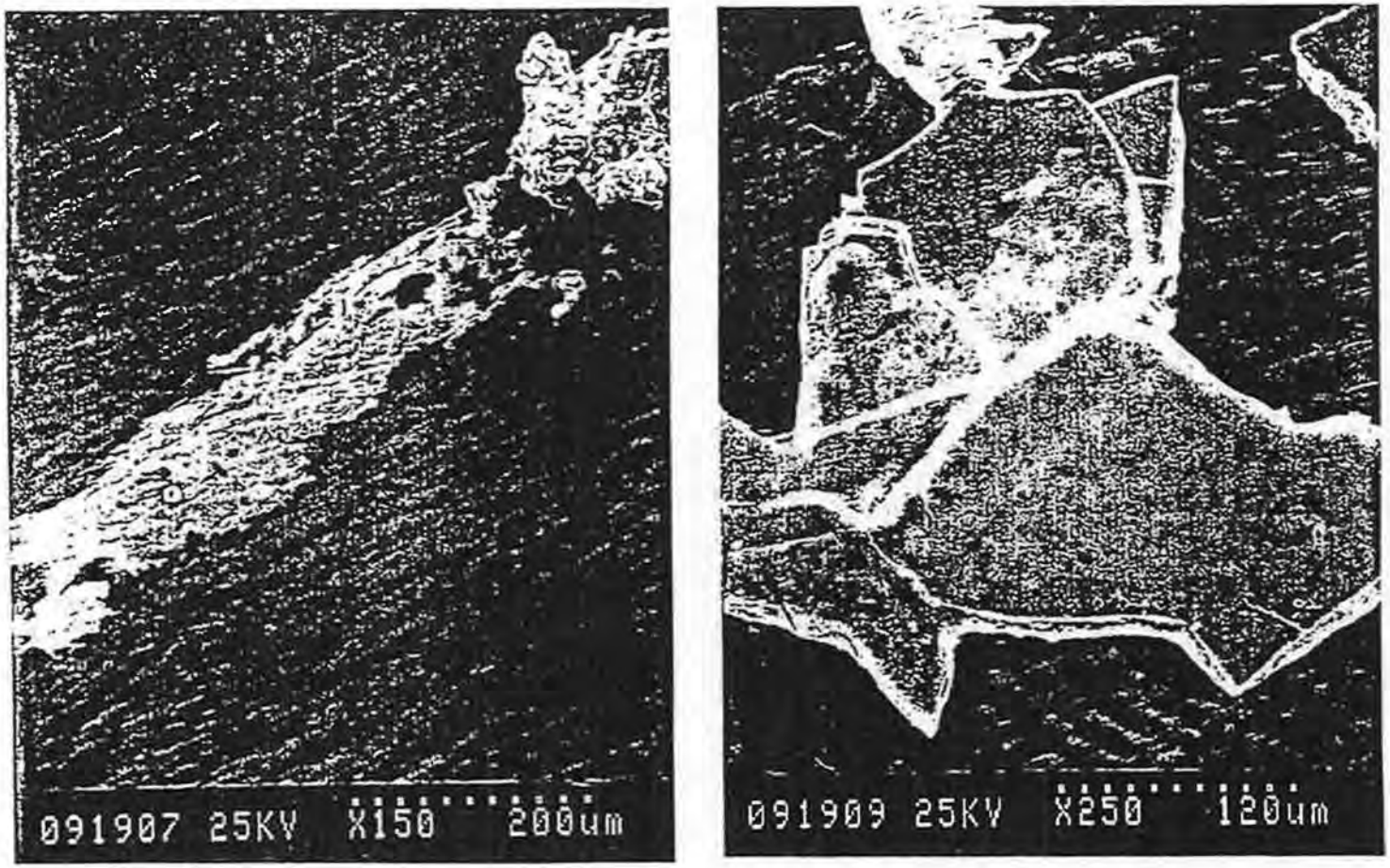

(a) (b)

FIGURE 4: Scanning Electron Micrographs (SEM) of Calcified Sections of Sample HSVT3 showing a) Calcium- and Carbon-Rich Ring with Mineral Growth Directly on Top and b) Flat Plates of Mineral Discovered Between the Washer and the Tissue

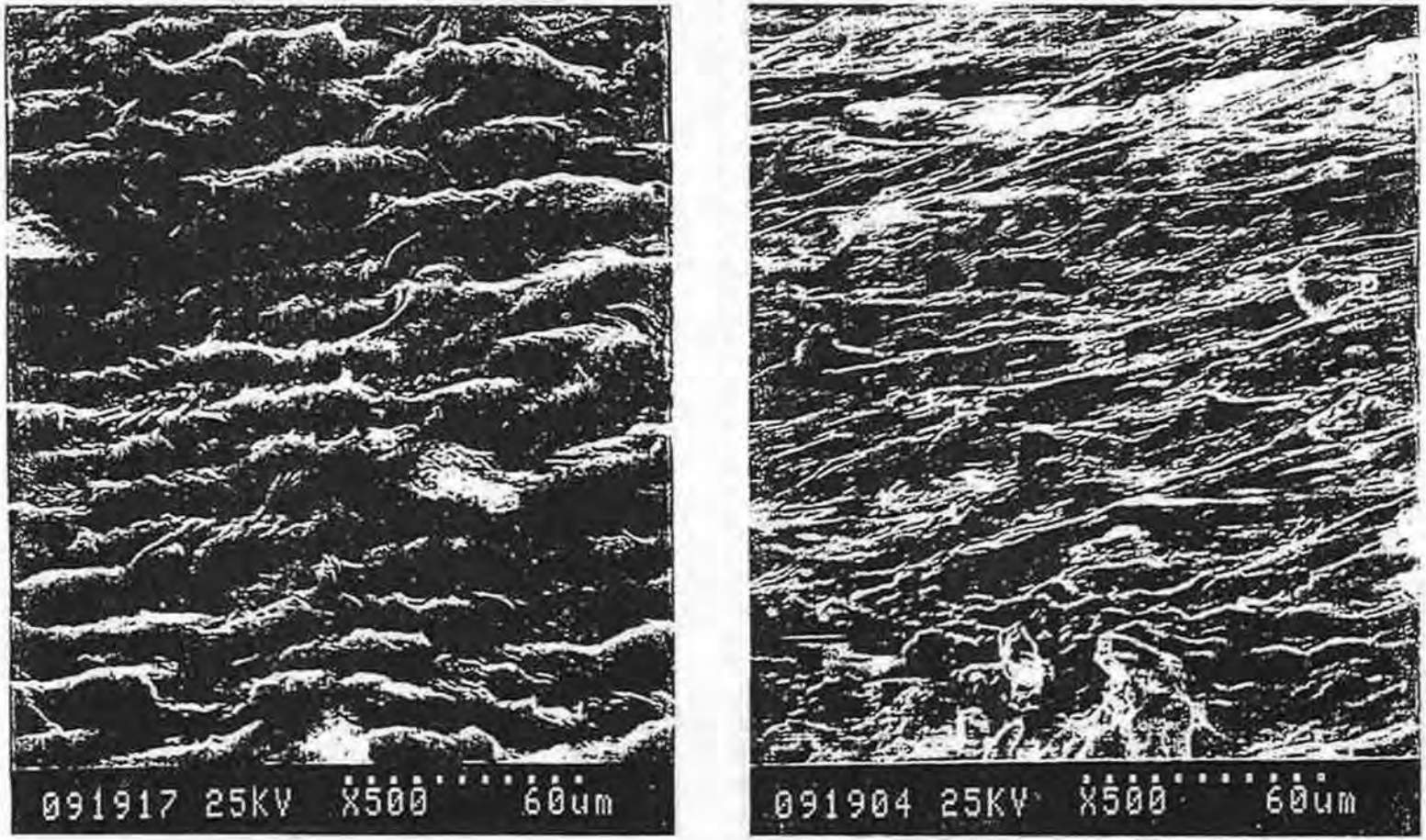

(a) (b)

FIGURE 5: SEM of Surfaces of Samples a) HSVT1D and b) HSVT4D showing damage to surfaces with increased cycling rate

comparable to naturally occurring defect HA (carbonated) mineral of teeth and bone [29]. Figure 6 presents SEM photomicrographs comparing the morphology of the dentin control with the mineral found on sample HSVT4D. Figure 7 shows the corresponding EDXray information. Notice the visual similarity between the mineral deposits formed during accelerated tests *in-vitro* and the dentin control. Further physical-chemical characterization, however, showed this dystrophic mineral to be more similar to octacalcium phosphate than hydroxyapatite[11].

The static and dynamic samples of HSVT1-4 also were checked using MAIR-IR spectroscopy to determine their superficial chemical compositions. Results from IR spectroscopy showed an increase in hydrocarbon and fatty-ester expression at the surfaces of the dynamic samples with increases in cycling rate. Figure 8 shows the IR results for the pericardium control and samples HSVT1D and HSVT4D. Note the increase in absorption band intensity at the wavenumbers 2800-3000 (hydrocarbons) and 1700-1800 (ester) with increasing sample number (increased cycling rate).

Energy-dispersive x-ray mapping of a cross-section of sample HSVT4D demonstrated a build up of calcium- and phosphorus-rich substance external to the original pericardial tissue. The absence of a dense accumulation of calcium and phosphorus within the tissue suggests the presence of an intermediate nucleating substance, possibly exuded at the surface of the tissue. Figure 9 contains an x-ray map taken at a cross section of sample HSVT4D near the mineralized rim. The calcium is highlighted in section A, and the phosphorus is shown in section B. The original boundary of the tissue specimen also is highlighted a contrasting shade, while white lines mark the final boundary of the sample.

The results from the bovine pericardium experiments suggest that, since both calcium- and phosphorus-based mineralization and obvious tissue damage are directly related to the cycling rate, some damage-induced process, structure, or chemical triggers calcium deposition. Mineral deposits were most abundant, but not entirely localized, at the region of maximum restraint of the tissue, specifically where the tissue was clamped into the high speed valve tester and at the marginal regions of tissue breakdown. The results from the IR analyses, in particular, suggest that there is a surface chemistry dependence for mineralization

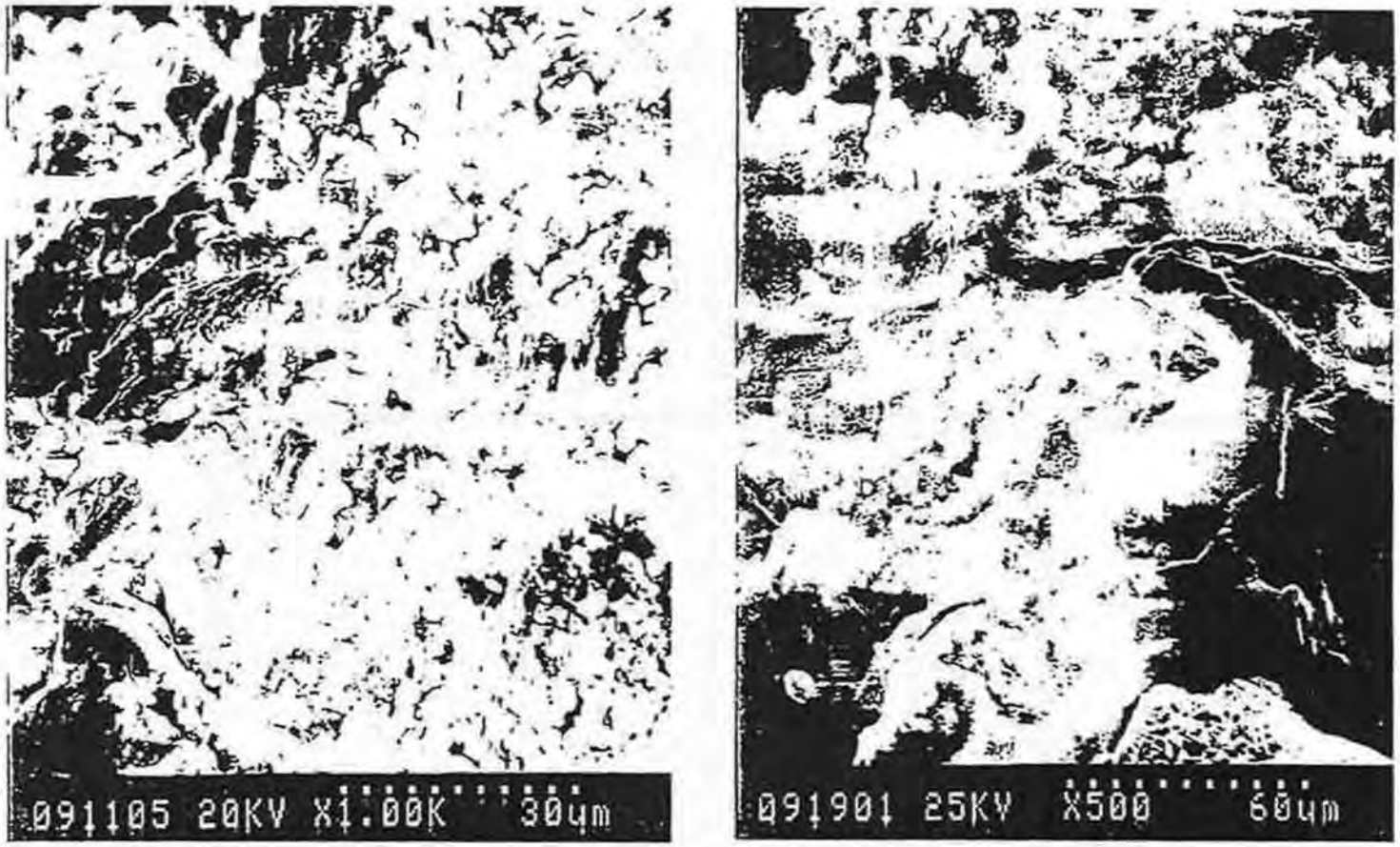

(a) (b)

FIGURE 6

SEM of a) Dentin Control, and b) Mineral Found on Surface of Sample HSVT4D

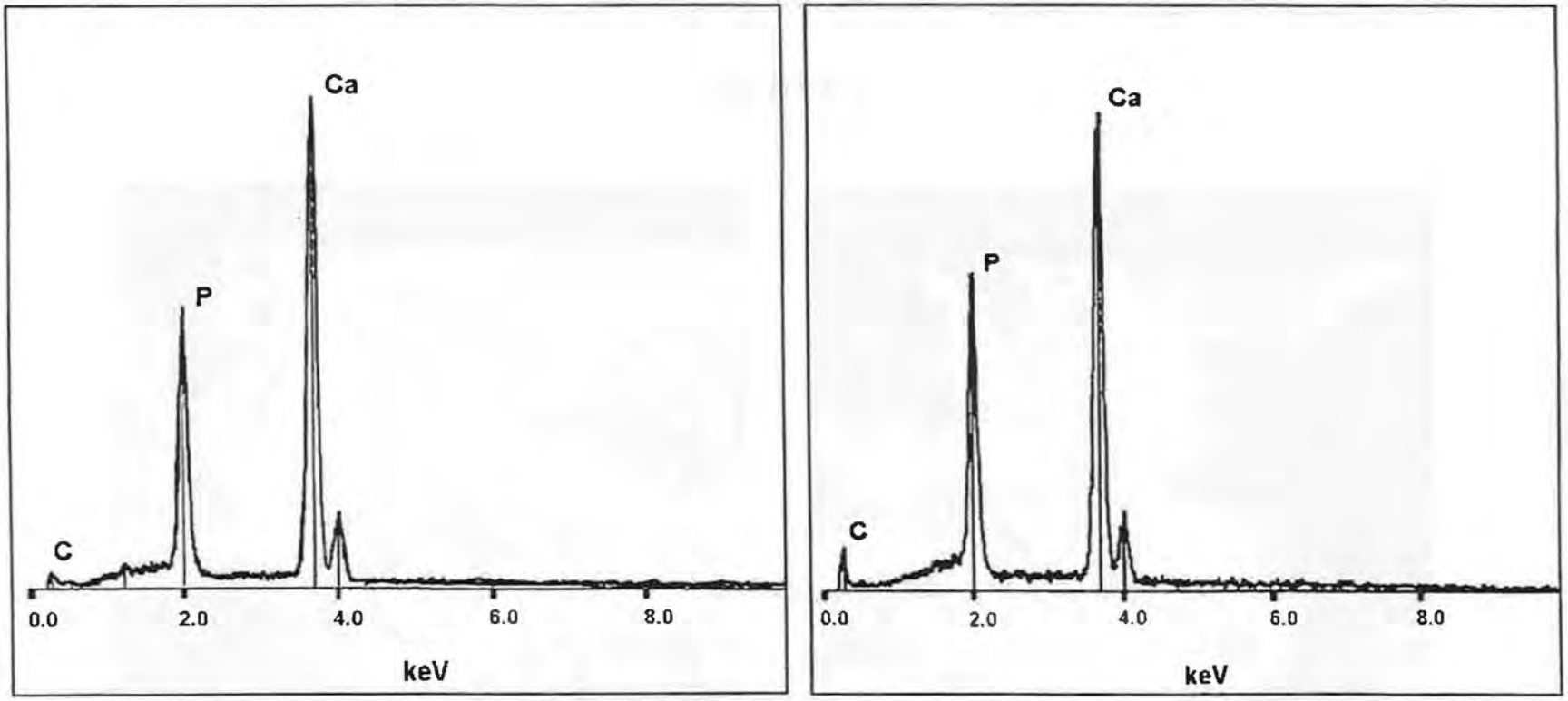

(a) (b)

FIGURE 7

Corresponding Energy-Dispersive X-ray Spectra for a) Dentin Control, and b) Mineral Found on Surface of Sample HSVT4D

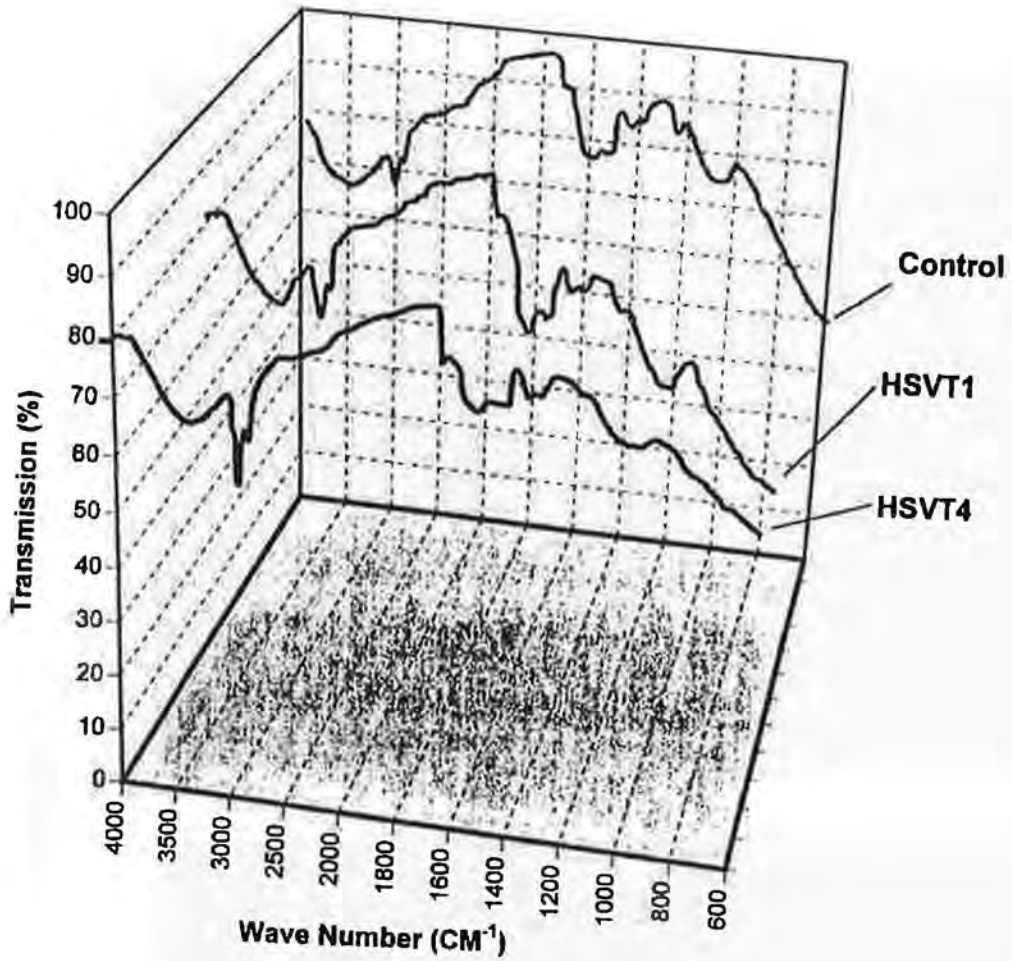

FIGURE 8

Multiple-Attenuated-Internal-Reflection Infrared Spectra of Pericardium Control and Samples HSVT1D and HSVT4D Showing Increased Expression of Hydrocarbons and Fatty-Esters at the Surfaces with Increased Cycling Rate

with the preference for localization of mineral to fatty-esters expressed at the surface of the pericardium. An increase in fatty-ester expression at the surface of the pericardium probably results from breakdown of remnant cell membranes, but could possibly be related to fibril rearrangement or other cellular damage from mechanical strain or stress on the tissue.

Digital subtraction radiography (DSR) [33] of the mineralization-solution-exposed, static/unflexed Hancock porcine bioprosthetic heart

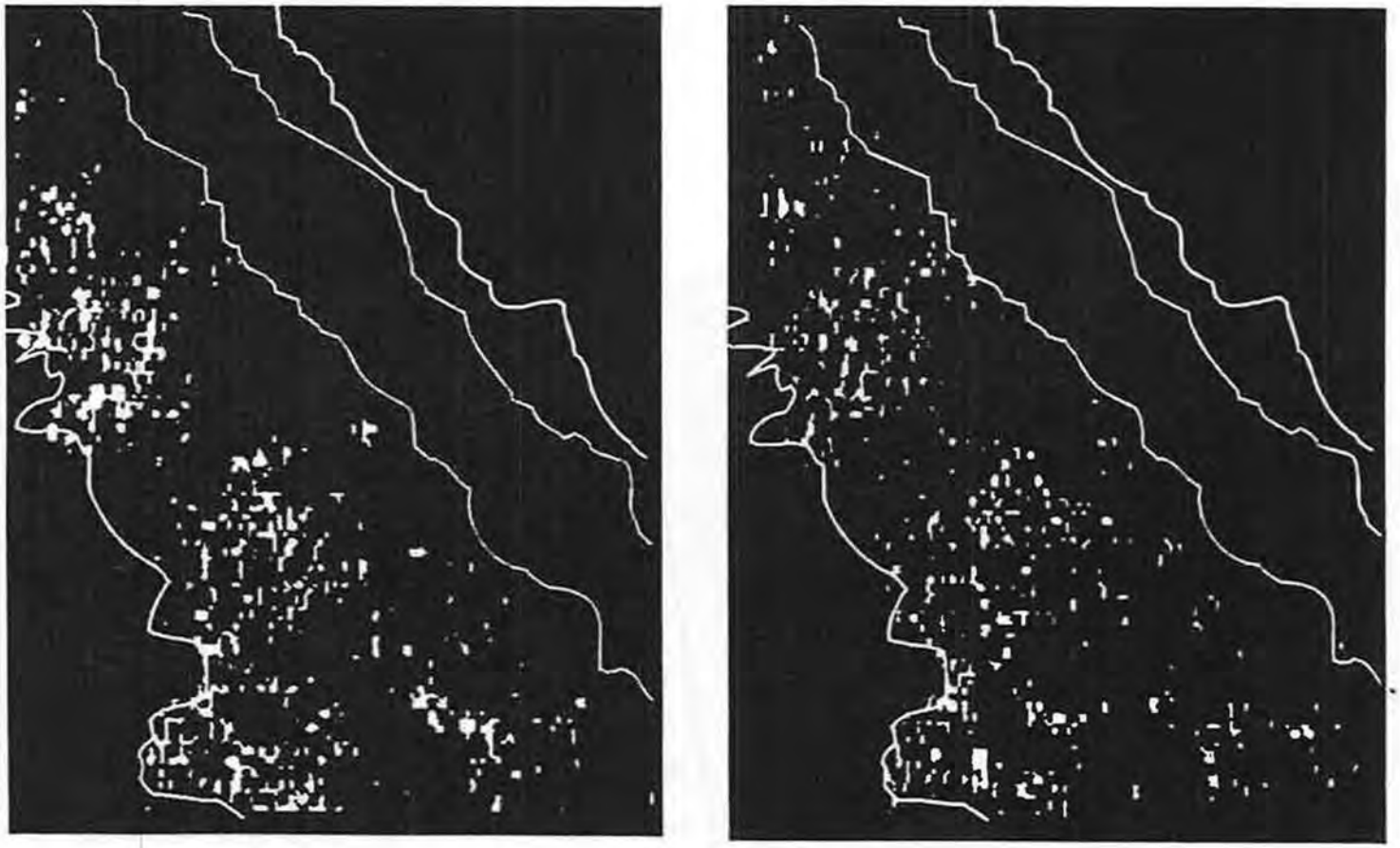

(a) (b)

FIGURE 9

X-ray map of magnified cross section of sample HSVT4D a) showing calcium b) showing phosphorus (interior lines mark original boundaries of tissue/ exterior lines mark final boundaries of specimen)

valve HV02 showed an apparently random and nonlocalized change in intrinsic density. Its dynamic counterpart HV01, however, showed a nonrandom and highly localized change in intrinsic density. Figure 10 shows the DSR results superimposed back on the original valve x-rays for samples HV01 and HV02. The change in intrinsic density of sample HV01 is located primarily around the cuspal commissures and basal attachment of the heart valve. The change in intrinsic density of the sample, attributed to calcium-phosphorus mineralization, is confirmed by SEM and EDXray analysis. The ratio of Ca/P of the mineral detected on the surface of sample HV01 by EDXray was found to be much smaller than that of the other samples including the hydroxyapatite controls. This is, possibly, the result of an amorphous precursor phase of dystrophic mineralization [36]. Table 3 summarizes these results. Note that these peak ratios are not to be taken as ratios of elemental abundance, since they have not been calibrated for electron capture "cross section" and x-ray efficiencies of the various elements.

X-ray photography of the human umbilical cord vein graft sample B1D showed an increase in intrinsic density at the central portion of the vessel after experimentation. The exit and entrance regions of the graft appeared

TABLE 3

Ratios of Calcium to Phosphorus detected in the mineral deposits of each sample

SAMPLE	Ca/P
Dentin	1.7
Macrosorb C	1.7
HSVT3	1.5
HSVT4	1.8
HV01	0.2

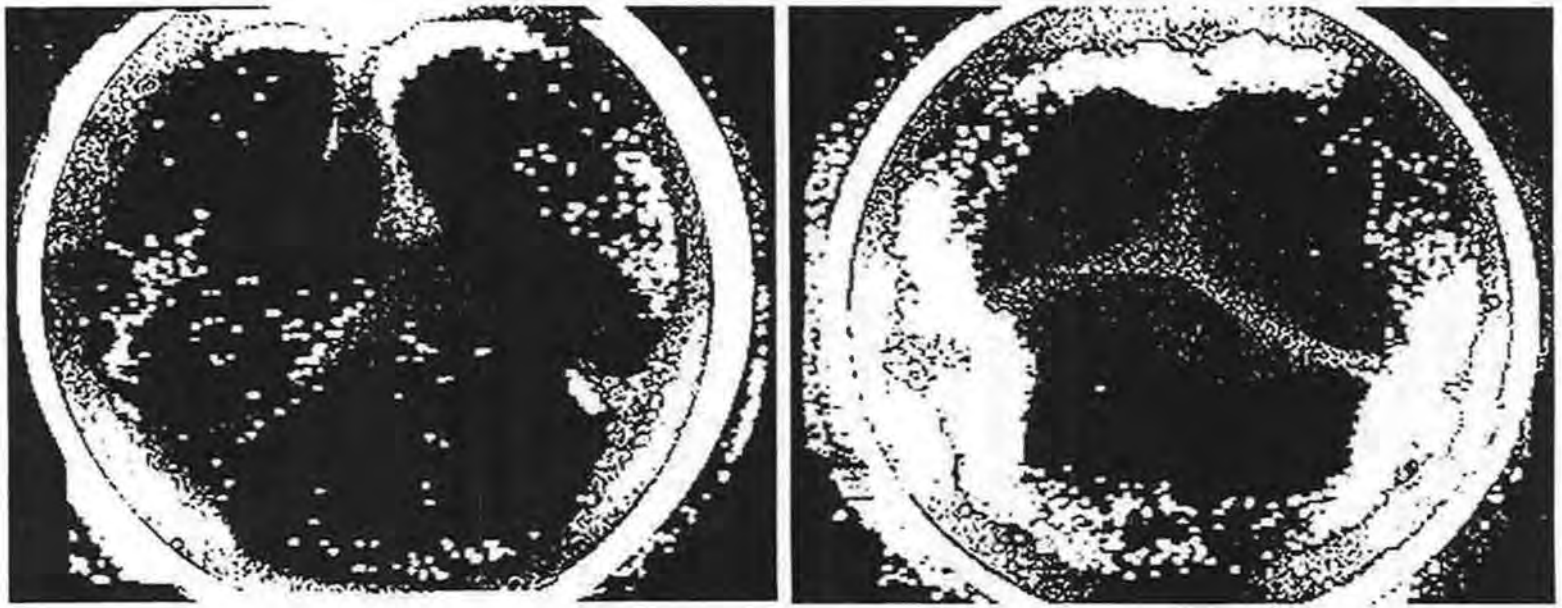

(a) (b)

FIGURE 10

Digital Subtraction Radiographs of a) static/unflexed heart valve, and b) dynamic/flexed heart valve with the subtraction image superimposed back onto the original x-ray of the valve

to be unchanged. Its static counterpart, sample B1S, showed no significant change in intrinsic density throughout the entire experiment. The SEM and EDXray information for sample B1 showed no indication of calcium or phosphorus on the inner surface or within the vein graft wall. Instead, the analyses indicated contamination by matter rich in silicon. The IR spectroscopy results showed that the silicon was associated with silicone rubber contamination from roller-pump-generated wear debris from the Masterflex silicone tubing used in the experimental apparatus [13, 22, 38, 39].

DISCUSSION

In vitro mineralization studies involving mechanically flexed glutaraldehyde-fixed bioprosthetic tissue subjected to flow have been frequent and numerous. Several noteworthy attempts also have been made to simulate the mineralization potential and composition of blood in order to study the formation of calcium-phosphate deposits on and within biologically relevant substrata [19, 24, 35, 50]. These studies have uncovered vital information on the effects of concentration, pH, temperature, and time on the mineralization process. Unfortunately, questions about the relationships between the mineralization process and the physical-chemical and engineering features remain, *eg* fluid dynamics, mechanical deformation, mechanical stress, and surface chemistry.

In vivo mineralization of glutaraldehyde-fixed bioprosthetic tissue and polymeric implants occurs most frequently at regions of maximum mechanical deformation [17, 40, 42, 43] and has been suggested to be favored at hemodynamic stress points [14, 21]. The formation of mineral on glutaraldehyde-fixed bioprosthetic implants in the cardiovascular system is a dynamic process which is most likely dependent on a number of yet-to-be elucidated complex biological interactions as well as being dependent on a number of more conventional chemical and mechanical properties. Even though the complex biological interactions of the human body cannot yet be duplicated, a suitable *in vitro* model is necessary for attaining a better understanding of mineralization and possibly predicting the localization of calcium-phosphate minerals on bioprosthetic implants and in stented vessels.

During this investigation, the mineralization potential of glutaraldehyde-fixed bioprosthetic tissue was examined under physiologic pressures, physiologic flows, and under accelerated flexing rates *in vitro*. Rather than attempting to simulate the exact chemical environment found in the human cardiovascular system, the mineralizing solution used in this investigation was deliberately and significantly increased in calcium and phosphate concentrations. The mineralizing solution was supersaturated with respect to calcium and phosphate (approximately 3 times that of blood) and was chosen to be on the "edge" of precipitation in order to promote the formation of mineral deposits in relatively "short" periods of time. It was successful in this regard, mineralizing the bovine pericardium in 17 hours (accelerated testing) and porcine heart valve leaflets in 9 days of investigation (pulse duplication), replicating the patterns of dystrophic mineralization seen clinically only after years of service.

The results from SEM, EDXray analysis, and MAIR-IR spectroscopy of the pericardium samples are worth summarizing again, together with the conclusions they suggest. Deposits were detected visually on the surfaces of the pericardium samples -- all pulsed to 1,000,000 cycles-- after 17 to 69 hours of investigation, with amounts directly depending on the cycling rate of the high speed valve tester. This suggests a rate-dependent and progressive chemical and/or mechanical change in tissue characteristics pre-disposing to nucleation of calcific deposits. The results from SEM and EDXray analysis of specimens, taken from the high speed valve tester, confirm that the increase in cycling rate led to an increase in the amount of mineral deposited on the surface of pericardium. They further suggest the increase in mineral seen on the surface of the samples is associated with breakdown and rearrangement of damaged pericardial surface fibers as observed (after high cycling rate) in the SEM. The nonlocalized increase in mineral deposits with increased solution cycling rate, observed on both the dynamic and static pericardium samples, suggests the release of some "tissue factor" into the solution, even though the dynamic samples were considerably more mineralized than their static counterparts. Heavy mineral deposits, absent from the free specimens in the solutions, were detected on the surface of the flexed pericardium mainly localized around the edge of the tissue where it was clamped (stented) into the HSVT. The localization of mineral on the tissue at this region suggests an increased mineralization potential for the restrained, or stented, areas of the samples. These mineral deposits, composed mostly of calcium and phosphorus in ratios approaching those of dentin and Macrosorb C controls (by EDXray analysis) seem to form

by paths similar to those known for eventual HA development [36]. The results from MAIR-IR showed an increased expression of hydrocarbons and fatty-esters at the surface of the flexed pericardium with an increased cycling rate of the high speed valve tester. No hydrocarbons or fatty-esters were detected on the surfaces of the high speed valve tester itself. It is possible that by increasing the cycling rate of the high speed valve tester, the collagen fibril structure may have become rearranged, creating void spaces, and possibly damaging the connective tissue cells, causing them to rupture and exude hydrocarbons and fatty-esters, especially from damaged membranes. The increase in calcium-binding sites provided by released membrane components at the surface of the pericardium may be the nidus for both nucleation and localization of mineral. Close examination of the ring-like mineral-deposit structure (the region of maximum restraint and bending of the tissue) discovered on sample HSVT3 by EDXray analysis showed that it was dominated throughout by calcium-rich substance. Calcium-phosphate mineral deposits were distributed unevenly along the surface of this ring. It has been suggested that the deposition of a calcium carbonate-like mineral may precede the formation of a more stable amorphous and then crystalline calcium-phosphate compound on the surface of orthopedic and dental implants [4]. This hypothesis is under test in current studies.

The results from SEM, EDXray analysis, x-ray photography, and MAIR-IR spectroscopy of the human umbilical cord vein graft samples are equally interesting, as summarized below. X-ray photographs of the dynamic sample B1 after 196 hours and 15 minutes (or approximately 2,300 liters of solution passage) showed an increase in intrinsic density around the central portion of the graft. There was no obvious change in the x-rays of the static control, subjected to uncirculated volumes of the same solution for the same amount of time. SEM and EDXray analysis of the central portion of the pump-driven graft showed that the surface was completely covered by a layer of silicon-rich material, apparently wear debris from the silicone tubing used in the experiment. No calcium was detected on the surface of the sample or throughout the cross section. The source of the silicon contamination at the central portion of sample B1 was confirmed by MAIR-IR. Silicone was detected on the surface of the sample with an absorption band at 1050 cm^{-1} indicating the presence of covalently bound Si-O, but little silicon-bound methyl CH_3 was detected (its absorption bands are typically located at 1260 cm^{-1} and 2980 cm^{-1}). In spite of the probable silicone-rubber particle contamination at the

surface of the graft --a condition predisposing to calcium phosphate nucleation [22] -- the glutaraldehyde-preserved umbilical cord vein graft did not show calcification, even under the accelerated, supersaturated conditions employed in these studies. The relative freedom of the vein graft from lipids, a quality control factor at the point of manufacture [1, 7], and its freedom from stenting-induced constraint during its pulsatile testing, are the probable reasons for this extraordinary resistance to dystrophic calcification.

The results from SEM, EDXray analysis, and digital subtraction radiography (DSR) of the porcine bioprosthetic heart valves are limited but compelling in their accurate reflection of much-longer-term clinical findings, as summarized below. Digital subtraction radiography of sample HV01 (the dynamic valve) showed a large increase in intrinsic density around the cuspal commissures and basal attachments after 1 million flexing cycles in the physiologic pulse duplicator. Sample HV02 (the static valve) unflexed, but nearby in the same solution and tester at the same time, showed a lesser, nonlocalized and random distribution of increased intrinsic density. Sample HV01 was considerably more mineralized than sample HV02. The localized increases in intrinsic density documented by DSR of the dynamic valve may be flow- and stress-related, of course, but there might also have been a biochemical (lipid) component present. This hypothesis prompts many current attempts to extract all lipids from newer generations of bioprosthetic valves, using surfactants, for example. Calcium- and phosphorus-containing mineral was detected by EDXray analysis on the inflow side of the heart valve at the region of stenting and maximum bending. Evidence from both clinical [20, 44, 45,] and experimental [15, 40, 49, 52] studies strongly suggests that dynamic mechanical stress and strain promote calcification. Macroscopic calcification of bioprosthetic valves has been said to begin and be enhanced in areas of leaflet flexion where deformations are maximal, especially the cuspal commissures and bases in valves [41]. This is what was observed with sample HV01 (the dynamic sample) after being physiologically flexed for 1 million cycles in the pulse duplicator. The mineral deposited, as analyzed by EDXray, was found to be composed of calcium and phosphorus, but with the calcium content much lower than observed in authentic hydroxyapatite samples or in the high-speed-valve-test samples from this investigation. The formation of calcium-deficient minerals such as brushite and octacalcium phosphate has been suggested to be a precursor to the formation of hydroxyapatite *in vivo* [27]. The actual physiologic path of dystrophic mineralization seems

to be mimicked in the pulse duplicator apparatus, with supersaturated solutions, as shown here. Follow-up studies are obviously required.

CONCLUSION

This investigation demonstrated accelerated mineralization of glutaraldehyde-fixed bioprosthetic tissues at room temperature using a supersaturated solution of calcium-phosphate. Extensive mineralization of dynamically flexed pericardium samples was observed after 1 million cycles in a high speed valve tester at frequencies greater than 12 Hz. Mineralization of a dynamically tested porcine bioprosthetic heart valve was observed after 1 million cycles in a pulse duplicator at physiologic pressures, flows, and rates. Unconstrained human umbilical cord vein grafts did not mineralize with respect to calcium and phosphorus after nearly 200 hours of exposure to the same solution. Internal stenting of these vessels, if it promotes mineralization under the same test conditions, will herald the introduction of a valuable new model for accelerated testing of new stenting concepts and materials.

REFERENCES

1. Baier, RE. Physical Chemistry of the Vascular Interface: Composition, Texture, and Adhesive Quality. In: Sawyer, PN, MJ Kaplitt (Editors). **Vascular Grafts**, Appleton-Century-Crofts, New York, 1978, 76-107
2. Baier, RE. Physical Chemistry of Blood-Surface Interface. In: Stanley, JC, et al. (Editors). **Biologic and Synthetic Vascular Prostheses**, Grune & Stratton, New York, 1982, 83-99
3. Baier, RE. Properties and Characteristics of Bioprosthetic Grafts. In: Kambic, HE, A Kantrowitz, P Sung (Editors). **Vascular Graft Update: Safety & Performance**, ASTM, Philadelphia, 1986, 95-107
4. Baier, RE. The Ocean is the Eye of the Earth: A World Biomaterials Overview. Trans Soc for Biomaterials 1993; XVI:xxx
5. Baier, RE, WM Abbott. Comparative Biophysical Properties of the Flow Surfaces of Contemporary Vascular Grafts. In: Dardik, H (Editor). **Graft Materials in Vascular Surgery**, Symposia Specialists, Inc., Miami, 1978, 79-103
6. Baier, RE, VA DePalma. The Relation of the Internal Surface of Grafts to Thrombosis. In: Dale, WA (Editor). **Management of**

Arterial Occlusive Disease, Year Book Medical Publishers, Inc, Chicago, 1971, 147-163

7. Baier, RE, CK Akers, S Perlmutter, et al. Processed Human Umbilical Cord Veins for Vascular Reconstructive Surgery. Trans Am Soc Artif Intern Organs 1976; XXII:514-524
8. Baier, RE, CK Akers, JR Natiella, et al. Physiochemical Properties of Stabilized Umbilical Vein. Vasc Surg 1980; 14(3):145-157
9. Ban, S, S Maruno. Effect of Temperature on Electrochemical Deposition of Calcium Phosphate Coatings in a Simulated Body Fluid. Biomaterials 1995; 16:977-981
10. Ban, S, S Maruno, H Iwata, H Itoh. Calcium Phospate Precipitation on the Surface of HA-G-Ti Composite Under Physiologic Conditions. J Biomed Mater Res 1994; 28:65-71
11. Batte, RT. **Evaluation of Specimen Preparation Methods for Calcium Phosphate Deposits on Biomaterials**, Masters Thesis, State University of New York at Buffalo, 1996
12. Bernacca, GM, TG Mackay, DJ Wheatley. In Vitro Calcification of Bioprosthetic Heart Valves: Report of a Novel Method and Review of the Biochemical Factors Involved. J Heart Valve Dis 1992; 1:115-130
13. Boretos, JW, FR Wagner. Communication to the Editor: Particle Fragmentation Generated in Pump Sets. J Biomed Mater Res 1971; 5:411-412
14. Bortolatti, U, A Milano, A Mazzucco, et al. Pregnancy in Patients with a Porcine Valve Bioprosthesis. Am J Cardiol 1982; 50:1051-1054
15. Coleman, D. Mineralization of Blood Pump Bladders. Trans Am Soc Artif Intern Organs 1981; 27:708-713
16. Damen, JJM, JM Ten Cate, JE Ellingsen. Induction of Calcium Phosphate Precipitation by Titanium Dioxide. J Dent Res 1991; 70:1346-1349
17. Davies, M. **Pathology of Cardiac Valves**, Butterworth, London-Boston, 1990
18. Deiwick, M, B Glasmacher, A Zarubin, et al. Quality Control of Bioprosthetic Heart Valves by Means of Holographic Interferometry. J Heart Valve Dis 1996; 5:441-447
19. Eanes, E, J Meyer. The Maturation of Crystalline Calcium Phosphates in Aqueous Suspensions at Physiologic pH. Calcif Tissue Res 1977; 23:259-269

20. Ferrans, V, S Boyce, M Billingham, et al. Calcific Deposits in Porcine Bioprostheses: Structure and Pathogenesis. Am J Cardiol 1990; 46:721-734
21. Fishbein, M, S Gissen, J Collins, et al. Pathologic Findings after Cardiac Valve Replacement with Glutaraldehyde-fixed Porcine Valves. Am J Cardiol 1977; 40:331-337
22. Hanlon, JG. **Development of Methodologies to Directly Characterize Calcium Phosphate Deposition Upon Various Biomaterial Substrata**. Masters Thesis, State University of New York at Buffalo, 1991
23. Hasson, JE, J Megerman, WM Abbott. Increased Compliance Near Vascular Anastomoses. J Vasc Surg 1985; 2:419-423
24. Heughebaert, J, S Zawacki, G Nancollas. The Growth of Non-Stoichiometric Apatite from Aqueous Solutions at 37 Degrees C. I. Methodology and Growth at pH = 7.4. J Colloid. Inter Sci 1990; 135:20-32
25. Hidaka, S, K Abe, SY Liu. A New Method for the Study of the Formation and Transformation of Calcium Phosphate Precipitates: Effects of Several Chemical Agents and Chinese Folk Medicines. Arch Oral Biol 1991; 36:49-54
26. Johnson, TP, J Boyd, FJ Schoen, RJ Levy. Prevention of Calcification of Bioprosthetic Heart Valves by Diphosphonate Pre-Treatment. Trans Soc Biomat 1987; 10:178
27. Johnsson, MSA, GH Nancollas. The Role of Brushite and Octacalcium Phosphate in Apatite Formation. Crit Rev Oral Biol and Med 1992; 3:61-82
28. Kessler, LG. FDA Postmarket Safety Notification, October 8, 1998
29. LeGeros, RZ. **Calcium Phosphates in Oral Biology and Medicine**, S. Karger AG, Basel, 1991
30. Levy, RJ, FJ Schoen, JT Levy, et al. Biologic Determinants of Dystrophic Calcification and Osteocalcin Deposition in Glutaraldehyde-Preserved Porcine Aortic Valve Leaflets Implanted Subcutaneously in Rats. Am J Path 1983; 113(2):143-155.
31. Levy, RJ, J Wolfrum, FJ Schoen, et al. Inhibition of Calcification of Bioprosthetic Heart Valves by Local Controlled-Release Diphosphonate. Science 1985; 228:190-192
32. L'Italien, GJ, J Megerman, JE Hassonet al. Compliance Changes in Glutaraldehyde-Treated Arteries. J Surg Res 1986; 41:182-188

33. Maggio, JJ, EM Hausmann, K Allen, TV Potts. A Model for Dentinal Caries Progression by Digital Subtraction Radiography. J Prosthet Dent 1990; 64:727-732
34. Mako, W, I Vesely. *In Vivo* and *In Vitro* Models of Calcification in Porcine Aortic Valve Cusps. J Heart Valve Dis 1997; 6:316-323
35. Nancollas, GH. *In Vitro* Studies of Calcium Phosphate Crystallization. In: Mann, S, J Webb, RJP Williams (Editors). **Biomineralization -- Chemical and Biochemical Perspective**, VCH Publishers, Dordrecht, The Netherlands, 1989, 157-187
36. Paschalis, EP. **Physicochemical Studies of Biologically Important Calcium Phosphates**, PhD Thesis, State University of New York at Buffalo, 1993
37. Paschalis, EP, AL Boskey, GH Nancollas. The Characterization of Biologically Important Apatite Surfaces Using the Dual Constant Composition and FTIR Microscopy Techniques. In: Kossowsky, R and N Kossovsky (Editors). **Advances in Materials Science and Implant Orthopedic Surgery**, Kluwer Academic Publishers, The Netherlands, 1995, 47-60
38. Pierce, WS, JW Boretos. The Dilemma of Patient Exposure to Ubiquitous Foreign Particles. J Biomed Mater Res 1983; 17:389-391
39. Pierce, WS, JW Boretos. Letter to the Editor: Particles and Analysis. Mag Reson in Med 1995; 34:505
40. Pierce, WS, JH Donachy, G Rosenberg, RE Baier. Calcification Inside Artificial Hearts: Inhibition by Warfarin-Sodium. Science 1980; 208:601-603
41. Schoen, FJ. Biomaterial-associated Infection, Neoplasia, and Calcification: Clinicopathologic Features and Pathophysiologic Concepts. Trans Am Soc Artif Intern Organs 1987; 33:8-18
42. Schoen, FJ, JJ Collins, LH Cohn. Long-Term Failure Rate and Morphologic Correlations In Porcine Bioprosthetic Heart Valves. Am J Cardiol 1983; 51:957-964
43. Schoen, FJ, H Harasaki, KM Kim, et al. Biomaterial-associated Calcification: Pathology, Mechanisms, and Strategies for Prevention. J Biomed Mater Res: Appl Biomat 1998; 22(A1):11-36
44. Schoen, F, C Hobson. Anatomic Analysis of Removed Prosthetic Heart Valves: Causes of Failure of 33 Mechanical Valves and 58 Bioprostheses. Hum Patho 1985; 16:549-559
45. Schoen, F, R Levy. Bioprosthetic Heart Valve Failure: Pathology and Pathogenesis. Cardiol Clin 1984; 2:717-739

46. Schoen, FJ, RJ Levy, AC Nelson, et al. Onset and Progression of Experimental Bioprosthetic Heart Valve Calcification. Laboratory Investigation 1985; 52:523-532
47. Schoen, FJ, JL Titus, GM Lawrie. Autopsy-Determined Causes of Death After Cardiac Valve Replacement. J Am Med Assoc 1983; 249:899-902
48. Smith, DB, MS Sacks, PM Pattany, R Schroeder. High-Resolution Magnetic Resonance Imaging to Characterize the Geometry of Fatigued Porcine Bioprosthetic Heart Valves. J Heart Valve Dis 1997; 6:424-432
49. Thubrikar, M, J Skinner, R Eppink, S Nolan. Stress Analysis of Porcine Bioprosthetic Heart Valves *in vivo*. J Biomed Mater Res 1982; 16:811-826
50. Tomson, M, G Nancollas. Mineralization Kinetics: A Constant Composition Approach. Science 1978; 200:1059-1060
51. Tsortos, A, S Ohki, A Zieba, et al. The Dual Role of Fibrinogen as Inhibitor and Nucleator of Calcium Phosphate Phases: The Importance of Structure. J Coll Interface Sci 1996; 177:257-262
52. Turner, S, M Bossart, J Milan, et al. Calcification in Chronically-Implanted Blood Pumps: Experimental Results and Review of the Literature. Texas Heart Inst J 1982; 9:195-205
53. U.S. Patent and Trademark Office website [http://www.uspto.gov]
54. Vossoughi, J, N Kipshidze, J Karanian (Workshop Organizers). Stent Grafts: An Interdisciplinary Workshop, October 5, 1998, Washington, DC
55. Webb, CL, JJ Benedict, FJ Schoen, et al. Inhibition of Bioprosthetic Heart Valve Calcification with Covalently Bound Aminopropane-hydroxydiphosphonate. Trans Am Soc Artif Intern Organs 1987; 33:592-595

Chapter 6

ACCELERATED TEST CRITERIA FOR STENTED GRAFTS

Narendra K Simha, PhD and Ned H C Hwang, PhD

Conventional treatment for an arterial aneurysm has been made through *in situ* surgical repair [1]. However, the intricate surgery has often been associated with complications, and complete protection from aneurysmal rupture has not been guaranteed [2].

A new approach in the treatment of aneurysms involves the catheter-directed endoluminal deployment of an endovascular stented graft (ESG) to bridge the diseased arterial segment [6, 12, 13]. An ESG is a device that uses a prosthetic graft, which is fixed to the arterial wall by means of an intravascular stent [5]. In 1990, Parodi performed the first repair of an abdominal aortic aneurysm using an ESG [12]. Since then, thousands of aneurysm patients have been treated with ESGs worldwide. However, long-term prognostic results are not yet conclusive.

From an engineering point of view, fatigue failure of the ESG remains a primary concern. One aspect is related to the wear of the material. Other factors include the possibility of stent dislodgment and subsequent graft migration. Since it is not practical to test ESGs *in vitro* for their expected period of longevity, which is more than 10 years, we have

Keywords: *Endovascular stented grafts, accelerated testing, fatigue, nitinol*

Ned H C Hwang, PhD (corresponding author), Medical Engineering Division, National Health Research Institute, 128 Yen-Chiu-Yea Road, Taipei 11529, Taiwan, ROC
Stent Graft Update, Edited by J Vossoughi, N Kipshidze, JW Karanian

developed an accelerated fatigue tester to simulate, through a bench-top experiment, the dynamic and fluid dynamic forces exerted on the ESGs. The complete bench-top life expectancy test can be accomplished within a few month's time. The system is designed to test twenty-four specimens simultaneously at a pulse rate up to twenty-five times the normal physiological heart rate in humans. Several sizes of both straight and bifurcated grafts can be mounted in the testing device. To our knowledge, this accelerated ESG fatigue tester is the first of its kind. Through this communication, we intend to discuss the criteria of accelerated testing of stented grafts from both the material's and hemodynamic viewpoints.

Materials Considerations

Treating the stent graft as a load bearing structure, we first analyze the loads and deformations that it has to withstand. Using this, we select the material properties that are relevant to the loading on a stent. Based on existing experimental understanding of these relevant material properties, we can then suggest guidelines for testing the stent grafts.

Strain Cycling in a Stent

In simple terms, an endovascular stent is a tubular structure whose diameter can be changed by applying appropriate forces. Since the stresses and strains in the stent are specific to the particular structure of the stent, we will describe the general material behavior of a stent by choosing a self-expanding endo-aortic stent example. However, the loading situations and the causes of failure that we identify will apply to other stents as well.

Consider the self-expanding stent shown in Figure 1. It may have a slightly larger diameter at the ends and tapers gradually to a constant smaller diameter in the middle. The stent is wound down to a smaller diameter before being placed into a catheter. The catheter is then inserted into a femoral or an iliac artery and maneuvered into an appropriate position in the aneurysm. Once the front end of the stent reaches the unaffected section upstream of the aneurysm, the catheter is retracted. The stent expands so that the ends touch the insides of the arterial wall.

Typically, the stent is covered by a graft layer made from a material such as Dacron (see Figure 1). Since the Nitinol stent is rigidly attached to the Dacron graft, there is negligible change in the diameter at the middle of the stent due to the pressure cycling, while the ends of the stent are less constrained by the graft and the end-diameter changes significantly

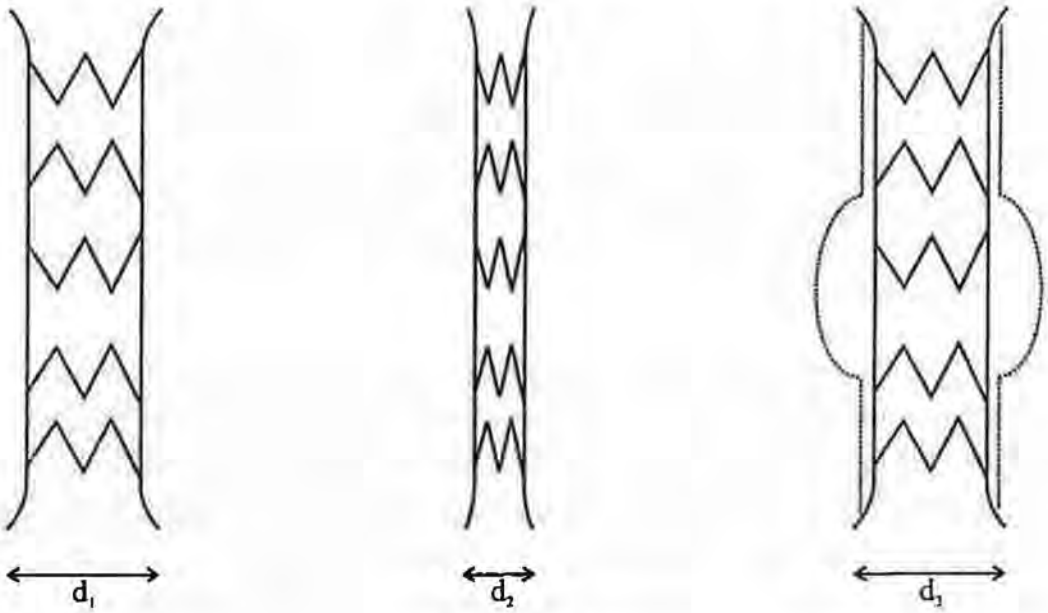

FIGURE 1

Stent shown in unconfined diameter (d_1), compressed diameter (d_2), and deployed diameter (d_3). The self-expanding stent is made of Nitinol and the graft covering is made of a polyester cloth (Dacron).

during the pressure cycling. Consequently, the Nitinol components in the middle region of the stent do not undergo any deformation due to the systolic/diastolic pressure changes. For the present example, we shall only consider the ends for finding the effects of pulse-pressure cycling.

A simple description of the end of the stent is to approximate it by a radial spring. It applies a radial force that seeks to expand when the radius is decreased. This radial spring consists of "V"-shaped components that are joined at the ends ("...VVV...") and this chain is wrapped into a cylindrical shape. Now let us compare the unconfined and compressed positions of the stent in Figure 1. When the end-diameter of the stent decreases, the distance between the ends of the "V"-shapes also decreases. This causes each of the two arms of the "V" to bend and thereby subjects the arms to *tensile* stresses and strains. Notice that as the diameter decrease, the arms bend more and more. Thus the magnitude of the tensile strain in the Nitinol component increases as the end-diameter of the stent decreases from the unconfined value.

Suppose that the artery in which the stent is to be deployed has the following diameters: d_s at the systolic pressure and d_d at the diastolic

pressure. Following U.S. Food and Drug Administration (FDA) guidelines, we may take $(d_d-d_s)/\frac{1}{2}(d_d+d_s) = 6\%$, where d_s and d_d are the systolic and diastolic diameters of the artery, respectively. The stent ends have to maintain contact with the artery during the pulse-pressure cycling; therefore, it follows that the end-diameter of the stent should be exactly the same as that of the internal diameter of the artery throughout the pressure cycling.

For a given stent, the strain depends on the end-diameter. Suppose that the maximum tensile strain occurs at a certain point P. Let the strain at point P be as follows: ε_i in the unconfined position, ε_s at the systolic position and ε_d at the diastolic position. Notice that the diameters follow the order $d_i > d_s > d_d$, consequently the strains satisfy $\varepsilon_d > \varepsilon_s > \varepsilon_i \geq 0$. Thus the strain at point P cycles according to a strain range $\Delta\varepsilon$, strain amplitude ε_a and mean-strain ε_m given by

$$\Delta\varepsilon = \varepsilon_d - \varepsilon_s; \qquad \varepsilon_a = \Delta\varepsilon/2; \qquad \varepsilon_m = (\varepsilon_d + \varepsilon_s)/2 \tag{1}$$

Thus we conclude that the strain in a generic stent cycles according to Equation (1). Only a very special stent structure will have $\varepsilon_m \leq 0$.

From the discussion above, we may extract the following generalization for all stents: *The strain in a stent cycles with a certain range $\Delta\varepsilon$ and about a mean strain $\varepsilon_m \neq 0$.* Thus to provide guidelines for accelerated tests of stent grafts, we need to understand the following material properties: (a) cycles-to-failure vs. strain amplitude with non-zero mean-strain and (b) effect of test frequency on property (a). These two properties are discussed for Nitinol in the next section.

Fatigue Properties of Nitinol

Nitinol is a Ni-Ti alloy that exhibits a superelastic behavior. Figure 2 shows a schematic quasistatic stress-strain curve for a NiTi alloy. When NiTi is stress-free, it has a cubic crystal structure, but under high stresses, it has a monoclinic structure. Consider a NiTi wire specimen and suppose that we start stretching it. At zero stress, the wire is in the cubic austenite phase, and on applying a stress, the wire first stretches elastically in the austenite phase (see Figure 2). When the stress reaches the critical stress σ_f, the material in a certain region of the wire transforms to martensite. Consequently, there are interfaces separating

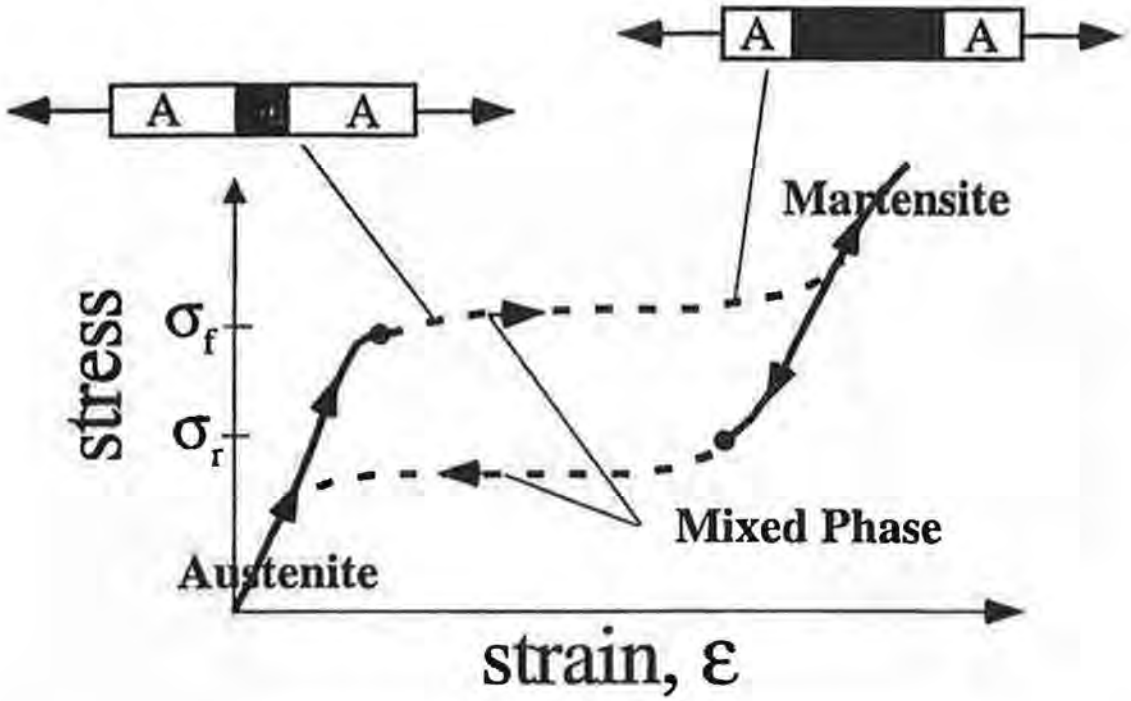

FIGURE 2

The superelastic stress-strain curve for Nitinol

the region of the wire in the austenite phase and the region in the martensite phase. When the wire is stretched further, the interfaces sweep across the specimen and this results in the large increase in strain with only a small increase in stress. Finally, after the entire wire has transformed to the martensite phase, the martensite starts to deform elastically. Now if we start decreasing the loads, at a lower critical value of σ_f, the reverse transformation starts and eventually all the martensite transforms back to austenite.

The rate at which the wire is stretched affects the stress-strain curve. Figure 3 shows that the forward transformation stress increases with the strain rate [15]. The austenite to martensite phase transformation in NiTi is exothermic. Consequently, when the phase transformation occurs at the austenite-martensite interface, latent heat is released which heats up the surrounding austenite [4]. Since increase in temperature stabilizes the austenite phase, more stress needs to be applied to transform it to the martensite phase. As the loading rate increases, less of the latent heat is dissipated by conduction, and consequently, the temperature rise of the austenite increases. Thus the critical stress for forward transformation increases with loading rate.

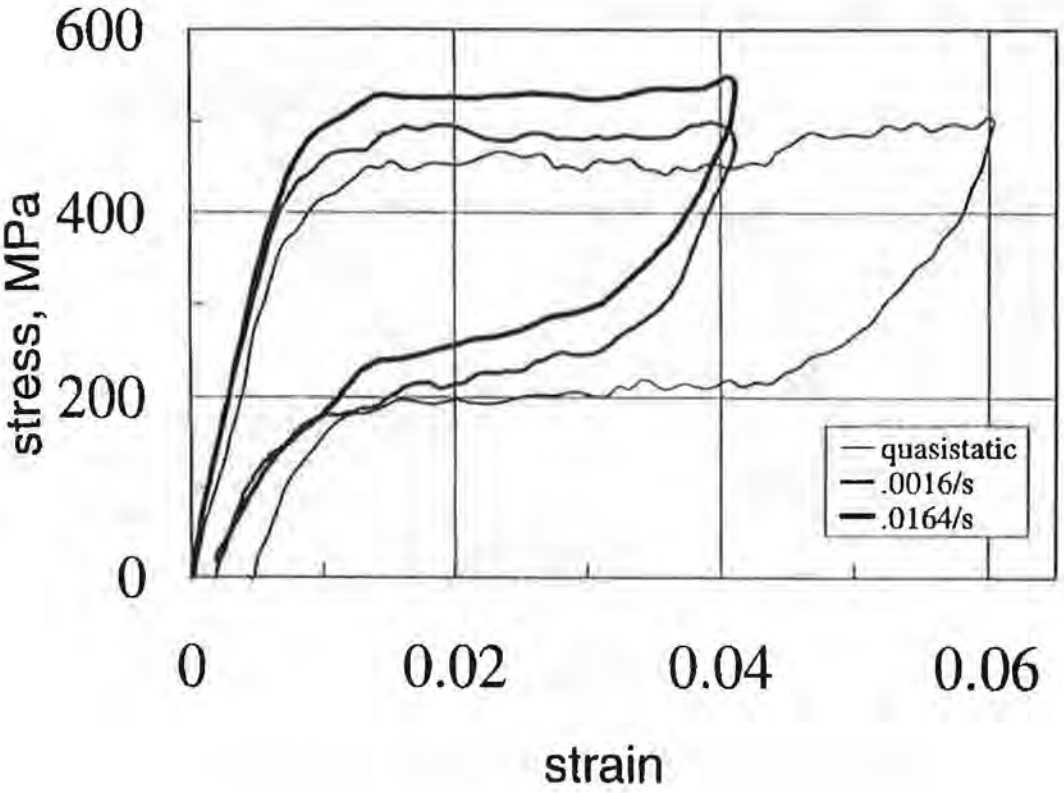

FIGURE 3

Strain-rate dependance of the stress-strain curves

Next we present a review of literature on mechanical fatigue of Nitinol. Melton and Mercier [7] studied the fatigue properties of NiTi by subjecting rod specimens to fully reversed loading. Fatigue crack growth rates and stress/strain amplitudes vs. cycles to failure were measured. Miyazaki notes that cycling with zero mean stress may be appropriate for structural materials, but does not correspond to the superelastic working cycle for NiTi. Instead, Miyazaki and coworkers have measured stress amplitude vs. cycles to failure (S-N) curves for loads that cycled between zero and maximum stress [8-11]. The deformation in the low and high cycle regions were different; in the low cycle region, stress-induced transformation was observed, whereas in the high cycle region, the deformation was mainly elastic. This is also reflected in the stress amplitude vs. cycles to failure (S-N) curves, where two lines with different slopes are needed to fit the data. They also show that heat treatments can increase the fatigue life by considering specimens made of Ti-50.8%Ni [10]. More recently, a temperature dependence of the S-N curves has been demonstrated using rotation-bending tests [3].

For stents, it is necessary to account for mean-strain (or mean-stress) effects. Also, we need to understand the effects of testing frequency on the S-N curves in order to interpret accelerated fatigue testing data. The above comprehensive literature survey shows that there are no studies that explicitly account for the effects of mean-stress and testing frequency on S-N curves for NiTi. Consequently, we have recently started examining these issues [14], and the results of our preliminary experiments are discussed below.

Experiments are conducted under strain control, since the stent diameter change is clearly defined by FDA guidelines, whereas the load changes are not. Table 1 shows the effect of mean strain on the number of cycles-to-failure for a NiTi alloy. All tests were conducted at a frequency of 20 Hz and at room temperature (~24°C). The mean-strain for test A lies on the austenite branch and test E on the martensite branch (see Figure 2). The mean-strain for tests C and D lies in the mixed-phase region; however, it is on the upper branch (austenite to martensite) for test C, whereas it is on the lower branch (martensite to austensite) for test D. For tests A and E, the specimens broke at the grips, hence the cycles-to-failure reported in Table 1 are lower bounds. The cycles-to-failure in the mixed-phase region (tests C and D) is an order of magnitude smaller than that in the single-phase austenite region (test A).

TABLE 1

MEAN-STRAIN EFFECTS
(* INDICATES SPECIMENS THAT FAILED AT GRIPS)

	Mean Strain, %	Strain Amplitude, %	Cycles-to-failure
A	0.25	0.21	185,000*
C	2.12	0.24	10,900
D	2.0	0.22	24,340
E	9.3	0.22	82,650*

Although the cycles-to-failure do not exceed $2X10^5$ in Table 1, we note that Nitinol has excellent strain properties when compared with other materials. For instance, 7075-T6 Al would break at less than 10^4 cycles for the values corresponding to test A in Table 1. Thus the low values for cycles-to-failure are a result of the relatively large strain-amplitude and mean-strain values.

To examine the effect of test frequency, tests were conducted at 2 Hz and 20 Hz (see Table 2). The cycles-to-failure almost doubles when the frequency decreases from 20 Hz to 2 Hz. Testing is under way at other frequencies. Nevertheless, these preliminary results indicate that the cycles-to-failure increase as the test frequency is lowered, at least in the mixed-phase region.

TABLE 2

STRAIN-RATE EFFECTS. THE STRAIN AMPLITUDE WAS ~0.22% AND THE MEAN-STRAIN WAS 6%

Phase	Frequency, Hz	Cycles-to-failure, N
Mixed Phase	20	22,900
Mixed Phase	2	42,400

Accelerated Testing of Stents

A stent usually has some sizing guidelines. For instance, suppose that a stent with an unconfined diameter d_0 is recommended for arteries with diameters between d_1 and d_2. Following the discussion in Section 1, we see that the strain in the stent depends on the ratio of the deployed and unconfined diameters. Consequently, the stent should be tested at the two extremes of the suggested diameters d_1 and d_2. It should perhaps be tested at intermediate diameters also, in view of the fact that the cycles-to-failure in the mixed-phase region are lower than that of the single-phase regions.

Since the cycles-to-failure depend on the strain amplitude, in principle, the stents should be subjected to the required 6% change in diameter. However, the issue of test frequency complicates this requirement. Since reducing the test frequency increases cycles-to-failure, if a stent does not fail under accelerated testing, it will not fail at physiological frequencies under the same testing conditions. This statement does not account for issues such as stress corrosion. Under accelerated testing, the decreased time may not result in stress corrosion, whereas under physiological conditions, stress corrosion may decrease the cycles-to-failure.

MATERIALS AND METHODS

The Pulse Flow Loop and Hydrodynamic Considerations

Theoretically, *in vitro* bench-top testing of any cardiovascular devices or prostheses should be carried out strictly according to the law of

hydrodynamic similarity. Unfortunately, this theory has not yet been developed for accelerated testing of the endovascular stented grafts (ESG). Therefore, a custom testing system must be carefully characterized and calibrated with all the test specimens in place before meaningful test data can be collected.

This paper presents the basic concept of an ESG fatigue-testing system, shown in Figure 4. The system is based on a concentric dual-cylinder design, which consists of a pressurized, rotating inner cylinder and a stationary outer cylinder. The inner cylinder has four circular openings, each with a one-inch diameter, spaced equally around the cylindrical wall. The outer cylinder contains twenty-four circular windows of a half-inch diameter, arranged equally around the outer cylindrical wall. Each of the twenty-four outer windows is connected to a Silastic conduit, which serves as the ESG testing chamber. The outlet of each testing chamber is then connected to tubing that joins all the ESG testing chambers and returns the testing fluid to a sump reservoir.

The testing fluid is pumped into the inner rotating cylinder at a constant pressurized level of 120 mmHg. When the inner cylinder opening matches with one of the outer windows, the pressurized testing fluid is discharged into the testing chamber with a systolic pressure of 120 mmHg. Through an estimated gap width between the two cylindrical walls, the testing fluid is allowed to leak slowly back to the sump reservoir through connecting drains at the bottom of the outer cylinder, shown in Figure 5. The sump reservoir has a free surface which is open to atmospheric pressure. This allows the testing chamber pressure to drop to a certain controlled diastolic pressure level (~80 mmHg) before the next systolic pressure pulse arrives.

The pressurized testing fluid enters the inner cylinder through the hollow shaft mounted on the top plate of the outer cylinder. A one horsepower stainless steel pump (TEEL™, Dayton Electric MFG Co, Niles, IL) is used to pump the testing fluid from the temperature-controlled reservoir to the pressurized chamber of the rotating inner cylinder. After passing through the Silastic testing chambers, the fluid drains back to the atmospheric sump reservoir. This arrangement allows the testing system to be maintained as a closed flow loop with a constant steady flow rate through each testing chamber. Considering the application of ESGs to the lower abdominal aorta, the flow rate of each test specimen is about 1/3 of the normal cardiac output of 5 liters per minute. Therefore, the total flow rate of the tester is chosen to be:

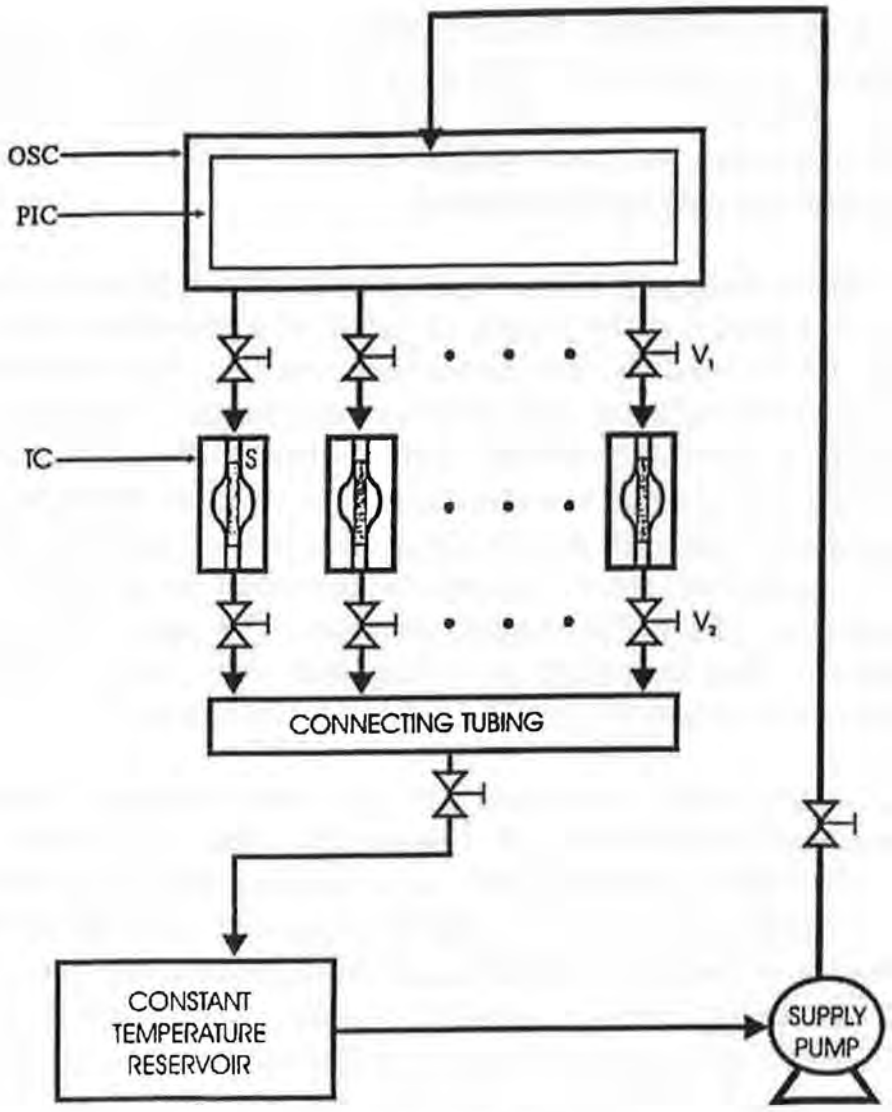

Legend

OSC - Outer Stationary Cylinder with Windows Connecting to Testing Chambers
PIC - Pressurized Inner Rotating Cylinder
TC - Testing Chamber
S - Specimen
V1 - Upstream Control Valve
V2 - Downstream Control Valve

FIGURE 4

Schematic Diagram of the ESG Testing System, where OSC is the Outer Stationary Cylinder with Windows connecting to Testing Chambers, PIC is the Pressurized Inner Rotating Cylinder, TC is the Testing Chamber, S is Specimen, V1 is Upstream Control Valve and V2 is Downstream Control Valve

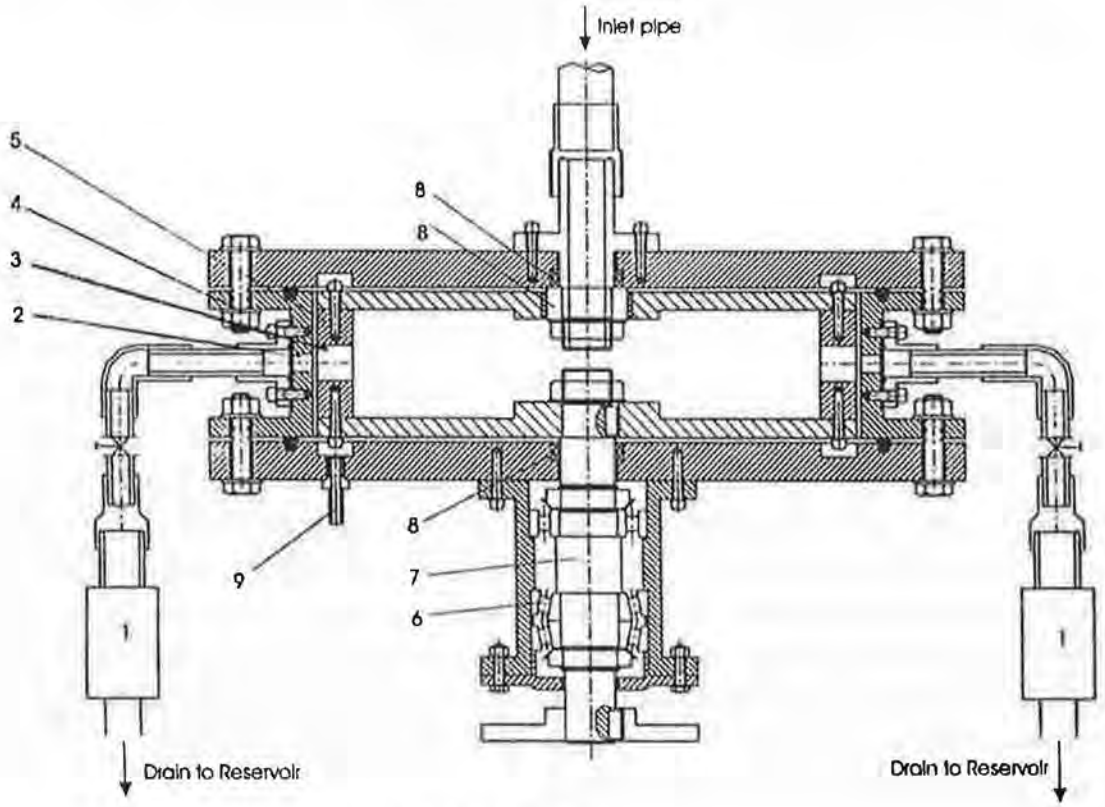

FIGURE 5

Essentials of the Dual Cylindrical Assembly:

1. **Specimen chamber**
2. **Outer cylinder windows**
3. **Inner cylinder windows**
4. **Outer cylinder**
5. **Inner cylinder**
6. **Bearings**
7. **Shaft**
8. **Bearing Seals**
9. **Drain**

$$\frac{1}{3} \times 5 liters / \min \times 24 specimens = 40 liters / \min$$

The testing fluid is a glycerin-water solution of viscosity 3.5 cP, and the fluid temperature is maintained at 37 ± 0.5 °C. Each stented graft sample in the fatigue tester is operated at the same Reynolds number as that of the natural human vessel for which the ESG is designed.

At the rate of 1800 beats/min, however the Womersley number (α) is about 5 times higher. The Womersley number

$$\alpha = \frac{d}{2}\sqrt{\frac{\rho\omega}{\mu}}$$

represents the ratio of the transient inertia force ($\rho\omega V$) to the shear force ($\mu V d^2$), where ρ is the fluid density, V is the mean velocity of flow, d is the diameter of the test conduit, and ω is the angular velocity of the oscillation. It is known that the effect of different α values on an oscillating flow in a given circular conduit is most noticeable in the center portion of the conduit where the transient inertia force is high, as demonstrated in Figure 6. While near the wall region, where the fluid shear stress dominates, the flow velocity reverses at each beat, but it remains practically the same magnitude for a wide range of α values. We believe it is this oscillating velocity profile, hence the corresponding wall shear stress, near the wall region that may lead to dislodgment and sequent migration of a stented graft.

The rotating mechanism consists of a five horsepower driving motor (Teco Electric & Machinery Co., Ltd., Taiwan) for rotational stability, a specially designed rotating shaft, and a series of seals and bearings. One end of the shaft is coupled to the motor, while the other end is keyed to the bottom plate of the inner cylinder. Two supporting bearing systems were designed for this rotating assembly. In order to provide support for the upper part of the inner cylinder during rotation, a cylindrical roller bearing is press fitted onto the top plate to function as a glide and maintain a uniform distance between the inner and outer cylinders. This inner bearing also supports to ensure that there is no wobbling of the cylinder under a rotational load.

For the lower support, a bearing housing with seals is mounted on the bottom plate of the outer cylinder using eight stainless steel screws. It contained three sets of bearings: a cylindrical roller bearing to support the radial load, and two tapered bearings to support axial load and share a portion of the radial loads. Each bearing is press fitted to its designed location in the bearing housing. Lock nuts and washers, specially designed for the bearing installations, were used to keep the bearings firmly in place.

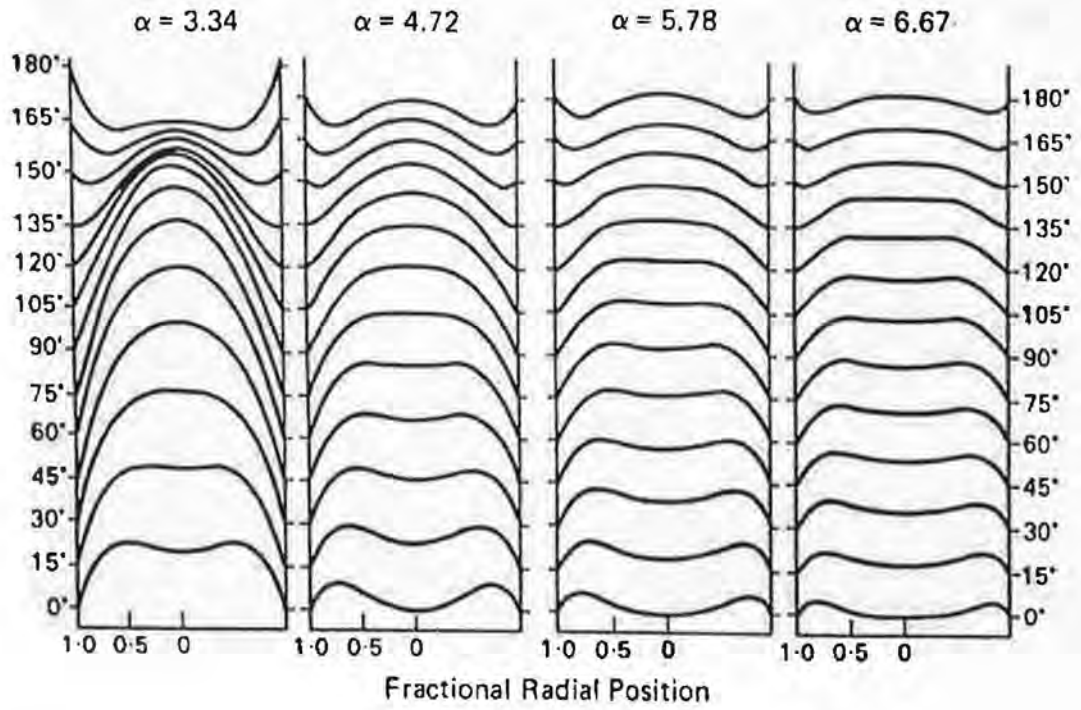

FIGURE 6

Oscillatory Velocity Profile at Different Womersely Numbers (α) (*Reproduced from DA McDonald, Blood Flow in Arteries, 1974, The Williams and Wilkins Co, Baltimore*)

One-inch nylon barbs were used to connect the twenty-four windows on the outer cylinder sidewall to the testing chambers. Each barb is connected to a hydraulic ball valve (Water Witz® PVC Ball Valve, Medley, FL) at the upstream of the testing chamber through the reinforced tubing. Another ball valve is mounted at the outflow end of the testing chamber. Thus, the pressure and flow rate in each testing chamber can be individually adjusted.

Silastic Testing Chambers

The testing chambers are Silastic conduits manufactured by dip molding over a glass mandrel. The thickness of each Silastic conduit is determined accordingly to match the compliance of the conduit wall with the compliance of the adult human abdominal aortic vessel wall. In order to approximate the geometrical and dynamic conditions of an aneurysmal vessel wall, the glass mandrels were also fashioned with a bulge in the region where the test ESG would reside. The hand-made Silastic conduits (Figure 7) were provided to us by Prof Dr–Ing H Reul of the

Helmholtz Institute of Biomedical Technology, RWTH Aachen, Germany.

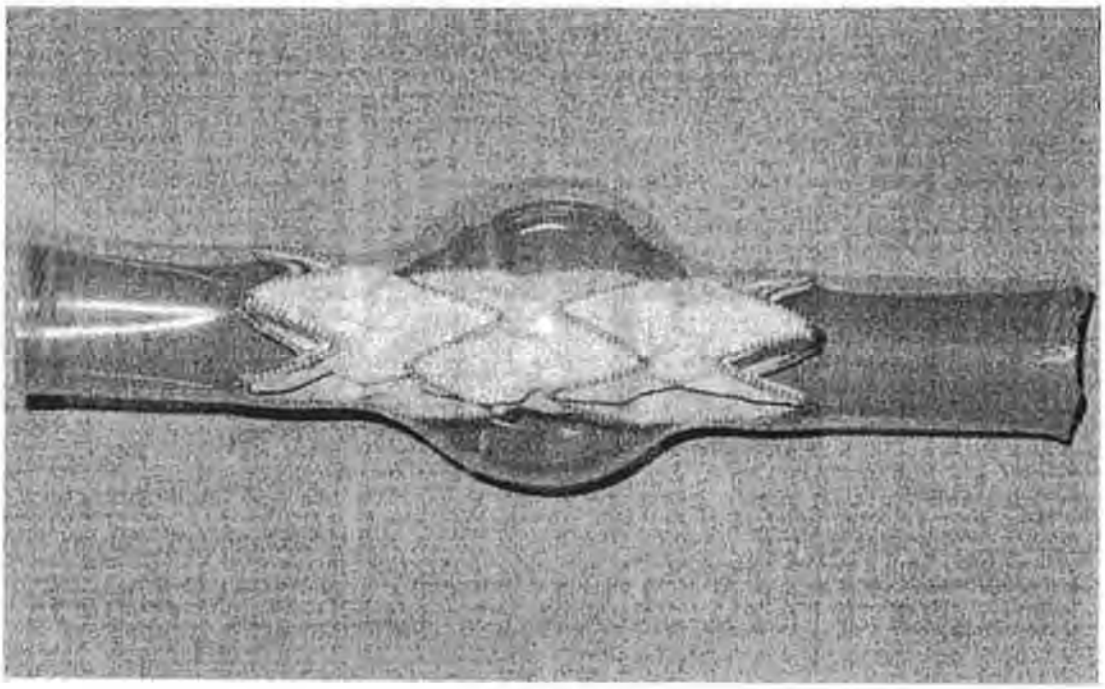

FIGURE 7

Silastic Test Conduit

All testing chambers were mounted vertically on barbs situated between the two horizontal platforms. A pressure tap is placed one-inch upstream of each testing chamber specimen. Signals from each pressure transducer (DTX Disposable Pressure Transducer, Ohmeda Medical Devices Division, Inc., Oxnard, CA) were acquired by an analog to digital acquisition board (DAP 800 Data Acquisition Processor; Microstar Laboratories, Inc., Bellevue, WA). A typical pressure waveform acquired from a testing chamber is depicted in Figure 8. The pressure waveforms are monitored in each testing chamber periodically; substantial changes from the initial 120/80 mmHg pressure differential are corrected using the hydraulic ball valves located above and below each of the testing chambers.

Each aneurysm-shaped Silastic test chamber is individually measured to ensure that its compliance matches that of the normal adult human abdominal aortic wall (6% ± 2%). Test conduit compliance (C) is defined as the change in external diameter of the test conduit proximal and distal to the bulge over a pressure differential of 120/80 mmHg, divided by the calculated mean diameter: where d_d is the external diameter at a pressure

of 80 mmHg, and d_s is the external diameter at a pressure of 120 mmHg. The conduit compliance:

$$C = \frac{d_s - d_d}{d_m} \times 100\% = \frac{d_s - d_d}{(d_s + d_d)/2} \times 100\% = 2\frac{d_s - d_d}{d_s + d_d} \times 100\% \tag{2}$$

is represented as a percentage, which is indicated as the percent change of diameter per 40 mmHg pressure difference at a normal human heart rate (70 beats/min).

Applying the laser dynamic compliance measurement technique (LCT) [7], the change of a single conduit diameter is quantitatively measured over the pressure range of 120/80 mmHg at 60 beats/min and under steady pressure levels. In the present study, LCT measurement of conduit compliance is made *in situ*. The system is capable of recording the instantaneous diameter and diameter changes at corresponding intravascular pressure levels, simultaneously.

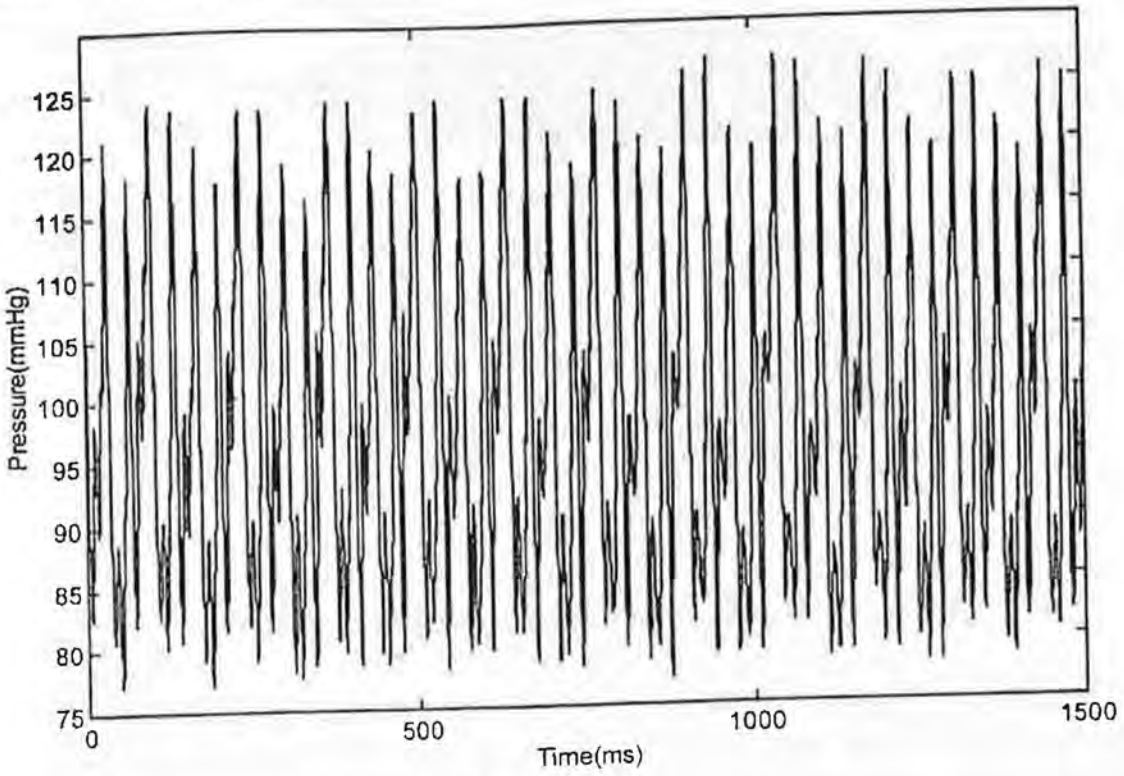

FIGURE 8

Pressure Waveform. Pressure from pressure tap Placed one inch upstream of the test chamber in mmHg versus time in milliseconds

The basic principle of the laser compliance measurement system is schematically shown in Figure 9. In this setup, a uniformly distributed, thin rectangular laser sheet is created by passing an 8 mw He-Ne laser beam through a cylindrical lens and a spherical collimating lens. A single elastic test conduit is placed at the center of the laser sheet to block a certain amount of the laser light, which is projected perpendicular to the test conduit. The remaining laser sheet that is not blocked by the conduit is focused through a downstream spherical lens onto a photodetector placed on the opposite side of the conduit. When the conduit increases its diameter, the intensity of light received by the photodetector will proportionally decrease, and vice versa, with no time delay. The photodetector generates an output voltage which is linearly proportional to the light received. A linear relationship between the conduit diameter, d, and the photodetector output, I, may then be established as follows:

$$I = Kd + C \tag{3}$$

where d is the instantaneous diameter, I is the output signal, K and C are the calibrated constants.

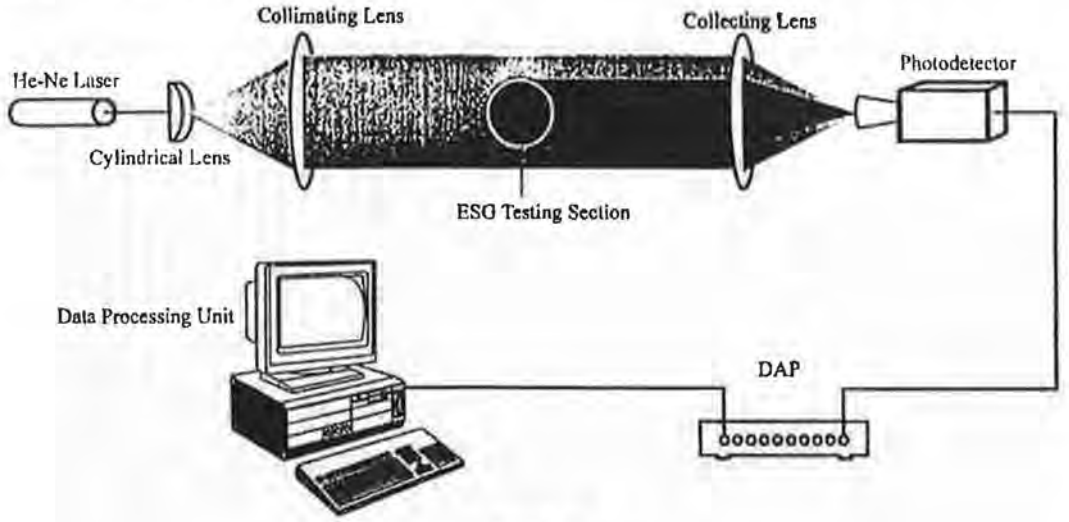

FIGURE 9

Schematics of laser dynamic compliance tester

The optical system is mounted on a vibration-free optic table with no direct contact with the pulsatile flow system for precise position measurement. The testing system is pre-calibrated using two solid cylinders of known diameter to determine K and C. The measured dynamic compliance of a typical Silastic conduit is shown in Figure 10. The compliance is measured and determined for all twenty-four testing conduits before the experiment.

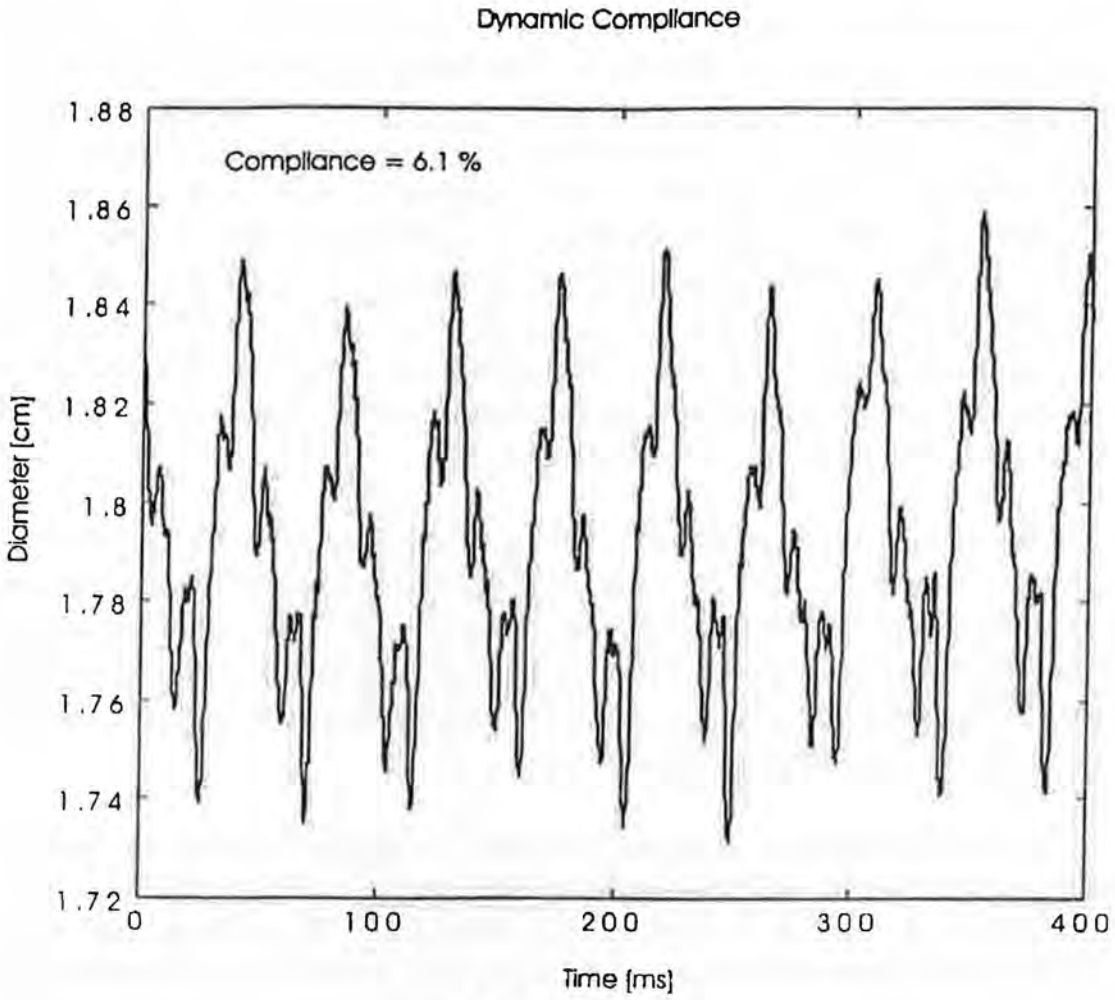

FIGURE 10

Typical conduit compliance measured by LCT. The compliance is calculated using equation (1); Taking the uppermost point in the plotted data to represent D_2 and the lowest point for D_1 over 100 milliseconds time.

Calibration of the ESG Fatigue Testing System

Theoretically, *in vitro* bench-top testing of any cardiovascular devices or prostheses should be carried out strictly according to the law of dynamic similarity. Unfortunately, this theory has not yet been developed for accelerated testing of the vascular stented grafts. Therefore, a custom testing system such as the presented ESG Fatigue Tester must be carefully calibrated and characterized together with all the test specimens in place before meaningful test data can be collected.

In addition to the 120/80 mmHg testing pressure levels, the testing flow rate, the testing conduit compliance, and the testing pulse rate for a specific set of specimens, important parameters are to be considered. In

the present tester, the pulse rate can be varied either by changing the speed of the rotating motor or by increasing the number of the inner cylinder openings from four to eight. By doing the latter, the systolic to diastolic ratios are inevitably altered. At the same time, the gap width between the inner and the outer cylindrical sidewalls has to be recalculated under eight openings by assuming Couette flow of a Newtonian fluid. The right amount of leakage between the gap will allow the pressure in the testing chambers to drop to the desired diastolic level, (i.e., approximately 80 mmHg). This procedure is largely trial-and-error, which can only be empirically achieved by operating the system with all test specimens installed in the testing system.

After initial adjustments, the testing flow loop will be operated at several pulse rates, each for a period of time until the system has reached stable equilibrium. The highest pulse rate, at which no apparent system resonance is observed, will be selected as the operating pulse rate. Once the testing procedure begins, no more adjustments will be made during the entire accelerating testing process.

The current testing system is designed to host 6 large size, 6 middle size, and 6 small size straight grafts with 2 study controls of each size; or 10 large size (36mm-20mm) and 10 small size (18mm-8mm) bifurcate ESGs for the abdominal aorta, with two study controls of each equivalent size; or three sizes (large, medium and small) each of 8 straight ESG samples, with two study controls of each equivalent size. Our experience with mock vascular conduits has indicated that the test specimens should be evenly distributed around the periphery of the tester in order to balance the load on the inner cylinder as it rotates at a high speed. Otherwise, cross-talk among the testing chambers may occur and mechanical resonance can follow. These aforementioned factors are what limit the accelerated rate of testing.

SUMMARY AND DISCUSSIONS

Industrial testing of endovascular stent grafts (ESG) for service expectance of 10 years or more can only be carried out at an accelerated rate. This paper reviews the accelerated test criteria from both the materials science and the hemodynamics viewpoints.

Treating the stent graft as a load bearing structure, we first analyzed the load and deformations in order to select material properties that are relevant to the loading of the stent. Based on existing understanding of

these relevant material properties, we suggested guidelines for accelerated testing of stent grafts.

Specifically, we discussed the effect of mean-strain on fatigue of Nitinol. We further noted the fact that the fatigue failure of most superelastic materials, such as Nitinol, often exhibits a dependency on the time rate of strain. Although the physiologic loading condition is often represented by a 6% change of conduit diameter at 40 mmHg pulse pressure and normal human heart rate, we expect that this strain rate dependency may be correlated to a high frequency accelerated test at a much lower strain amplitude. Based on this hypothesis, a rotary type accelerated ESG tester was designed. The tester system is capable of testing simultaneously 24 ESG specimens at pulse rates up to 1800 beats/min at normal physiologic pressure levels (120/80 mmHg). Each test specimen is installed inside a transparent, Silastic conduit, which has wall properties similar to that of the normal human aortic wall (conduit compliance approximately 6% with 40 mmHg pressure pulse under physiologic pulse rates).

Mechanical failure may occur in a surgically implanted ESG by either strain fatigue or dislodgement followed by migration. The tester system is designed considering conduit hydrodynamics which includes Reynolds and Womersley number simulations. At accelerated rates, the oscillatory Womersley number, which represents the ratio of the transient inertia force to the shear force, also increases. The theoretically different values of computed velocity profiles showed that the transient velocity in the pipe center was affected by different values of the Womersely number, while the shear stress in the wall region remained relatively unvaried. Taking cognizance of the fact that the relationship between the normal force that the stent exerted on the vessel wall and the oscillatory shear force in the wall region determines the stability (or dislodgment) of an implanted ESG, we believe that testing ESG specimen in a conduit, which mimics the elastic wall properties of the natural aortic wall, would represent a close imitation for studying ESG dislodgment under oscillatory conditions.

ACKNOWLEDGEMENTS

The authors acknowledge a donation made by the World Medical Manufacture Corporation (Sunrise, FL 33325), which provided partial funding for construction of the device reported in this paper. The authors also wish to express appreciation to their graduate students, Julie X Yun, Matthew Tingom, and Bruce Z Gao, who participated in this project.

REFERENCES

1. Carola, R, JP Harley, CR Noback. ***Human Anatomy & Physiology***. New York: McGraw-Hill, 1990: 609
2. Edwards, JM, SA Teefey, RE Zierler, TR Kohler. Intraabdominal Paraanastomotic Aneurysms after Aortic Bypass Grafting. J Vasc Surg 1992; 15:344-353
3. Kim, YS, S Miyazaki. Fatigue Properties of Ti-50.9 at %Ni Shape Memory Wires. Proceedings of the Second International Conference on Shape Memory and Superelastic Technologies, Pacific Grove, CA, 1997: 473-478
4. Leo, PH, TW Shield, OP Bruno. Transient Heat Transfer effects on the Pseudoelastic Behavior of Shape-Memory Wires. Acta Metall. Mater 1993; 41:2477-85
5. Marin, ML, FJ Veith. Endovascular Stents and Stented Grafts for the Treatment of Aneurysms and other Arterial Lesions. Advances in Surgery 1996; 29:93-109
6. Marin, ML, JV Frank, TF Panetta, *et al.* Transfemoral Endoluminal Stented Graft Repair of a Popliteal Artery Aneurysm. J Vasc Surg 1994; 19:754-757
7. Melton, KN, MO Mercier. Fatigue of NiTi Thermoelastic Martensites, Acta Met 1979; 27:137-144
8. Miyazaki, S, T Imai, Y Igo, K Otsuka. Effect of Cyclic Deformation on the Pseudoelasticity Characteristics of Ti-Ni alloys. Metallurgy Transactions 1986; 17A:115-120
9. Miyazaki, S, Y Igo, K Otsuka. Effect of Thermal Cycling on the Transformation Temperatures of Ti-Ni alloys. Acta Metall 1986; 34: 2045-2051
10. Miyazaki, S. Development and Characterization of Shape Memory Alloys. In: ***Shape Memory Alloys***; CISM lecture No. 351, Springer-Verlag, Wien, 1994, 69-147
11. Miyazaki, S. Thermal and Stress Cycling Effects and Fatigue Properties of Ni-Ti Alloys. In: Duerig, TW, KN Melton, D Stoeckel, CM Wayman (Editors.) ***Engineering Aspects of Shape Memory Alloys***, Butterworth-Heinemann, 1990, 3-20
12. Parodi, JC, JC Palmaz, HD Brone: Transfemoral Intraluminal Graft Implantation for Abdominal Aortic Aneurysms. Ann Vasc Surg 1991; 5:491-499
13. Parodi, JC, ML Marin, FJ Veith. Transfemoral, Endovascular Stented Graft Repair of an Abdominal Aortic Aneurysm. Arch Surg 1995; 130:549-552

14. Tabanli, RM, NK Simha, BT Berg. Mean Stress effects on the Fatigue of NiTi, Materials Science and Engineering (Proceedings of ICOMAT), 1998
15. Tabanli, RM. Fatigue of NiTi, PhD Thesis, University of Miami, 1998

Chapter 7

TISSUE ENGINEERED VASCULAR GRAFTS

Lee K Landeen, MS, Joan Zeltinger, PhD, Ann A Lee, PhD, Holly G Alexander, BA, Dionne A Graham, MS, Michael R Fino, BS, Anthony Ratcliffe, PhD , Gail K Naughton, PhD

Clinical intervention is often necessary to restore proper circulation in persons afflicted with cardiovascular disease. Over one million vascular procedures are performed annually in the United States, including over 500,000 coronary artery bypass graft procedures and over 80,000 peripheral graft procedures [28, 37, 53]. Although improvements in the understanding of the etiology and pathology of cardiovascular and vascular diseases have been made, treatment options such as angioplasty, stents, transmyocardial revascularization, and bypass generally prolong the interval between repeat procedures but do not correct for the actual predisposition towards disease.

Vascular grafts are used by vascular and cardiothoracic surgeons to repair or replace segments of arterial and venous blood vessels that are weakened, damaged, or obstructed due to trauma or disease such

Keywords: *Vascular graft, tissue engineering, smooth muscle cell, fibroblast, endothelial cell, extracellular matrix*

Gail K Naughton, PhD (corresponding author), Advanced Tissue Sciences, Inc, 10933 North Torrey Pines Road, La Jolla, CA 92037
Stent Graft Update, Edited by J Vossoughi, N Kipshidze, JW Karanian

as aneurysm, atherosclerosis, and diabetes mellitus. Vascular bypass grafts for small-diameter applications (<4-6 mm) are frequently prepared from autologous saphenous veins or internal mammary arteries. Of the autologous tissues, the saphenous vein maintains approximately 50% patency after 7.5 years, while the internal mammary artery has greater than 90% patency over seven years [20]. A second approach for coronary and below-the-knee vessel repair is the Rapidgraft Arterial Vessel Substitute™, a vascular graft comprised of autologous pericardial tissue, from Ramus Medical Technologies [32]. Although autologous Rapidgrafts may provide benefits, this approach could not be used for repeated procedures.

Synthetic materials such as expanded polyester polytetrafluoroethylene (ePTFE) or poly(ethylene terephthalate) (PET, Dacron®) have traditionally had poor patency rates in small-diameter sites, but have had greater usage in medium- to large-diameter applications (>6 mm) [8, 62]. However, one synthetic vascular prosthesis, the Perma-Flow® Coronary Bypass Graft by Possis Medical, Inc., is showing clinical promise for small-diameter vessel repair [14, 15, 16]. This graft utilizes a proprietary, flow-control design to maintain adequate blood velocities and to reduce the possibility of thrombosis, the leading cause of failure of synthetic grafts positioned in high resistance outflow tracts. Long-term patency of Perma-Flow has yet to be determined.

The clinical complications of synthetic prostheses commonly result from an immune response to and pathologic remodeling of the prosthetic material. These failure modes have increased interest in new approaches for designing vascular grafts, such as tissue engineered products, for improving biocompatibility and long-term function.

Tissue engineering is an emerging technology that is changing the field of transplantation by developing new medical devices for wound healing and tissue repair [40]. This technology comprises the disciplines of cell and molecular biology, gene therapy, polymer chemistry, and bioengineering to create tissues or cell-based therapies that could correct problems associated with current vascular and cardiovascular devices. The first tissue engineered products to be successfully marketed were for skin applications [4, 7, 34]. Through various designs, these tissue engineered skin products have demonstrated the feasibility of tissue engineering and have paved the way for other applications.

The earliest production of a tissue engineered blood vessel was by Weinberg and Bell [57], in which a contracted collagen gel was formed using bovine arterial cells and a Dacron mesh sleeve. This landmark graft was able to withstand burst pressures of 323 mmHg; however, those values are considerably less than reported burst pressures for human saphenous veins (3,900-9,400 mmHg) [44, 61]. More recently, L'Heureux and associates [30] have reported that their tissue engineered blood vessels, made by sequential culture of human dermal fibroblasts and umbilical smooth muscle cells in the absence of a support scaffold, withstood burst pressures over 2000 mmHg. These tissue engineered blood vessels required a three-month development/culture process.

A different approach to vascular tissue engineering incorporates a supporting scaffold to reduce culture time without compromising mechanical strength. Researchers at Massachusetts Institute of Technology and Children's Hospital, Boston have tested the utility of this tissue engineering approach for larger diameter vessel repair [48]. In these studies, tissue engineered ovine pulmonary conduits were made after one week of culture using autologous vascular cells seeded onto poly(glycolic acid) felt, reinforced with a poly(glycolic acid)/poly(lactide-co-glycolide) knitted scaffold. These conduits resisted mechanical failure over five months when implanted into growing juvenile sheep. Additionally, these conduits grew with the native proximal and distal vessels such that the diameters of the TEVGs matched the adjacent native vessels within 95%.

In this report, we present the feasibility of applying our tissue engineering approach of cells grown on a biocompatible scaffold for small-diameter cardiovascular applications. Our results showed that growth by smooth muscle cells on cylindrical scaffolds produced living, three-dimensional tissue. These conduits of tissue and residual scaffolding were capable of withstanding significant burst pressures and, when sutured to small-diameter vessels, established a uniform transition at the vessel-implant interface.

MATERIALS AND METHODS

Scaffold Fabrication

Porous sponges were fabricated using a solvent-casting and particulate-leaching method [17]. Poly(ε-caprolactone) (PCL) polymer (1.2 - 1.5 dL/g inherent viscosity) (Birmingham Polymers, Inc., Birmingham, AL) was dissolved in acetone or methylene chloride. Sodium chloride (ground and

sieved to 106-150 μm particle size) was added to achieve a 90% w/w ratio of salt to polymer. The mixture was thoroughly agitated to create a homogeneous suspension, immediately cast into a Teflon Petri dish, covered, and left undisturbed at room temperature for 18-24 hours. The resulting hardened mixture was heated to 60°C for at least 1 hour and immediately quenched in liquid nitrogen to maintain the polymer in an amorphous state. After removal from the liquid nitrogen and warming to room temperature, the polymer scaffold was soaked at room temperature in successive changes of reverse osmosis water (Milli-Q system, Millipore, Bedford, MA) to leach residual salt. One-centimeter, disc-shaped, porous scaffolds (approximately 1-mm in thickness) were cut.

Cylindrical scaffolds were fabricated using a similar approach as described above. Teflon mandrels (3-mm outer diameter) were repeatedly dipped into the salt/polymer mixture to cast cylindrical scaffolds approximately 1 mm in wall thickness. After leaching and removal from the mandrel, scaffolds were cut to 6 cm in length. All scaffolds were sterilized by electron-beam irradiation (2.0 MRad).

Cell Culture

Primary cell isolates of adult canine dermal fibroblasts (DmFb) and coronary artery smooth muscle cells (SMC) were obtained by enzymatic digestion. Neonatal human foreskin DmFb were obtained from qualified master cell banks, similar to those used to produce Dermagraft® and TransCyte™ [22, 38]. Fibroblasts were passaged on tissue culture plastic in culture medium consisting of 10% fetal bovine serum (FBS; Hyclone, Logan, UT), Dulbecco's Modified Eagle Medium (DMEM; Gibco, Gaithersburg, MD), sodium pyruvate (Gibco), non-essential amino acids (Gibco), L-glutamine (Gibco), and antimicrobial agents (Gibco). Canine microvascular endothelial cells (MVEC), generously provided by Dr. Stuart Williams (University of Arizona Health Sciences Center, Tucson, AZ), were cultured in endothelial cell growth medium (Clonetics, San Diego, CA). All cell types were used between the fourth and eighth passage and were cultured at 37°C, 5% CO_2, and >90% humidity.

Porous PCL scaffolds were prepared for cell seeding by briefly dipping in 70% ethanol, rinsing in phosphate buffered saline (PBS) for 5 minutes at room temperature, and incubating for 18-24 hours at 37°C in culture medium. Scaffolds were seeded at densities of $1x10^6$ cells per disc or $1x10^7$ per cylinder under rotation (3-4 rpm) for 24 hours. The seeded disc scaffolds were transferred into multi-well dishes and grown statically with

culture medium containing 50 μg/ml ascorbate (Baker, Phillipsburg, NJ). Seeded cylindrical scaffolds were placed into bioreactors [12] with recirculating ascorbate-containing medium. The medium for all cultures was changed weekly for up to 8 weeks.

Canine SMC TEVGs were endothelialized by seeding $5x10^6$ MVEC onto the luminal surface under rotation (0.25 rpm) for 4 hours. After seeding, the endothelialized TEVGs were placed in bioreactors and cultured under flow (100 ml/min).

Biochemical Analysis

TEVG discs and cylinders were collected at 24 hours and at weekly intervals (up to 8 weeks) and analyzed as described below. Estimation of cell numbers and activity was accomplished using the MTT assay [27, 36, 52]. Briefly, samples were incubated in MTT solution (0.5 mg/ml in 2% FBS culture medium) (Sigma, St Louis, MO) for 2 hours and rinsed with PBS for 5-10 minutes. The insoluble precipitant was extracted in isopropanol for 24 hours at room temperature, and optical density (OD) was determined at 540 nm. Linear correlations between OD and cell numbers were established (unpublished results).

Collagen content was quantified using the Sirius Red Assay [3, 29, 54]. TEVG samples were treated with 1% Triton X-100 in PBS at room temperature for 1 hour to remove cellular and minor extracellular (ECM) components. After rinsing in PBS, samples were stained with Direct Red 80 dye (0.1% in picric acid) (Aldrich, Milwaukee, IL) which has a strong affinity for collagens. After a minimum of 3-4 successive rinses in PBS to remove unbound dye, samples were treated with collagenase (2 mg/ml in PBS without Ca^{++} or Mg^{++}) (Boehringer Mannheim, Indianapolis, IN) to liberate collagen-bound dye, and OD was measured at 540 nm. Collagen concentration was determined against a standard curve of purified collagen type I (Sigma).

Histology and Immunohistochemistry

Cell type of each established canine tissue isolate was confirmed by immunostaining monolayer cultures with monoclonal primary antibodies against smooth muscle-specific alpha actin (SM α-actin) (pre-diluted) (Enzo, Framingdale, NY) and calponin (1:1000 dilution) (Sigma), and polyclonal antibodies against von Willebrand factor (vWF) (1:200 dilution) (Dako, Carpenteria, CA). Monolayers were grown in chamber slides and fixed with cold methanol just before confluency. All monolayer

cultures were blocked for non-specific binding with 5% normal goat serum (30 minutes at room temperature), incubated with the primary antibodies and rinsed with Tris-buffered saline (TBS). Indirect immunofluorescent slides were treated with an anti-mouse or anti-rabbit fluorescein-tagged secondary antibody (1:200 dilution) (caltag, Burlingame, CA), and visualized under ultraviolet light. Immunohistochemical slides were treated with a biotinylated universal secondary antibody (prediluted) (DAKO), followed by addition of streptavidin (1:200 dilution) (Zymed, San Francisco, CA) and visualized using a DAB substrate chromagen. All incubations were at room temperature for 15 minutes. SMCs stained positive for SM α-actin and calponin and negative for vWF (data not shown). Endothelial cells (EC) stained positive for vWF and negative for the other markers and were positive when cultured with DiI-labeled low density lipoprotein (Molecular Probes, Eugene, OR) (data not shown).

Histological specimens were fixed in 10% buffered formalin and embedded in either paraffin or plastic for sectioning and staining. Samples used for plastic sections were embedded in catalyzed glycol methacrylate and allowed to polymerize at room temperature for approximately 1 hour. The blocks were sectioned using an automated microtome with tungsten carbide knife (Leica Model RM2065, Deerfield, IL), and sections (3-4 μm thickness) were mounted on glass slides. After drying for approximately 1 hour at room temperature, the slides were stained with hematoxylin and eosin to visualize cell and tissue components by light microscopy (Zeiss, Thornwood, NY).

Native canine artery or TEVGs samples were formalin-fixed and paraffin-embedded. Sections were cut to 5 μm and mounted on glass slides. Slides were rehydrated in a graded series of alcohol and rinsed in TBS. Tissue sections were stained for elastin using an anti-elastin monoclonal antibody (1:50 dilution) (Sigma) as described above. Control slides of equivalent tissues received no primary antibody.

Scanning Electron Microscopy (SEM)

Tissue and scaffold samples were fixed at least 1 hour in glutaraldehyde or formalin, washed in PBS, and treated with osmium tetroxide (1% in water) for 1 hour at 0-4°C in the dark. Samples were washed with water, alcohol-dehydrated, and critical point dried in liquid CO_2. Specimens were mounted to posts, sputter-coated with gold for visualization, and viewed on a Hitachi (Model S-520) microscope.

Mechanical Testing

Circumferential burst tests were performed using a custom-designed, pneumatically-actuated testing device (EH Mead Instruments, La Jolla, CA). Samples were placed over mandrels sheathed with a distensible silicone tube (Specialty Manufacturing, Inc., Saginaw, MI) and were immersed in a recirculating 37°C PBS bath. A dry nitrogen air source was used to inflate the silicone tube and apply a radial load to the surrounding sample. Samples were inflated to complete failure without pre- or cyclic-loading. A pressure transducer monitored the applied load and a video capture system recorded the deforming vessel. The recorded video simultaneously captured the transducer output and elapsed time, respectively, with video voltage and timer display devices (Vista Electronics, Ramona, CA). A 200 MHz Pentium computer with frame grabber board digitized the video signal for use with image analysis software (Image-Pro Plus; Media Cybernetics, Silver Spring, MD). The burst pressure of the sample was determined by subtracting the mechanical contribution of the silicone tube [9].

In Vivo Feasibility Study

Handling characteristics and short-term suture retention of PCL cylinders and TEVGs were assessed in canines. The study followed guidelines of the National Institutes of Health for care and use of laboratory animals (NIH publication #85-23 REV.1985) and was conducted in accordance with Good Laboratory Practice Regulations (21 CFR Part 58). Animals were housed in facilities approved by the American Association for Accreditation of Laboratory Animal Care. After anesthetization with intravenous pentothal followed by inhalation of halothane and oxygen, 3-cm graft sections were anastomosed using 6-0 Prolene suture into the arteries of adult mongrel dogs that were administered anticoagulants (pre-operative aspirin for 1 day and 3,000 units of heparin prior to vessel clamping). SMC TEVGs (n=4) were sutured into the carotid artery, while unseeded PCL cylindrical scaffolds were implanted into the carotid and femoral arteries (n=1 for each vessel). The unseeded PCL scaffolds were monitored for up to 30 minutes, while the TEVGs were monitored for up to 2 hours.

Statistical Analysis

Data were collected in triplicate and errors are reported as standard deviations. Statistical analysis for multiple comparisons consisted of one-way ANOVA followed by Bonferonni-Dunn's post hoc test.

RESULTS

PCL Scaffold Fabrication

A representative PCL cylindrical scaffold and SEM showing ultra-structural details of the interconnected pores are shown in Figures 1 and 2a, respectively. Porous PCL scaffolds were created with porogens of 106-150 μm and void fractions (porosity) of approximately 90%, based on percent weight ratios of polymer and salt. Pore size was selected based on feasibility cell culture studies (unpublished data); void fraction was selected to obtain interconnected pores [5].

Tissue Characterization

SEM analysis of canine SMC TEVGs showed formation of a three-dimensional tissue. The *en face* view of the unseeded scaffold (Figure 2a) shows the open pored structure of the scaffold. After culture for 4 weeks, a dense network of cells and ECM have filled the scaffold pores (Figure 2b). Histological analysis of time course samples (0 - 8 weeks) confirmed the SEM findings. A 4-week TEVG is shown in Figure 3, demonstrating that SMCs colonized the porous scaffolds. The SMCs appear non-pyknotic and are randomly oriented within the ECM that encompasses the residual PCL scaffold.

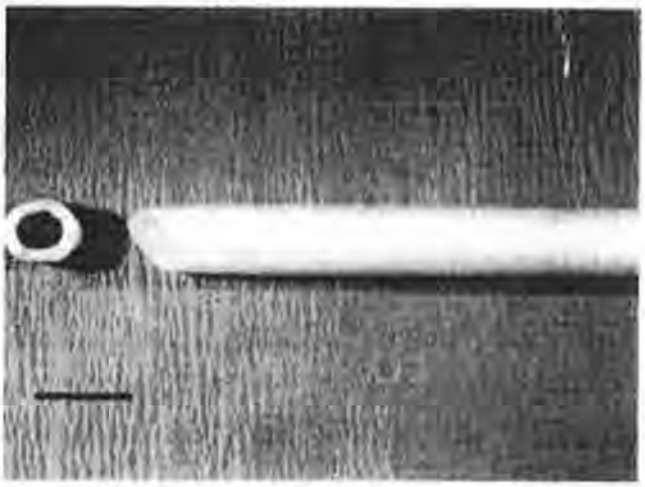

FIGURE 1

Porous PCL cylindrical scaffolds. Scaffolds were fabricated using a solvent casting / particulate leaching method to achieve 90% void fraction and 106-150 μm pore size. Bar represents 1 cm.

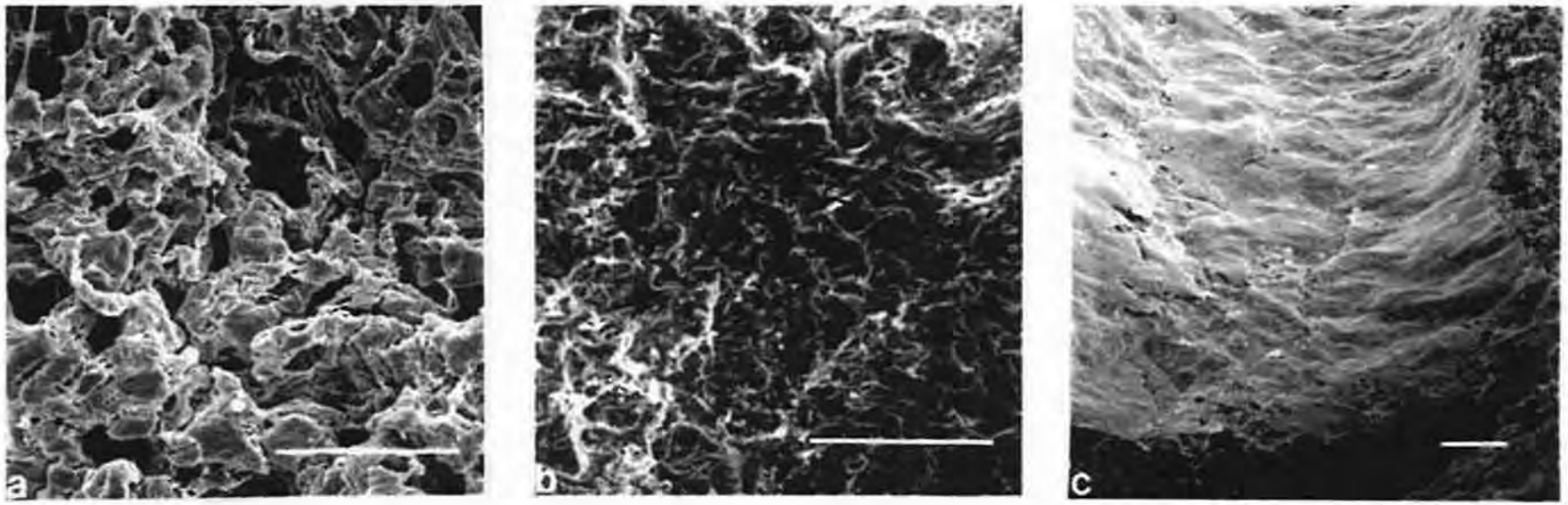

FIGURE 2

Scanning electron micrographs of PCL scaffold and 4-week TEVGs with and without MVEC for 48 hours. The highly porous surface of the PCL scaffold (a) becomes colonized and densely filled with ECM by 4 weeks (b). Seeded MVECs attach to TEVG lumen and form a continuous endothelium by 48 hours (c). Bar represents 300 μm.

FIGURE 3

Histological section of a 4-week canine SMC TEVG. Cells and ECM form an integrated tissue throughout the scaffold. Photographed at 10X magnification.

PCL disc scaffolds were shown by the MTT assay to support increasing numbers of canine SMCs over several weeks in static culture (Figure 4).

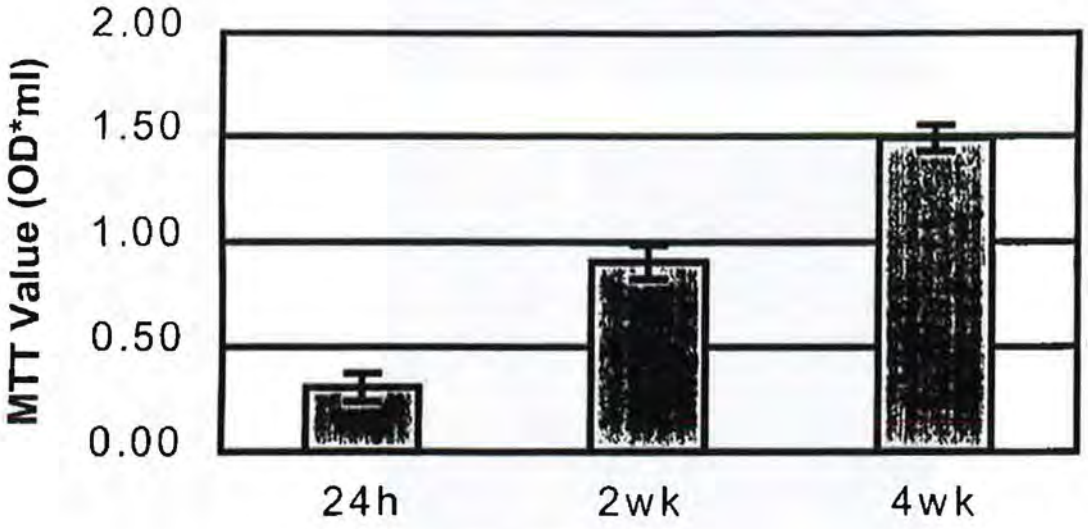

FIGURE 4

MTT analysis of TEVGs. Canine SMC numbers increased during culture on PCL scaffolds.

Cell numbers increased approximately 5-fold from 24 hours to 4 weeks. As the SMCs proliferated and colonized the scaffolds, they deposited increasing amounts of collagen (Figure 5). Similarly, disc scaffolds cultured with human DmFb or canine DmFb increased in MTT and Sirius Red values over time; these results were also observed when using cylindrical scaffolds and cultured under dynamic flow conditions (data not shown).

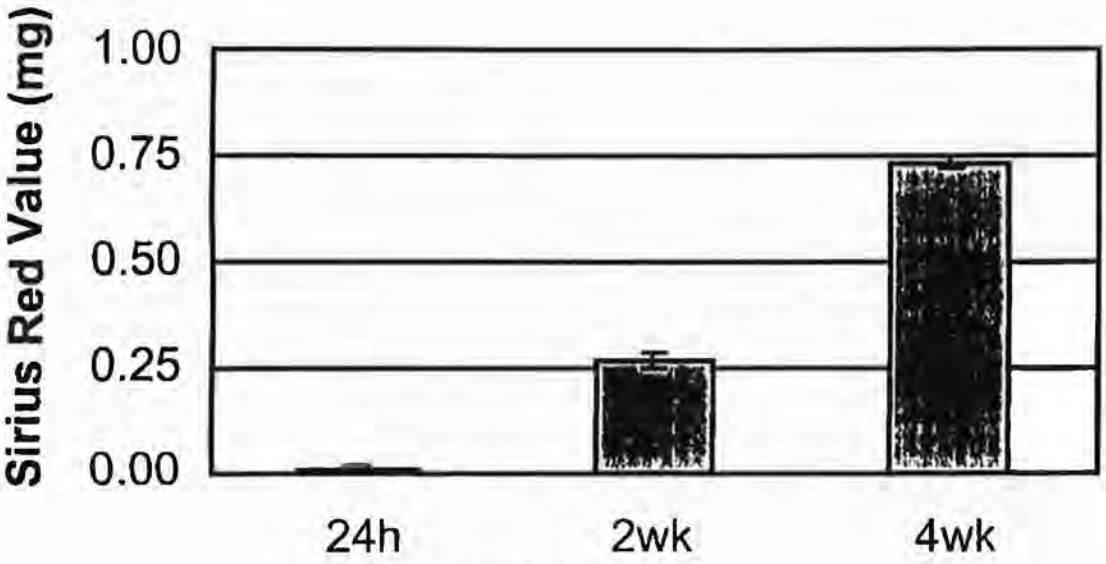

FIGURE 5

Sirius Red analysis of TEVGs. Collagen deposition from canine SMCs increased during culture on PCL scaffolds.

Immunohistochemical staining of a 6-week TEVG (Figure 6) using an anti-elastin antibody demonstrated positive staining compared with equivalent control sections receiving no primary antibody. Characteristic localized staining of the elastic laminae was observed in native canine arterial tissue, further demonstrating antibody specificity.

Canine MVECs seeded onto the lumens of canine SMC TEVGs began to attach within 4 hours. By 48 hours, the MVEC had established a confluent endothelial lining over the fibrous ECM of the TEVG (Figure 2c). This MVEC endothelium remained attached to the TEVG while subjected to low fluid low rates (100 ml/min) up to 2 weeks post-seeding (data not shown).

Mechanical Testing

Circumferential burst strengths of replicate canine SMC TEVGs (n=3) were measured at 2-week intervals during the 8-week culture period

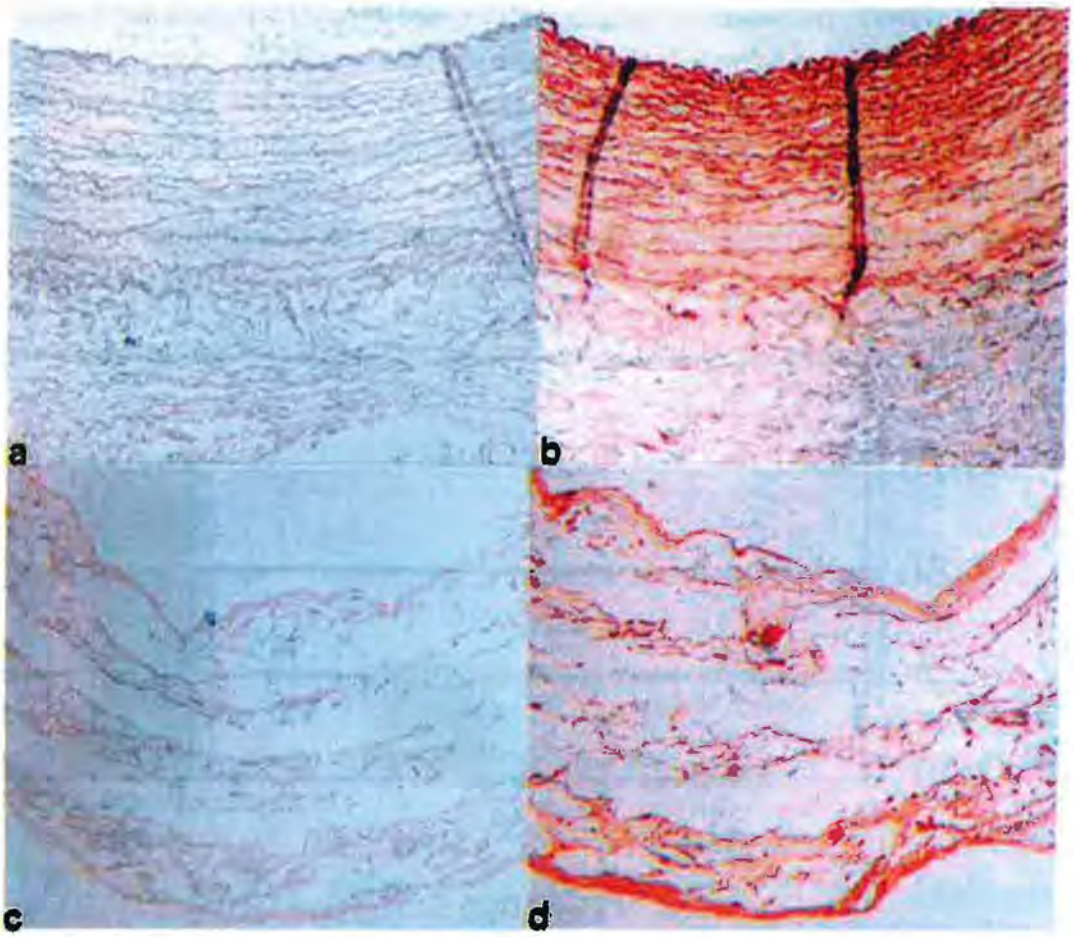

FIGURE 6

Immunohistochemical staining for elastin. Native canine artery (b) and 6-week canine SMC TEVG (d) showed positive staining when compared with control sections (a, c) which received no primary antibody. Photographed at 10X magnification.

(Figure 7). Baseline burst strengths for porous PCL scaffolds were 540 ± 65 mmHg. The strengths of the unseeded PCL scaffolds that were soaked in culture medium at 37°C did not change during the 8-week culture time (data not shown), due to the slow degradation rate of PCL. Canine SMC TEVGs at 4, 6 and 8 weeks demonstrated significantly increased burst strengths over the unseeded PCL scaffolds ($p<0.0001$). Dynamically cultured TEVGs obtained strengths of over 800 mmHg by 4 weeks. Increasing the culture time to 8 weeks further enhanced burst strengths ($p<0.005$) to over 1300 mmHg. Comparison of TEVG burst strengths from three individual canine SMC lines (n=3 each) showed uniform behavior and were comparable to PCL scaffolds seeded with canine DmFbs (approximately 800 mmHg at 6 weeks) (data not shown).

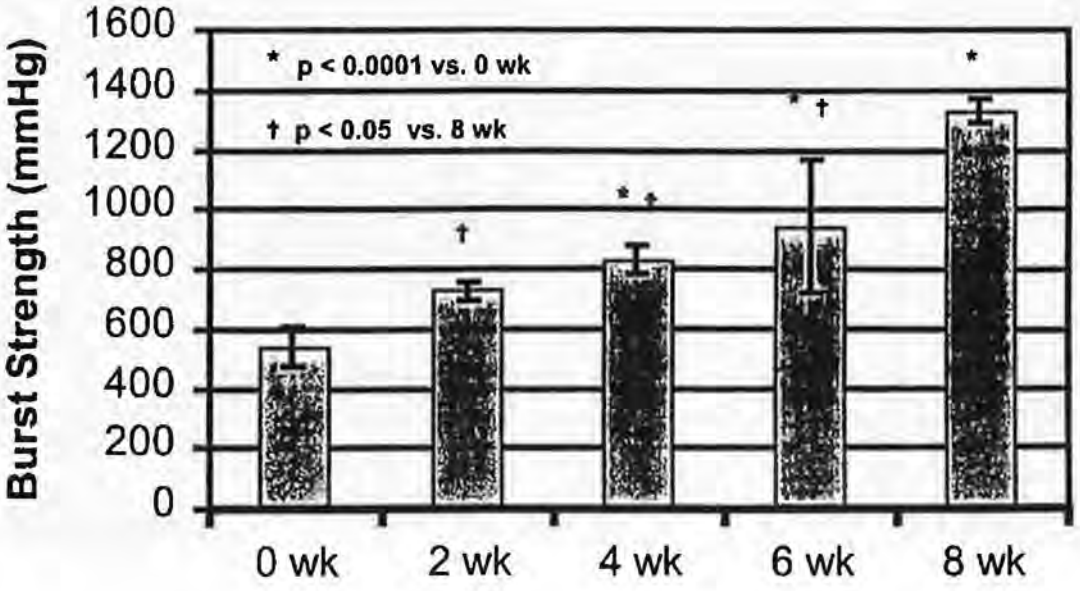

FIGURE 7

Burst pressures for PCL cylinders cultured with and without canine SMCs up to 8 weeks in a bioreactor.

Assessment of Suture Take and Handling Characteristics

Eight-week TEVGs composed of canine SMC or unseeded PCL scaffolds were sutured in place to native carotid or femoral arteries of adult dogs. Both the TEVGs (Figure 8a) and unseeded scaffolds (Figure 8b) were capable of holding 6-0 sutures for 30 and 120 minutes, respectively. Neither unseeded scaffolds nor TEVGs exhibited structural failures such as suture pull out or tearing during the implant period. TEVGs conformed better than scaffolds alone at the anastomotic sites to yield a smooth transition from native vessel to implant.

DISCUSSION

We have demonstrated that SMA-based TEVGs have burst strengths suitable for small-diameter peripheral and coronary applications in a canine implant model. TEVGs made from canine SMCs and cultured on porous PCL scaffolds developed into an integrated tissue comprised of collagen and elastin. The burst strengths obtained after 4 weeks in culture (800 mmHg) and 8 weeks in culture (1300 mmHg) are an order of magnitude greater than physiological blood pressures experienced by veins and arteries, respectively [45]. The TEVGs withstood suturing without tearing or leaking at the needle punctures.

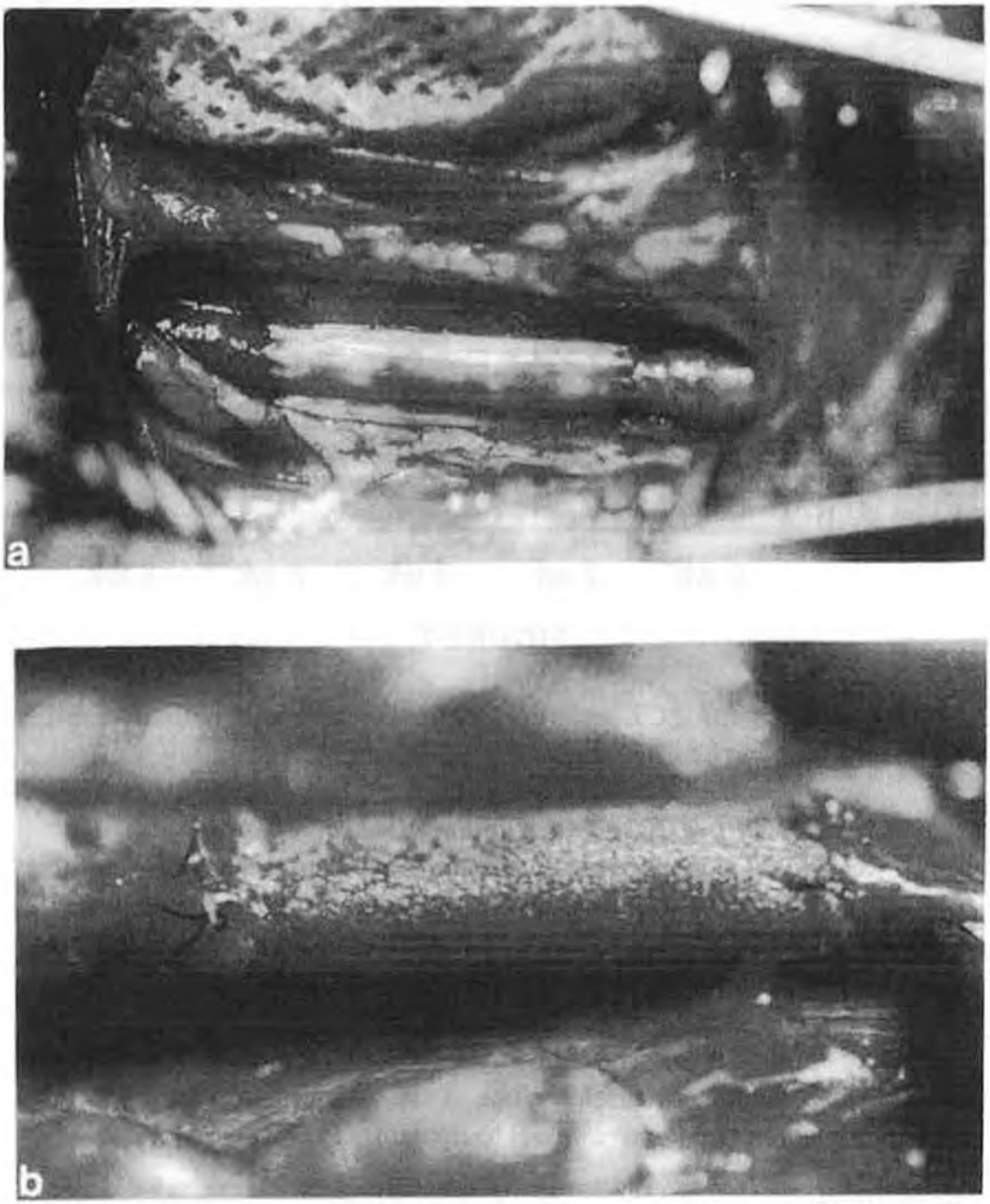

FIGURE 8

Handling characteristics of PCL scaffold and canine SMC TEVGs. Unseeded PCL scaffolds (b) accepted suture without tearing when positioned into carotid or femoral arteries of adult dogs. Eight-week TEVGs implanted into adult canine carotid arteries (a) were easily anastomosed into position.

Compliance mismatch has previously been attributed to graft failure [2, 56]. Although the mechanical properties of PCL do not match those of

native arteries, this slowly degrading polyester [17] can exist in a rubbery state at body temperature (glass transition temperature, $T_g \cong -60°C$). We have shown that SMC and DmFb will form a dense tissue matrix that can enhance the mechanical properties of the scaffold. The relatively slow degradation time of PCL may provide an advantage of gradual remodeling *in vitro* and *in vivo* without risk of structural failure. Additionally, PCL has an established use as an implant material and device component [35, 46].

Collagen and elastin are ECM proteins that compose the bulk tissue in native arteries and are responsible for the viscoelastic properties of these vessels [43, 58]. Elastin is produced within the smooth muscle layer and collagen types I and III are primarily found associated with SMCs and adventitial fibroblasts, respectively. As shown by other researchers using three-dimensional cultures of SMCs [25], we have demonstrated that our canine SMCs can form an ECM rich in collagen and elastin. Additionally, our DmFb-based TEVGs produced a mechanically strong matrix that could be used in combination with SMCs or by itself to function as an adventitia that anchors the TEVG.

The synthesis of collagen types I and III and elastin over the 8-week culture period most likely resulted in the increased strength of TEVGs compared with unseeded scaffolds. Potentially, an implant composed of living cells embedded within natural biomolecules would be more responsive to physiomechanical changes and, therefore, be more likely to maintain a normal blood flow profile [41]. Increasing the amount of collagen and elastin through chemical [10] or mechanical stimulation [42, 47] during culture could provide additional methods for increasing TEVG elasticity and may result in increased compliance matching and longer-term patency.

In healthy vessels, an intact endothelium covers the luminal face of the tunica media (the smooth muscle layer). These confluent ECs maintain smooth muscle function and prevent thrombosis through the secretion of anticoagulation factors. Rapid and complete endothelialization of TEVGs could be accomplished through EC sodding. While MVECs are different than arterial ECs, they are easily accessible for clinical treatment and have improved graft patency when sodded onto prostheses [59]. Thus, as an approach to preventing thrombosis, we tested the ability of MVECs to resurface the lumen of our TEVGs to conceal ECM proteins and SMC from blood components [1, 55]. These MVEC seeding studies

demonstrated that our TEVGs promoted EC attachment under dynamic flow conditions. EC adhesion on synthetic prostheses pre-coated with ECM proteins has been shown to be enhanced for prolonged periods under fluid shear flow [6], and ECs have been reported to migrate readily *in vitro* on ECM proteins [23, 63] such as those identified in the TEVGs. *In vivo*, however, human ECs from vessels generally migrate only 1-2 cm beyond the point of anastomosis and onto the prosthetic implant.

Recent advances in revascularization have been made with the use of EC-targeted growth factors to encourage perianastomotic and transmural endothelialization [11] and growth of new collateral vessels [51]. Of particular interest is vascular endothelial growth factor (VEGF), an angiogenic and vasculogenic molecule produced by SMCs [19] and activated macrophages [18]. As an independent therapy, VEGF has been inserted into occluded vessels by direct injection or through delivery of naked genetic material [60]. This marks two approaches in which growth factors stimulate the body to utilize its natural regenerative capacity. Tissue engineered grafts made of human DmFbs grown on three-dimensional scaffolds have been reported to secrete a number of growth factors including VEGF as well as basic fibroblast growth factor (bFGF), platelet-derived growth factor (PDGF), and transforming growth factor-beta (TGF-β) [31]. Similarly, SMCs also produce such growth factors [19, 21, 26, 49]. We hypothesize that a TEVG capable of secreting such biomolecules will provide an added benefit of delivering physiologic and therapeutic doses of growth factors that would encourage endothelialization and host tissue integration.

A TEVG could potentially have unique benefits such as promoting seamless integration at the anastomoses, providing healthy tissue to replace diseased autologous tissue, responding to physiological cues by growing with the adjacent tissue, and adapting mechanically to the *in vivo* hemodynamic environment to maintain normal blood flow profiles.

Treatment of artherosclerotic and stenotic vessels using angioplasty, coupled with endoscopically-guided intraluminal stent delivery, has gained acceptance as a minimally invasive procedure to increase the patency of constricted vessels. Traditional stent designs, however, further damage the already abraded and diseased vessel wall and poorly integrate with the adjacent vessel tissue, leading to a high rate of restenosis and limiting long-term patency [13, 33, 50].

We believe that the principles applied to developing a TEVG could also be relevant for developing tissue engineered stents. While the creation of a tissue engineered stent is not without its challenges, a living, bioengineered stent comprised of cells grown into a porous scaffolding may overcome several limitations of current stent therapy: in particular, it may integrate more uniformly with the native vessel to form a smooth vascular lining, the healthy tissue may help reduce the propensity for restenosis, or it may minimize thrombosis at the stent-blood interface by secreting anti-thrombotic or thrombolytic agents [24].

Advanced Tissue Sciences' tissue engineering technology has recently been extended to include gene therapy to address a broad range of diseases, including cardiovascular applications [39]. Using our core technology, genetically modified cells may be seeded onto a biocompatible scaffold to form a structural tissue capable of secreting therapeutic proteins. Sustaining long-term expression is one of the key technical hurdles facing the gene therapy industry. Implantation of living and physiologically functioning three-dimensional, tissue-engineered products may provide a safe and effective means for local or systemic delivery of therapeutic proteins to patients with cardiovascular pathologies.

Through continued applied research and incorporation of break-through discoveries, tissue engineering may provide treatment solutions for vascular disease.

ACKNOWLEDGEMENTS

The authors wish to thank John Wright and Sheila Dela Cruz for their assistance in the preparation of this manuscript.

This research was funded in part with the United States Government support under cooperative agreement 70NANB7H3060 awarded by the National Institute of Standards and Technology Advanced Technology Program.

REFERENCES

1. Badimon, L, JJ Badimon, A Galvez. Influence of Arterial Damage and Wall Shear Rate on Platelet Deposition: *Ex vivo* Study in a Swine Model. Arteriosclerosis 1986; 6:312-320

2. Ballyk, PD, C Walsh, J Butany, M Ojha. Compliance Mismatch May Promote Graft-Artery Intimal Hyperplasia By Altering Suture-Line Stresses. J Biomech 1998; 31:229-237
3. Bedossa, P, G Lemaigre, JM Bacci. Quantitative Estimation of the Collagen Content in Normal and Pathologic Pancreas Tissue. Digestion 1989; 44:7-13
4. Bell, E, HP Ehrlich, DJ Buttle, T Nakatsuji. Living Tissue Formed in vitro and Accepted As Skin-Equivalent Tissue of Full Thickness. Science 1981; 211:1052-1054
5. Bonny, JD, H Leuenberger. Matrix Type Controlled Release Systems: Effect of Percolation on Drug Dissolution Kinetics. Pharm Acta Helv 1991; 66:160-164
6. Bujan, J, N Garcia-Honduvilla, L Contreras, et al. Coating PTFE Vascular Prostheses with a Fibroblastic Matrix Improves Cell Retention When Subjected to Blood Flow. J Biomed Mater Res 1998; 39:32-39
7. Burke, JF, IV Yannas, WCJ Quinby, et al. Successful Use of a Physiologically Acceptable Artificial Skin in the Treatment of Extensive Burn Injury. Ann Surg 1981; 194:413-428
8. Canver, CC. Conduit Options in Coronary Artery Bypass Surgery. Chest 1995; 108:1150-1155
9. Carmines, DA, JH McElhaney, R Stack. A Piece-Wise Non-Linear Elastic Stress Expression of Human and Pig Coronary Arteries Tested in vitro. J Biomech 1991; 24:899-906
10. Davidson, J, O Zoia, J Liu. Modulation of Transforming Growth Factor-Beta 1 Stimulated Elastin and Collagen Production and Proliferation in Porcine Vascular Smooth Muscle Cells and Skin Fibroblasts by Basic Fibroblast Growth Factor, Transforming Growth Factor-Alpha, and Insulin-Like Growth Factor-I. J Cell Physiol 1993; 155:149-156
11. Doi, K, S Satoh, T Oka, T Matsuda. Impregnation of Basic Fibroblast Growth Factor on a Microporous Small Caliber Graft Enhances Vascularization. ASAIO J 1996; 42:M394-M398
12. Dunkelman, N, AE Peterson, LK Landeen, J Zeltinger. Apparatus and Method for Sterilizing, Seeding, Culturing, Storing, Shipping and Testing Tissue, Synthetic or Native, Vascular Grafts. US Pat No 5,792,603. Advanced Tissue Sciences, Inc, USA. 1998
13. Elderman, ER, C Rogers. Pathobiologic Responses to Stenting. Am J Cardiol 1998; 81:4E-6E

14. Emery, RW, LD Joyce, KV Arom. Operative Considerations in Implantation of the Perma-Flow Graft. Ann Thorac Surg 1994; 58: 1770-1773
15. Emery, RW, NL Mills, FJ Teiheira, et al. North American Experience with the Perma-Flow Prosthetic Coronary Graft. Ann Thorac Surg 1996; 62:691-696
16. Emery, RW, R Petersen, C Baumgard, DM Nicoloff. First Clinical Use of the Possis Synthetic Coronary Graft. J Card Surg 1993; 8: 439-442
17. Engelberg, I, J Kohn. Physio-Mechanical Properties of Degradable Polymers Used in Medical Applications: a Comparative Study. Biomaterials 1991; 12:292-304
18. Fava, R, et al. Vascular Permeability Factor/Endothelial Growth Factor (VPF/VEGF): Accumulation and Expression in Human Synovial Fluids and Rheumatoid Synovial Tissue. J Exp Med 1994; 180:341-346
19. Ferrara, N, J Winer, T Burton. Aortic Smooth Muscle Cells Express and Secrete Vascular Endothelial Growth Factor. Growth Factors 1991; 5:141-148
20. Fitzgibbon, GM, HP Kafka, AJ Leach, WJ Keon, et al. Coronary Bypass Graft Fate and Patient Outcome: Anigiographic Follow-Up of 5,065 Grafts Related to Survival and Reoperation in 1,388 Patients During 25 Years. J Am Coll Cardiol 1996; 28:616-626
21. Gospodarowicz, D, et al. Basic Fibroblast Growth Factor: Expression in Cultured Bovine Vascular Smooth Muscle Cells. Eur J Cell Biol 1988; 46:144-151
22. Hansbrough, JF, DW Mozingo, GP Kealey, et al. Clinical Trials of a Biosynthetic Temporary Skin Replacement, Dermagraft-Transitional Covering, Compared with Cryopreserved Human Cadaver Skin for Temporary Coverage of Excised Burn Wounds. J Burn Care Rehabil 1997; 18:43-51
23. Hoch, J, BE Jarrell, T Schneider, SK Williams. Endothelial Cell Interactions with Native Surfaces. Annals of Vascular Surgery 1989; 3:153-159
24. Katzen, BT, GJ Becker, JF Benenati, G Zemel. Stent Grafts for Aortic Aneurysms: the Next Interventional Challenge. Am J Cardiol 1998; 81:33E-43E
25. Kim, B-S, DJ Mooney. Engineering Smooth Muscle Tissue with a Predefined Structure. J Biomed Mater Res 1998; 41:322-332

26. Kirschenlohr, HL, et al. Adult Human Aortic Smooth Muscle Cells in Culture Produce Active TGF-Beta. Am J Physiol 1993; 265:C571-C576
27. Klein, MB, D Shaw, S Barese, et al. A Reliable and Cost-Effective in vitro Assay of Skin Viability for Skin Banks and Burn Centers. J Burn Care Rehabil 1996; 17:565-570
28. Kruger, KA, H Tabuteau, ES Snitkin. Healing Hearts, Getting Paid: a Preview of the American College of Cardiology Conference. Montgomery Securities, San Franciso, CA, 1997
29. Lee, DA, E Assoku, V Doyle. A Specific Quantitative Assay for Collagen Synthesis by Cells Seeded in Collagen-Based Biomaterials Using Sirius Red F3B Precipitation. J Mat Sci: Mater Med 1998; 9: 47-51
30. L'Heureux, N, L Germain, R Labbe, FA Auger. Structural Analysis of a Tissue Engineered Vascular Equivalent: Photonic and Electronic Microscopy Studies. J Cell Biochem 1994; Supplement 18C 1994: 281
31. Liu, KK, E Pinney, J Mansbridge. Cryopreservation of the Three Dimensional Fibroblast-Derived Tissue, Dermagraft, Induces Cellular Responses that Promote Wound Healing. 8th Annual Meeting of the European Tissue Repair Society, Copenhagen, Denmark, 1998: P78
32. Love, CS, T Zelenovic, TJ Dahl. An Intro-Operatively Constructed Autologous Tissue Small Diameter Blood Vessel Substitute. International Society for Applied Cardiovascular Biology Sixth Biennial Meeting, Wildbad Kreuth, Munich, 1998: IV-10
33. Mak, KH, G Belli, SG Ellis, DJ Moliterno. Subacute Stent Thrombosis: Evolving Issues and Current Concepts. J Am Coll Cardiol 1996; 27:494-503
34. Mansbridge, J. Skin Substitutes to Enhance Wound Healing. Expert Opinion on Investigational Drugs 1998; 7:803-809
35. Middleton, JC, AJ Tipton. Synthetic Biodegrable Polymers as Medical Devices. Medical Plastics and Biomaterials 1998:30-39
36. Miki, I, N Ishihara, M Otoshi, H Kase. Simple Colorimetric Cell-Cell Adhesion Assay Using MTT-Stained Leukemia Cells. J Immunol Meth 1993; 164:255-261
37. Motwani, JG, EJ Topol. Aortocoronary Saphenous Vein Graft Disease. Circulation 1998; 97:916-931
38. Naughton, G, J Mansbridge, G Gentzkow. A Metabolically Active Human Dermal Replacement for the Treatment of Diabetic Foot Ulcers. Artif Org 1997; 21:1203-1210

39. Naughton, G, B Naughton. Three-Dimensional Genetically Engineered Cell and Tissue System. US Pat No 5,785,964. Advanced Tissue Sciences, Inc, US.1998
40. Naughton, GK, WR Tolber, TM Grillot. Emerging Developments in Tissue Engineering and Cell Technology. Tiss Engin 1995; 1: 211-219
41. Noishiki, Y, Y Tomizawa, Y Yamane, et al. Acceleration of Neointima Formation in Vascular Prostheses by Transplantation of Autologous Venous Tissue Fragments. J Thorac Cardiovasc Surg 1993; 105:796-804
42. Owens, G. Role of Mechanical Strain in Regulation of Differentiation of Vascular Smooth Muscle Cells. Circ Res 1996; 79:1054-1055
43. Ozola, BO, G Svikis, D Mungalov, L Slutskii. Statistical Analysis of the Effect of Biochemical Composition Morphometric Indices on the Mechanical Properties of the Cardiac Coronary Arteries Relative to Age. Mech Comp Mater 1984; 20:105-111
44. Parodi, EN, GA Kaiser, M Wolff, ATW Kovalik, JR Malm. Comparative Study of the Tensile Strength of Autogenous Systemic Veins and Preserved Venous Homografts. J Surg Res 1972; 12:99-104
45. Patton, HD, AF Fuchs, B Hille, et al. Introduction and Physical Principles. In: Scher, AM, EO Feigl (Editors). **Textbook of Physiology: Circulation, Respiration, Body Fluids, Metabolism, and Endocrinology Vol. 2,** WB Saunders Co, Philadelphia, PA, 1989: 778
46. Pitt, CG. Poly-ε-caprolactone and its Copolymers. In: Chasin, ML (Editor). **Biodegradable Polymers and Drug Delivery Systems,** Marcel Dekker, New York, 1990: 71-120
47. Reusch, P, H Wagdy, R Reusch, E Wilson, H Ives. Mechanical Strain Increases Smooth Muscle and Decreases Nonmuscle Myosin Expression in Rat Vascular Smooth Muscle Cells. Circ Res 1996; 79: 1046-1053
48. Shin'oka, T, D Shum-Tim, PX Ma, RE Tanel, N Isogai, R Langer, JP Vacanti, JE Mayer, Jr. Creation of Viable Pulmonary Artery Autografts Through Tissue Engineering. J Thorac Cardiovasc Surg 1998; 115:536-546
49. Sjolund, M, et al. Arterial Smooth Muscle Cells Express Platelet-Derived Growth Factor (PDGF) A Chain mRNA, Secrete a PDGF-Like Mitogen, and Bind Exogenous PDGF in a Phenotype- and Growth State-Dependent Manner. J Cell Biol 1988; 106:403-413

50. Sniderman, KW. Noncoronary Vascular Stenting. Prog Cardiovasc Dis 1996; 39:141-164
51. Tabata, H, M Silver, JM Isner. Arterial Gene Transfer of Acidic Fibroblast Growth Factor for Therapeutic Angiogenesis in vivo: Critical Role of Secretion Signal in Use of Naked DNA. Cardiovasc Res 1997; 35:470-479
52. Triglia, D, S Braa, C Yonan, G Naughton. Cytotoxicity Testing Using Neutral Red and MTT Assays on a Three-Dimensional Human Skin Substrate. Toxic in vitro 1991; 5:573-578
53. US Dept of Health and Human Services. Vital and Health Statistics: Ambulatory and Inpatient Procedures in the United States, 1995. US Dept of Health and Human Services, Centers for Disease Control, National Institute of Health, Washington, DC, 1998
54. Valderrama, R, S Navarro, E Campo, J Camps, A Gimenez, A Pares, J Caballeria. Quantitative Measurement of Fibrosis in Pancreatic Tissue: Evaluation of a Colorimetric Method. Int J Pancreatol 1991; 10:23-29
55. van Zanten, GH, E Saelman, K Schut-Hese, Y Wu, P Slootweg, H Nieuwenhuis, P de Groot, J Sixma. Platelet Adhesion to Collagen Type IV Under Flow Conditions. Blood 1996; 88:3862-3871
56. Walden, R, GJ L'Italien, J Megerman, WM Abbott. Matched Elastic Properties and Successful Arterial Grafting. Arch Surg 1980; 115: 1166-1169
57. Weinberg, CB, E Bell. A Blood Vessel Model Constructed from Collagen and Cultured Vascular Cells. Science, 1986; 231: 397-400
58. Wight, T. Arterial Wall. In: Wight, T (Editor). **Extracellular Matrix,** Harwood Academic Publisher, London,1996
59. Williams, SK, BE Jarrell, DG Rose. Human Microvessel Endothelial Cell Isolation and Vascular Graft Sodding in the Operating Room. Ann Vasc Surg 1989; 3:146-152
60. Witzenbilcher, B, T Asahara, T Murohara, M Silver, I Spyridopoulos, M Magner, N Principe, M Kearney, JS Hu, JM Isner. Vascular Endothelial Growth Factor-C (VEGF-C/VEGF-2) Promotes Angiogenesis in the Setting of Tissue Ischemia. Am J Pathol 1998; 153:381-394
61. Yu, A, H Dardik, F Wolodiger, et al. Everted Cervical Vein for Carotid Patch Angioplasty. J Vasc Surg, 1990; 12: 523-526
62. Zdrahala, RJ. Small Caliber Vascular Grafts. Part I: State of the Art. J Biomater Appl 1996; 10:309-329

63. Zilla, P, R Fasol, M Grimm, et al. Growth Properties of Cultured Human Endothelial Cells on Differently Coated Artificial Heart Materials. J Thorac Cardiovasc Surg 1991; 101:671-680

Part III

BIOLOGIC RESPONSE

Chapter 8

LASER SCANNING CONFOCAL FLUORESCENCE MICROSCOPY: AN EMERGING TECHNIQUE FOR THE PATHOLOGIC EVALUATION OF CARDIOVASCULAR DEVICES

Stephen L Hilbert, MD, PhD, Zu-Xi Yu, MD, PhD,
Steven Archuleta, BA, Victor J Ferrans, MD, PhD

The purpose of this communication is to briefly describe our experience with the use of laser scanning confocal fluorescence microscopy for the assessment of cardiovascular device-related pathology. This emerging technology allows for the simultaneous multicolor imaging of paraffin or frozen sections stained with fluorochrome-labeled antibodies and/or specific fluorescent reagents. This imaging can be combined with other modes of microscopy, such as Nomarski differential interference contrast (DIC), phase contrast or incident polarized light microscopy. In addition, Z-scans (optical cross sections at multiple levels within the tissue section) can be obtained and used for three-dimensional reconstruction of the topographic distribution of the fluorescent labeling.

Keywords: *Confocal microscopy, histopathology, cardiovascular prosthetic device, immunohistochemistry, apoptosis*

Stephen L Hilbert, MD, PhD (corresponding authors), Center for Devices and Radiological Health, Food and Drug Administration, 12725 Twinbrook Parkway, Rockville, MD 20852
Stent Graft Update, Edited by J Vossoughi, N Kipshidze, JW Karanian

Through the appropriate selection of primary and secondary antibodies or specific stains (*eg*, for nuclear DNA) and laser excitation and fluorescence emission wavelengths, confocal microscopy makes it possible to visualize up to four fluorescent markers or stains with minimal fluorescent quenching (fading or photobleaching). In our laboratory, we routinely employ a confocal microscope (Model TCS-4DMIR-BE, Leica, Heidelberg, Germany) to obtain images of histologic sections stained using secondary antibodies labeled with fluorescein isothiocyanate (FITC; green fluorescence) and Texas Red (red fluorescence) and nuclear DNA stains with 2,6-diamidino-4-phenylindole (DAPI; blue fluorescence). These methods provide unique information concerning the colocalization of intra- or extracellular components in normal and pathological conditions.

The practical application of these methods will be illustrated by describing our experience with the use of laser scanning confocal fluorescence microscopy to study explanted allograft heart valves. We will also discuss potential applications of this technology for the investigation of: 1) the biological and pathological effects of cardiovascular prosthetic devices being developed as viable tissue-engineered prostheses (*eg*, blood vessels and heart valves), and 2) the effects of biomechanical factors on tissue remodeling in valved conduits or within vascular walls in response to angioplasty or the placement of vascular stents or stented-grafts.

ALLOGRAFT HEART VALVES

We have recently reported [5] our pathological findings on a series of allograft heart valves that were implanted in the systemic circulation in juvenile sheep for periods of time ranging from 2 days to 20 weeks. In these animals, both cryopreserved and fresh allograft aortic valves were implanted in the mid-thoracic aorta (left thoracotomy, 4th intercostal space) using proximal and distal end-to-end anastomoses following the temporary placement of a bypass shunt to prevent spinal cord ischemia and subsequent paraplegia. It was also necessary to create a shunt (5 mm diameter expanded polytetrafluoroethylene vascular graft) between the distal aortic arch (approximately 2 cm proximal to the allograft anastomosis) and the left atrium. This shunt increased the aortic pulse pressure by decreasing the diastolic pressure by approximately 10 - 15 mmHg, and increased the left atrial pressure by 12 - 14 mmHg. However, this shunt did not result in the development of congestive heart failure in chronic animals (20 weeks). The creation of this shunt provided the appropriate hemodynamic conditions needed to ensure the

full range of motion and coaptation of the leaflets of the allograft valve, as confirmed by Doppler echocardiography. When the shunt was either cross-clamped or occluded, the leaflets would simply flutter throughout the cardiac cycle.

Fifteen aortic valves, including five native unimplanted valves and 10-explanted allograft conduits (six fresh allografts and four cryopreserved), were studied. Histopathologic examination showed that the cusps of the allograft valves had become acellular by the 20th week after implantation. In an effort to determine the pathogenesis of this loss of cell viability, explanted allograft valves were studied at the following intervals after implantation: 2 days, 8 days, 10 days, 14 days, 30 days and 20 weeks. Initial histologic and ultrastructural observations following 30 days of implantation demonstrated that the cusps already had undergone a significant reduction in cellularity (Figures 1 and 2). In addition, changes suggestive of apoptosis [2] (programmed cell death), such as pyknotic and fragmented nuclei (Figure 3) and deeply eosinophilic cytoplasm, were observed in endothelial cells and connective tissue cells of the allografts (Figure 4A).

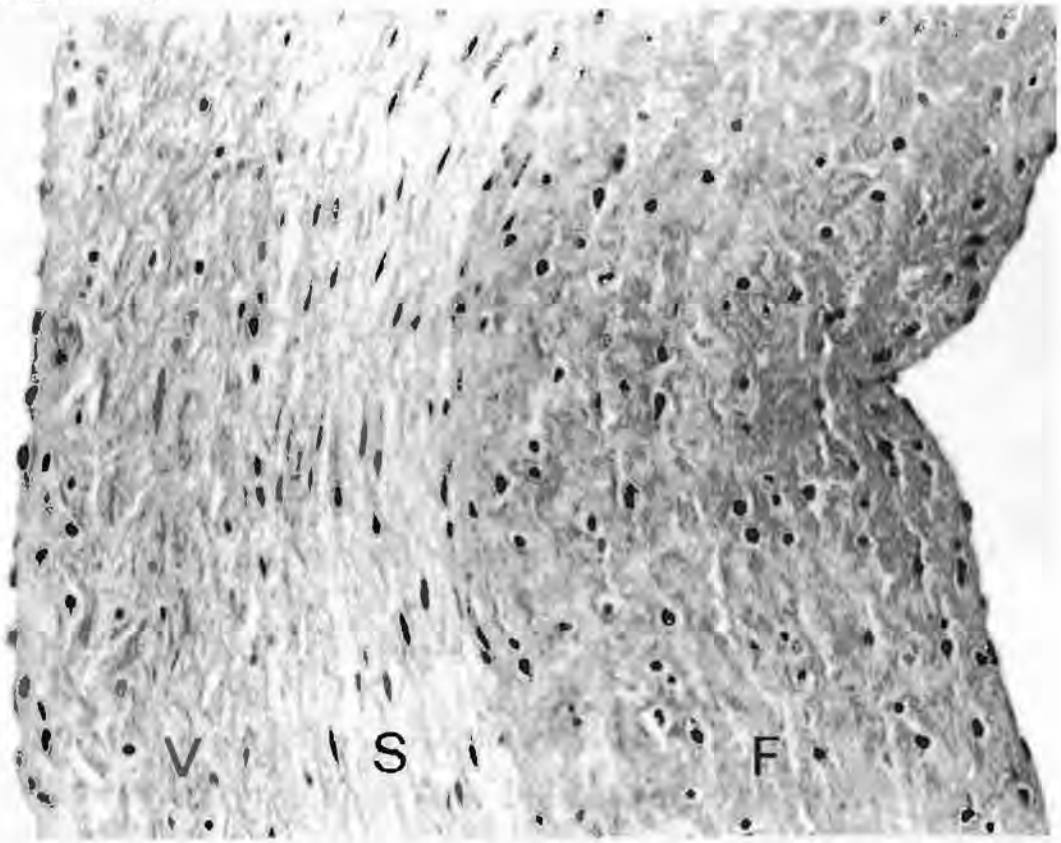

FIGURE 1

Light micrograph demonstrating the characteristic histologic trilaminar structure and the cellularity of a native ovine aortic valve cusp. F: fibrosa; S: spongiosa; V: ventricularis. H&E stain. X 630

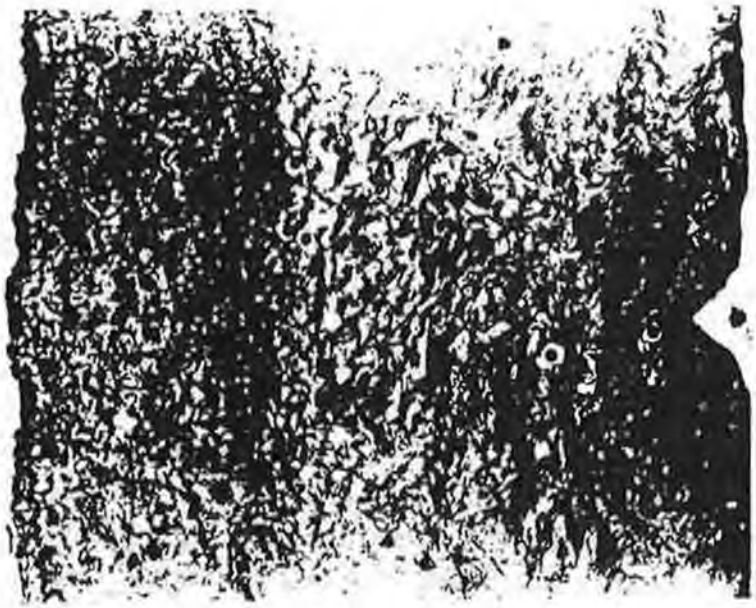

FIGURE 2

Histologic section of a cryopreserved ovine aortic valve allograft implanted for 30 days. A marked decrease in cuspal cellularity is depicted. Note the loss of the trilaminar architecture characteristic of the aortic valve cusp. Compare with Figure 1. H&E stain. X 630

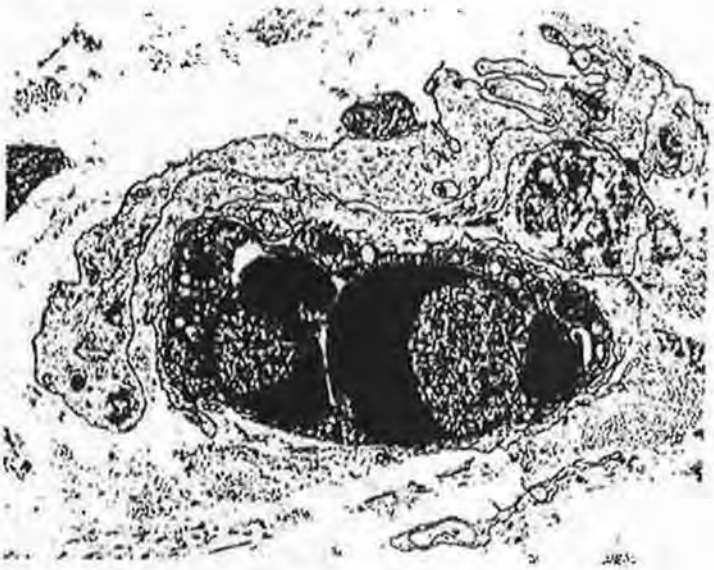

FIGURE 3

Transmission electron micrograph depicting an apoptotic body that consists of condensed and fragmented nuclear chromatin: apoptotic bodies are derived from cells undergoing apoptisis and are clearly indicative of this phenomenon. Cryopreserved ovine aortic valve allograft implanted for 30 days. Uranyl acetate/lead citrate stain. X 6,000

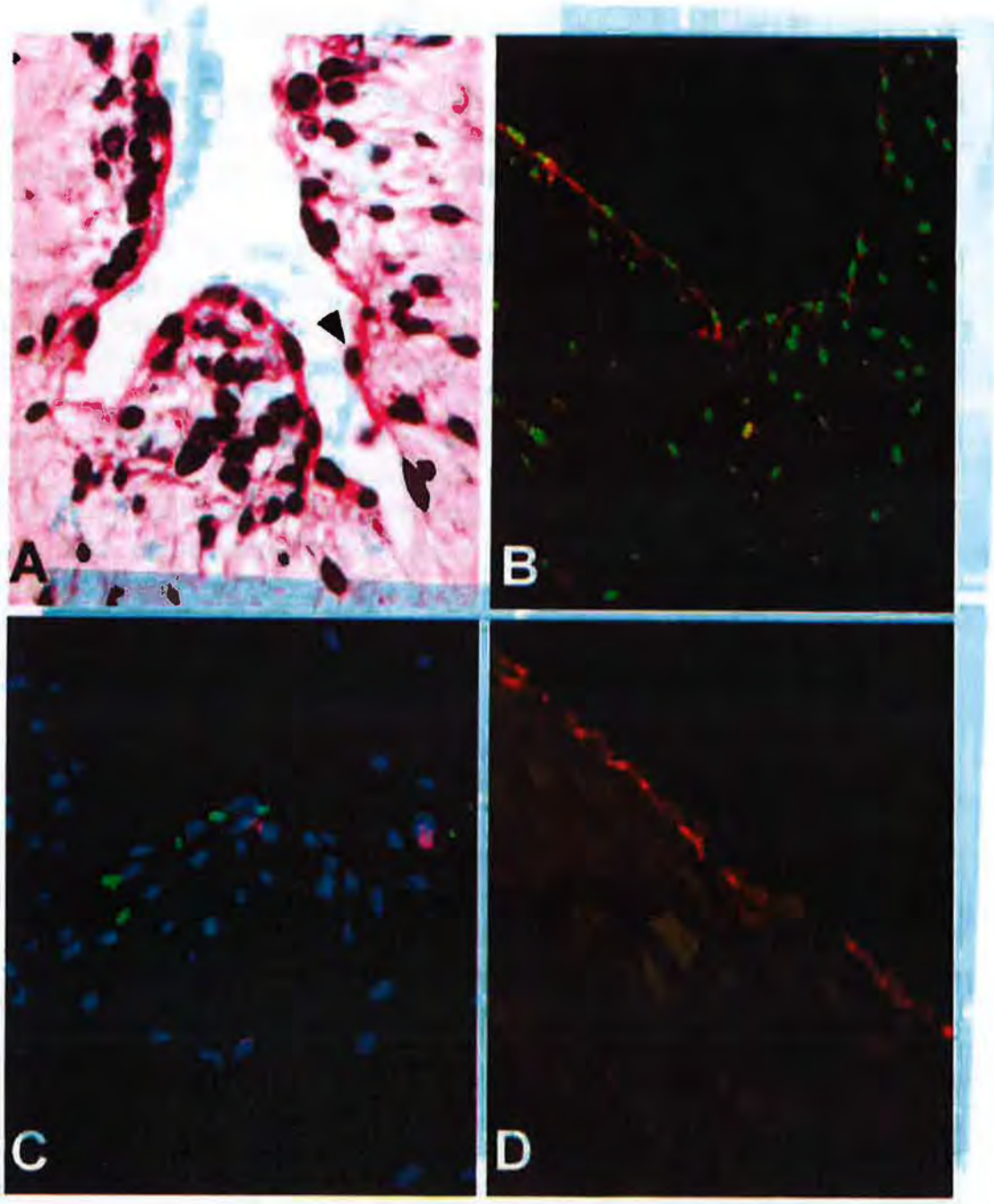

FIGURE 4

A. Light micrograph depicting pyknotic nuclei in endothelial and cuspal cells. Increased cytoplasmic eosinophila is also noted in cell containing pyknotic nuclei (arrowhead). Cryopreserved ovine aortic valve allograft implanted for 10 days. H&E stain, X 1000,
(caption continued on next page)

FIGURE 4 (Caption continued from page 119)

B. Confocal image of a native aortic valve cusp illustrating PCNA-reactive nuclei (green fluorescence) in myofibroblasts and endothelial cells. The latter cells are identified by their reactivity for Factor VIII (red fluorescence). X 200

C. Fresh ovine aortic valve allograft implanted for 10 days. In situ nick end labeling shows apoptotic nuclei (yellow green fluorescence) in the fibrosa. Non-apoptotic nuclei are stained with DAPI (blue fluorescence). Compare with Figure 4A, which illustrates pyknotic nuclei. X 400

D. Confocal image of the fibrous sheath encasing the cusp of a fresh ovine aortic valve allograft implanted for 20 weeks. The endothelial cells lining the surface of the fiberous sheath show a positive reaction for Factor VIII (red fluorescence) and are believed to be of host origin. PCNA-positive nuclei (green fluorescence) are not observed in myofibroblasts or endothelial cells, X 400

To evaluate the loss of cuspal cell viability and the occurrence of apoptosis, paraffin sections of routinely fixed tissues (phosphate-buffered 10% formalin) were prepared from the central third of each allograft cusp (cut from the base to the free edge). Immunohistochemical staining protocols were developed for the simultaneous demonstration of: 1) nick end labeling for the detection of apoptosis, by means of the incorporation of FITC-labeled deoxynucleotides by terminal dexoynucleotidyl transferase (ApopTag direct in situ apoptosis detection kit #S7160, Oncor, Inc, Gaithersburg, MD); 2) Factor VIII-related antigen (rabbit polyclonal antibody; DAKO, Corp, Carpinteria, CA) using a Texas red-conjugated secondary antibody (Vector Laboratories, Burlingame, CA) and 3) nuclear DNA staining using a 0.01% aqueous solution of DAPI (Sigma Chemical Co, St Louis, MO). In a second protocol for triple labeling, staining for PCNA (Figure 4B), with a mouse monoclonal antibody (DAKO) and an FITC-conjugated secondary antibody, was employed instead of the first step of the method outlined above. Negative controls consisted of the omission of the primary antibody and substitution of normal goat or rabbit IgG for the primary antibody. Positive controls for apoptosis included: 1) treatment of tissue sections with DNAse I to induce DNA cleavage similar to that found in apoptotic cells, and 2) simultaneous staining of sections of rat mammary gland undergoing postpartal involution, in which apoptotic cells are known to be numerous.

The results of the immunohistochemical studies described above indicate that a marked reduction in the mitotic activity of cuspal cells occurred within two days of implantation, as demonstrated by the loss of PCNA reactivity normally present in valvular endothelial cells and connective tissue cells. Reactivity for PCNA was rarely seen after 30 days of implantation and was essentially absent at 20 weeks. Apoptosis, as demonstrated by in situ nick end labeling and by transmission electron microscopy, was observed in both endothelial cells and connective tissue cells two days after implantation and reached a peak between 10 (Figure 4C) and 14 days, resulting in nuclear fragmentation (Figure 3) and the formation of intra- and extracellular apoptotic bodies, which were most numerous at 30 days of implantation. Neither apoptosis nor PCNA reactivity was observed in the fibrous sheath (of host origin) encapsulating the cusp at 20 weeks after implantation (Figure 4D). Analysis of this data suggests that multiple factors associated with the harvesting, processing and implantation of allograft valves may contribute to the initiation of apoptosis and the subsequent loss of cuspal cellularity.

FUTURE APPLICATIONS

Tissue Engineering: Viable Cardiovascular Prostheses

Various prototypes of viable vascular grafts and valved conduits are being developed as new concepts in tissue engineering evolve. Immunohistochemical methods are expected to play an important role in the characterization of unimplanted prostheses as well as in the identification of specific device-related postimplantation changes. Knowledge gained from these studies will help identify the specific mechanisms that are responsible for alterations in the expected performance of tissue-engineered prosthetic devices. Such studies will also serve to facilitate the development of tissue processing methods capable of mitigating or reducing device-related pathological alterations. For example, it is reasonable to hypothesize, based on our findings on allograft heart valve, that viable tissue-engineered valved conduits may be rendered nonviable by the loss of cellularity due to apoptosis [5]. Further studies defining initiators, promoters and suppressors of apoptosis in valvular tissue may provide a scientific basis for the development of tissue processing methods designed to prevent this type of cell death.

In addition to tissue processing and biochemical factors, which may be responsible for the initiation of bioprosthetic device-related pathology, biomechanical factors also must be considered in this regard. The influence of cyclic [illegible]

residual stresses within the tissue-engineered bioprostheses also should be expected to result in observable postimplantation changes in both the cellular and extracellular matrix components of these viable cardiovascular devices. The effects of biomechanical factors on gene expression, cellular proliferation and the synthesis and stability of extracellular matrix components are not known. It is interesting to note that apoptosis of smooth muscle cells has been reported to be induced by biomechanical factors (compressive and tensile stresses) associated with angioplasty [3, 8]. Apoptosis also has been demonstrated to develop in cardiac myocytes [1] subjected to excessive mechanical stretching and in endothelial cells and epithelial cells being mechanically detached from their underlying connective tissue matrix [9]. The latter phenomenon constitutes a special type of apoptosis known as anoikis [9]. Furthermore, stretching of cardiac fibroblasts also has been shown to increase the expression of activators of matrix metalloproteinases (MMPs) [13], enzymes that mediate the breakdown of extracellular components of connective tissue [12]. These enzymes are secreted as inactive proenzymes (pro-MMPs), which are activated in the extracellular space by cleavage of their carboxy terminus by membrane-type metalloproteinases (MT-MMPs). Membrane-type MMP-2 has been reported to be increased in cardiac fibroblasts that have been exposed to cyclic stretching [13].

Immunohistochemical and confocal microscopy studies have been initiated in our laboratory to characterize the activity of MMPs in muscular arteries, native heart valves and bioprosthetic valves, as well as in various tissue engineered vascular prostheses and valved conduits. Initial studies of this type have resulted in recognition of the importance of MMPs in the pathogenesis of the aortic aneurysms and aortic valvular lesions that develop in patients with the Marfan syndrome [11].

Tissue Remodeling: Biomechanical Factors

Tissue remodeling is mediated by a complex and integrated series of mechanisms involving cell proliferation, apoptosis and the synthesis and degradation of the extracellular matrix [2, 7, 8]. The extensive clinical use of stents for the treatment of coronary artery stenosis and the investigational use of stent-grafts for the treatment of abdominal aortic aneurysms has raised fundamental scientific questions concerning the long-term influence of biomechanical factors (particularly the retention of residual stresses [6] within the vessel wall) on vascular remodeling. To the best of our knowledge, no studies have been conducted to assess: 1) the magnitude of residual stresses within the vessel wall after the placement of a stent or a stent- graft, or 2) the biological responses to

these residual stresses. Immunohistochemical and laser scanning confocal fluorescence microscopy methods are being developed in our laboratory to evaluate the occurrence of apoptosis and the immunoreactivity for PCNA and MMPs in muscular and elastic arteries in which residual stresses have been documented. Studies of these basic biological mechanisms are expected to provide information addressing: 1) tissue remodeling and the pathogenesis of coronary artery restenosis after stent placement, and 2) the development of proximal and distal neck dilatation of abdominal aortic aneurysms following the long-term use of stent-grafts.

SUMMARY

The application of immunohistochemical staining methods and the use of laser scanning confocal fluorescence microscopy for the evaluation of allograft heart valve pathology is described. These methods have led to the demonstration of apoptosis as a cause of the loss of cuspal cell viability in implanted allograft valves. Thus, these studies present a specific example of the capability of these methods for the elucidation of pathologic mechanisms. In addition, various preliminary and ongoing studies are described to further illustrate the utility of these methods for the assessment of fundamental problems in tissue engineering and tissue remodeling, with emphasis on the long-term performance of cardiovascular bioprosthetic devices.

REFERENCES

1. Anversa, P, L Annarosa, A Beltrami, et al. Myocyte Death and Growth in the Failing Heart. Lab Invest 1998; 78:767-786
2. Bauriedel, G, S Schluckebier, R Hutter, et al. Apoptosis in Restenosis Versus Stable-Angina Atherosclerosis: Implications for the Pathogenesis of Restenosis. Arterioscler Thromb Vasc Biol 1998; 18:1132-1139
3. Cummings, MC, CM Winterford, NI Walker. Apoptosis. Am J Surg Pathol 1997; 21:88-101
4. Fujiwara, OJ, A Kawamura, M Katsuragawa, et al. Acute Cellular Damage in Medial Smooth Muscle Cells Following Experimental Coronary Angioplasty in Dog. Damage of Cytoskeleton and Apoptosis. Heart Vessels 1997; 12:157-166
5. Hilbert, SL, RE Luna, J Zhang, et al. Allograft Heart Valves: The Role of Apoptosis-Mediated Cell Loss. J Thorac Cardiovasc Surg 1999; 117:454-462

6. Hong, MK, J Vossoughi, GS Mintz, et al. Altered Compliance and Residual Strain Precede Angiographically Detectable Early Atherosclerosis in Low-density Lipoprotein Receptor Deficiency. Arterioscler Thromb Vasc Biol 1997; 17:2209-2217
7. Kearney M, A Pieczek, L Haley, et al. Histopathology of In-stent Restenosis in Patients with Peripheral Artery Disease. Circulation 1997; 95:1998-2002
8. Kollum, M, S Kaiser, R Kinscherf, et al. Apoptosis after Stent Implantation Compared with Balloon Angioplasty in Rabbits. Role of Macrophages. Arterioscler Thromb Vasc Biol 1997; 17:2383-2388
9. Li, AE, H Ito, KS Kim, et al. The Role of Reactive Oxygen Species in Anoikis. Circ Res, (Submitted)
10. Perlman, H, L Maillard, K Krasinsi, K Walsh. Evidence for the Rapid Onset of Apoptosis in Medial Smooth Muscle Cells after Balloon Injury. Circulation 1997; 95:981-7
11. Segura, AM, RE Luna, K Horiba, et al. Immunohistochemistry of Matrix Metalloproteinase and their Inhibitors in Thoracic Aortic Aneurysms and Aortic Valves of Patients with Marfan's Syndrome. Circulation 1998; 98:II-331-338
12. Stetler-Steveson, WG. Dynamics of Matrix Turnover during Pathologic Remodeling of the Extracellular Matrix. Am J Pathol 1996; 148:1345-1350
13. Tyagi ,SC, K Lewis, D Pikes, et al. Stretch-Induced Membrane Type Matrix Metalloproteinase and Tissue Plasminogen Activator in Cardiac Fibroblast Cells. J Cell Physiol 1998; 176:374-382

Chapter 9

THROMBOSIS AND THROMBOEMBOLISM IN STENT GRAFTS: EVALUATING VIRCHOW'S TRIAD

William R Wagner, PhD, Kenneth L Gage

Stent grafts present artificial surfaces to ongoing blood contact and thus have an associated risk of thrombosis and thromboembolism. In this report, the incidence of thrombosis and thromboembolism in stent graft patients will briefly be reviewed, followed by a discussion of the potential mechanisms contributing to thrombosis in these cardiovascular devices. Methodologies for assessing and modeling factors controlling stent graft thrombosis will be addressed for *in vitro*, animal, and clinical environments.

INCIDENCE OF THROMBOSIS AND THROMBOEMBOLISM

In Table 1, recent reports citing the occurrence of thrombosis and/or thromboembolism are summarized for a variety of stent graft devices. Of particular note is the large difference seen in the rate between devices placed in the aorto-iliac position (3-10%) and those placed peripherally in the femoro-popliteal location (36-44%) [5, 6, 9, 12, 18, 20, 32, 39].

Keywords: *Thrombosis, thromboembolism, platelets, endovascular graft, biomaterials, fluid dynamics, computational fluid dynamic analysis*

William R Wagner, PhD (corresponding author), University of Pittsburgh, Center for Biotechnology and Bioengineering, Room 407, 300 Technology Drive, Pittsburgh, PA 15219

Stent Graft Update, Edited by J Vossoughi, N Kipshidze, JW Karanian

Experience with peripheral placement is certainly limited with respect to the increasing number of patients with aorto-iliac stent grafts. An increased incidence of thrombosis and thromboembolism would be expected for smaller diameter endovascular grafts; however, simply based on analogous differences in thrombotic complications for traditional synthetic vascular graft placement.

TABLE 1

SELECTION OF CLINICAL REPORTS OF THROMBOSIS &/OR EMBOLISM

Investigators	Device(s)	Patients	%Thrombosis &/or Embolism
Stelter et al ('97) [39]	Stentor/Vanguard Talent	201	10%
Blum et al ('97) [5]	Stentor/Vanguard	154	3%
Chuter et al ('97) [9]	Chuter-Gianturco	55	9%
Broeders et al ('97) [6]	EVT	77	6%
Dereume et al ('97) [12]	Corvita	35	6%
Parodi et al ('97) [6]	Parodi System	88	3%
Hayoz et al ('97) [18]	Cragg EndoPro*	9	44%
Henry et al ('96) [20]	Cragg EndoPro*	67	36%

* Femoro-poplital, all others aorto-iliac

The learning curve associated with the development and placement of any cardiovascular device will often lead to decreasing rates of complications such as thrombosis. With stent grafts a major potential instigator of thrombosis is graft kinking. Increasing experience has lead clinicians to develop maneuvers for kink avoidance, and better imaging has assisted in the diagnosis of the problem and verification of smooth placement. On the device design front, manufacturers have improved

stent support schemes and introduced appropriate graft material crimping to reduce the propensity for kink generation.

The source of emboli associated with stent graft placement and residence remains somewhat undefined. The disturbance of atherosclerotic plaques with device positioning and stent expansion may generate emboli in the periprocedural period. Plaque components or thrombi formed on subluminal vessel constituents exposed by device placement may provide this embolic source. The exposed polymeric biomaterial of the graft or the exposed metallic components of the stent will serve as sites for thrombotic deposition and present an ongoing risk for clinically significant thromboemboli generation. Preexisting patient coagulopathy or, possibly, the existence of a subclinical prothrombotic state [36] believed to exist in many individuals with cardiovascular disease may serve to elevate the thrombotic risk associated with damaged vascular and device surfaces.

GENERAL ISSUES IN CARDIOVASCULAR DEVICE THROMBOSIS

An excellent framework for the discussion and investigation of cardiovascular device thrombosis is provided by the observations of the famous 19th century German pathologist, Rudolf Virchow, on venous thrombosis. Virchow's triad of blood, surface, and flow as determinants in the development of venous thrombosis similarly describe the factors by which cardiovascular device thrombosis can both be initiated and controlled. Here we will discuss each component of the triad in turn and suggest methodologies for analyzing that particular variable to aid in the characterization stent graft (or more generally, cardiovascular device) thrombotic risk.

FLOW

An artificial surface in contact with blood has a propensity for generating platelet agonists. These platelet agonists can come from the activation of enzyme cascades by the surface, such as the generation of complement products C3a, C5a, and C5b-9 or coagulation activation resulting in thrombin generation. Platelets previously deposited and activated on the surface can support platelet agonist generation by providing a catalytic surface for cascade reactions (e.g. thrombin production) or by the release of platelet derived agonists such as ADP and thromboxane A_2. The net result of this process may be thought of as a flux of platelet agonists from the surface. The surface flux is dependent upon the characteristics of the

artificial surface and on the propensity of the blood to generate agonists (the other two components of Virchow's triad). Assuming that the condition of the blood and the artificial surface(s) are fixed, the concentrations of platelet agonists experienced by platelets in blood passing over the surface is controlled by the flow through the device. This concept is illustrated schematically in Figure 1.

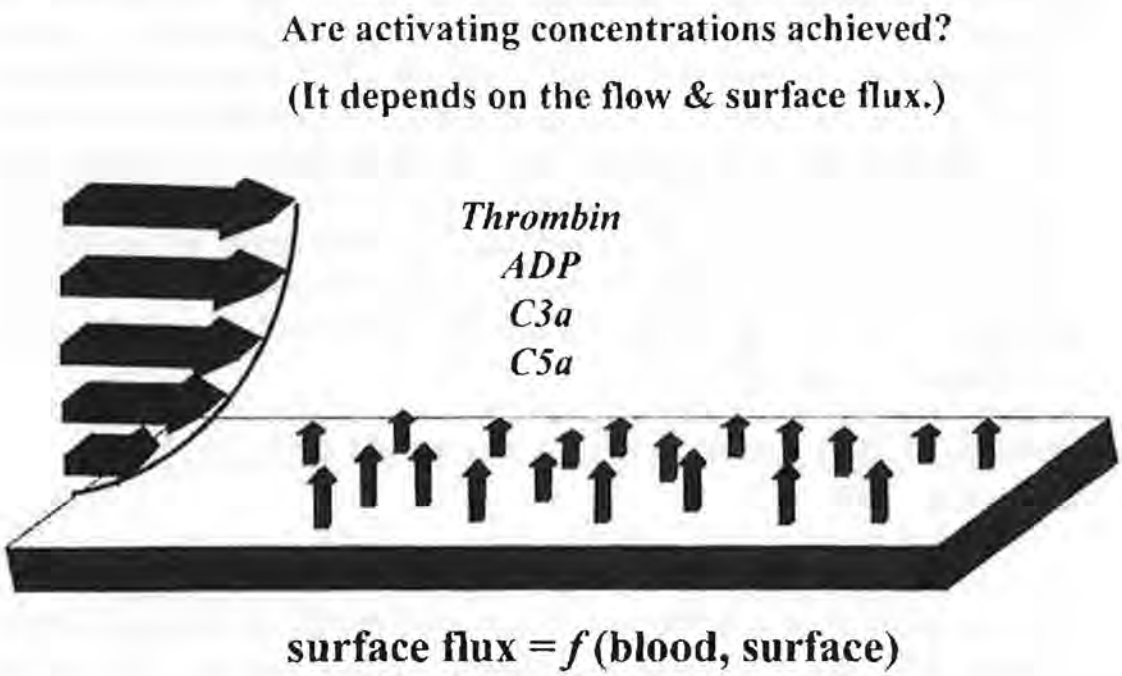

FIGURE 1

The regions near an artificial surface at risk for achieving concentrations capable of activating platelets are dependent upon the flux from the surface of platelet agonists and the flow field above the surface. The surface flux will depend upon the characteristics of the surface and the contacting blood.

Relating a flux of platelet agonists from a surface to the concentrations of platelet agonists found in the vicinity of the surface in the presence of blood flow can be modeled mathematically by solving the equations for the conservation of mass and momentum [13, 22]. Using this technique one can model whether activating thresholds of particular platelet agonists are achieved within the device and the location of these regions of risk. The availability of increasingly sophisticated computational fluid dynamics (CFD) software packages combined with similarly advancing computational power allow the modeling of transport phenomena in increasingly complex geometries [10, 28, 30]. Such models are useful in quantitatively illustrating the role of flow in device thrombosis.

With regard to stent graft thrombosis, some simple CFD models are presented here to illustrate the potential insights one might gain with this technique. These models were solved using a commercial, finite volume based CFD code, Fluent 5.0 (Lebanon, NH). In Figure 2, flow through a two-dimensional representation of a femoral stent graft is presented. In this model, flow is well-developed (parabolic velocity profile) and non-pulsatile. An arbitrarily fixed flux of a theoretical platelet agonist is assumed to be generated on the artificial surface. For blood volumetric flow rates similar to that experienced in the femoral artery, it can be seen that the regions achieving activating concentrations of platelet agonist are limited to near the wall. Considering the same biomaterial, or rather the same wall flux of platelet agonist, with a flow rate reduced by 80%, the regions within the graft achieving platelet activating levels of agonist increase markedly in Figure 3. To illustrate the effects of a kink within a stent graft, the two-dimensional model presented in Figure 4 was constructed. The flux of platelet agonist generated from the wall is the same as for the previous examples, and the blood flow rate is the normal rate used for Figure 2. Distal to the kink, a region of reduced fluid velocities leads to the buildup of platelet agonist and creates a location theoretically at risk for thrombotic deposition.

The results presented here with the simplified CFD models are useful for comparative purposes and support what is already intuitive: regions of poor perfusion are at risk for thrombotic deposition. The value of CFD models lies in their ability to make quantitative comparisons and to potentially investigate complex geometries. Three-dimensional models incorporating kinks and bifurcations are readily achievable, as are investigations of microflows near crimped surfaces and the incorporation of pulsatile flow. The modeling of actual platelet agonist flux rates for specific biomaterials would offer more meaningful data, but much work remains to develop and verify the parameters required for such models.

Another means of investigating flow issues in cardiovascular devices is to map local fluid velocities within the device. Flow visualization techniques utilizing transparent models of device geometries and a transparent blood analogue fluid seeded with fluorescent microsphere tracers have been utilized to map velocity fields in a number of devices [41, 45]. Using pulsed laser illumination of the microspheres in specific imaging planes, the velocity field in a region of interest can be mapped using digital image processing of particle traces. An alternative velocity mapping technique, frequently utilized in the assessment of prosthetic

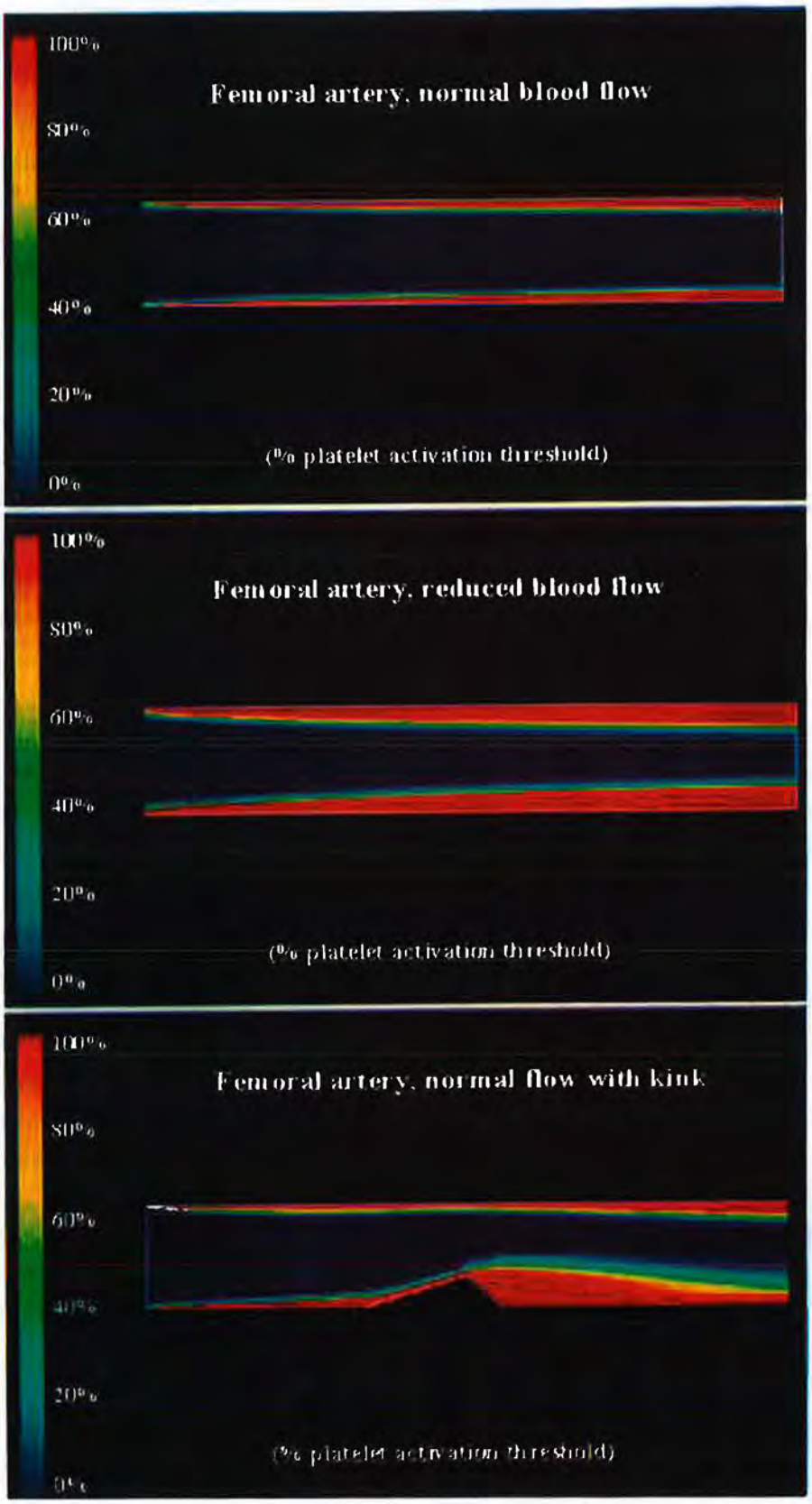

FIGURE 2 (Top), FIGURE 3 (Middle), FIGURE 4 (Bottom)
(captions on page 131)

FIGURE 2 Caption (for Figure on page 130)

The concentrations of a theoretical platelet agonist generated on an artificial surface are modeled using a two-dimensional CFD model of a femoral artery graft. The geometry shown has a 6mm width (or diameter) and a 36mm length. A parabolic, constant velocity profile was introduced at the graft inlet on the left, with flow from left to right. The mean blood velocity at the inlet was 12 cm/s, corresponding to a typical average velocity in a femoral artery. An arbitrary scale was applied to demonstrate the regions at risk for achieving activating concentrations of a theoretical platelet agonist generated with a constant flux from the surface.

FIGURE 3 Caption (for Figure on page 130)

The same model of a femoral artery graft as in Figure 2 was modeled with the same wall flux of theoretical platelet agonist. In this case, the flow was reduced by 80% to an average flow rate of 2.4 cm/s. The reduction in flow is seen to markedly increase the regions possessing activating concentrations of the platelet agonist.

FIGURE 4 Caption (for Figure on page 130)

An idealized kink is introduced into the geometry of the femoral graft of Figure 2 while maintaining the blood flow rate and the surface flux of platelet agonist of that earlier model. Distal to the kink, the region theoretically capable of activating platelets is extended into the graft cross section.

---

heart valves, is laser Doppler velocimetry [29]. With flow mapping techniques, features such as recirculation and turbulent flow can be identified and device design can potentially be altered to minimize these features. In the case of stent grafts, the risks associated with specific levels of tortuosity and kinking for a relevant range of blood flow rates could be illustrated.

SURFACE

Protein adsorption occurs rapidly upon the exposure of an artificial surface to blood. The proteins which adsorb, the extent to which they adsorb, and the orientation and unfolding of these adsorbed proteins is believed to dictate the biological response to the implanted material [15].

Two major consequences of blood protein adsorption onto biomaterial surfaces are the activation of enzymatic cascades and the facilitation of cell adhesion. The coagulation and complement cascades are triggered by specific proenzyme adsorption and activation. Platelet and leukocyte adhesion is mediated by the adsorption of proteins such as fibrinogen, vitronectin and C3b. When both processes occur on an implanted surface, synergistic interactions can occur. For instance, surface generated thrombin can activate nearby platelets and provide a catalytic phospholipid surface for more efficient thrombin generation. Platelets activated by increasing concentrations of surface generated thrombin are more likely to upregulate adhesion receptors and deposit onto the biomaterial surface.

Under Virchow's hypothesis as applied to cardiovascular devices, if the state of the blood and the flow environment are kept constant, device thrombogenicity will be a function of material thrombogenicity. Since the ability of a material to mediate platelet deposition is determined by protein adsorption, it would seem rational to focus on relating protein deposition profiles to the risk for thrombosis. Unfortunately, although attempts have been made [7, 31], specific relationships between complex protein deposition profiles and thrombogenic risk remain largely undefined. One is left with relating thrombotic deposition, or secondary effects due to this deposition, to material properties.

Surface thrombogenicity is commonly assessed *in vitro* using the perfusion of whole blood over material surfaces of interest. A number of methodologies have been employed to measure cellular deposition following perfusion. Radiolabeling of platelets, as well as visible light and electron microscopic evaluation of surface platelet deposition are common. Epifluorescence microscopy used with fluorescently labeled platelets in whole blood allows the visualization of platelet deposition, in real time [23]. With this temporal assessment technique, thromboembolization can be observed on a microscopic scale. Given the potential for some material surfaces to remain relatively free of substantial thrombotic deposition while still consuming platelets, presumably by generating thromboemboli [8], one must be cautious about reaching conclusions regarding thromboembolism based on end-point deposition data alone.

In vitro surface evaluation has the potential advantage of separating the flow effects of a given device from material effects. Utilizing material-coated components such as coverslips, perfusion systems can be designed to provide a well-defined, constant flow environment [24].

Comparative testing between candidate materials or material coatings can be conducted at the desired wall shear rate with human blood. Some of the disadvantages of such a system are artifacts introduced by blood contact with non-test surfaces, the requirement for relatively high levels of anticoagulation, and the limitation of acute contact times. Mock circulatory loops containing the device can be employed to provide complex flow environments, but these systems generally require large blood volumes (making the use of human blood less feasible) and remain limited by the constraints outlined above.

An animal model offers advantages over *in vitro* models by allowing chronic blood-material contact at reasonable levels of anticoagulation (or in the absence thereof). Arterio-venous shunts can be created in larger animals to permit the testing of surfaces under controlled flow environments [8]. Alternatively, the actual device, or an appropriately scaled version can be evaluated in situ to combine flow and material effects. The major disadvantage of animal models stems from differences in hemostatic system reactivity between the various animal models and the human [38].

A primary means for quantifying material thrombogenicity in the animal model is careful explant analysis of the surface or device. As described by Anderson [2], a systematic approach addressing a wide variety of biocompatibility concerns including thrombosis is appropriate. Specific issues relating to thrombosis and thromboembolism include: 1) the evaluation of spatial variations in thrombotic deposition, which may reflect flow effects; 2) assessment of thrombosis on nearby tissue surfaces; 3) documentation of embolic damage evident in distal organ beds; and 4) evaluation of the healing or foreign body response on all device surfaces. During the animal implant, a number of techniques are available to assess thrombosis and thromboembolism. Flow variations and tissue perfusion distal to the device can be quantified [27], and radiolabeling of platelets can be combined with gamma camera imaging of the device or distal tissue beds. The latter technique is well illustrated by the work of Schneider et al [37], where increased emboli shedding to the feet of baboons was reported distal to Dacron versus ePTFE containing shunts.

Surface thrombogenicity assessment in the clinic often depends upon documentation of tissue ischemia resulting from thromboembolism or device occlusion and the evaluation of subclinical thrombosis using radiography, ultrasonography, and distal perfusion or pressure measurements. Direct imaging of platelet deposition is possible using

^{111}In-oxine labeled platelets [33, 40]. Although explant analysis presents a greater challenge logistically, the importance of a careful device retrieval and analysis protocol is essential for acquiring data from the most relevant of settings. The issues addressed in animal trials should likewise be pursued and reported for devices explanted from patients.

BLOOD

The status of the coagulation enzymes, platelets, and, to some extent, inflammatory cells and proteins will determine the capacity of an artificial surface with a given hemodynamic environment to support thrombosis and thromboembolism. Many control points exist for the down-regulation of coagulation and inflammatory reactions as well as cellular activation and adhesion. Indeed, pharmaceutical control of blood coagulability opened the door for a wide variety of procedures and therapies involving extensive blood-material contact. In that blood transports many of the participants and byproducts of the reactions occurring near the surface of the cardiovascular device to distal sites in the vasculature, remote evaluation of subclinical thrombosis and thromboembolism can often be achieved by assaying this blood for appropriate factors. The feasibility of such an approach will depend upon factor dilution or clearance occurring prior to the distal sampling site and the thrombotic activity generated by the device. With regard to stent grafts, the thrombotic signal generated may be expected to be measurable for many indices based upon studies with traditional vascular grafts [11, 42].

For *in vitro* studies, the opportunity to directly evaluate the surface for thrombosis at various time points reduces the need for evaluation of thrombotic byproducts. Furthermore, the problems associated with blood contact with non-test surfaces and time spent removed from the body often lead to the loss of the signal attributable to the material of interest in the noise of the background activation reactions. Under well-controlled conditions and with well-designed experimental set-ups, the measurement of thrombotic byproducts can be used for evaluation purposes [19, 26]. More commonly, a simple blood assay such as the reduction of platelet count is employed to indirectly verify deposition of platelets onto the surface or device of interest.

Animal models are much more appropriate than *in vitro* studies for the utilization of blood sampling for the characterization of material or device thrombogenicity. Measurements of the platelet count, or better, platelet life span through the use of radiolabeled or biotinylated platelets

allow interpretation of the consumption of platelets due to participation in thrombotic processes [1, 3, 17]. The use of assays for specific participants and byproducts of thrombotic reactions remains a challenge in most animal models, with the possible exception of primates such as baboons [21, 34]. This limitation is due to a lack of cross-reactivity for many of the monoclonal antibodies used in commercial immunoassay kits for coagulation and platelet factors. Likewise, the lack of cross-reactivity of anti-human monoclonal antibodies used in flow cytometric evaluation of cellular participants is problematic. There have been reports, however, where cross-reactivity has been found or where monoclonal antibodies specific for the animal model of interest have been characterized and employed [4, 16].

Blood sampling offers the greatest potential in the clinical setting and has been used to characterize the performance of a wide variety of cardiovascular devices. An increasingly diverse array of immunoassays is available for the measurement of plasma concentrations of coagulation, inflammation, fibrinolytic, and platelet activation byproducts. Likewise, reports utilizing flow cytometric evaluation of circulating platelet microaggregates, platelet-leukocyte aggregates, activated platelets, and activated leukocytes for the characterization of device performance have become more common in the literature [43]. With these assays, the potential exists for the determination of critical pathways related to thrombotic complications associated with a particular device as well as comparative studies between device designs or distinct patient groups. The ability to use such assays for the prediction of an impending adverse event appears less likely at present, however.

THROMBOSIS AND STENT GRAFT DESIGN

Although intraluminal thrombus formation on the stent graft surface is not desirable, the opposite is true on the vessel wall side, where thrombotic sealing and the encouragement of tissue incorporation of the graft material are beneficial (Figure 5). Achieving these differential device requirements will likely require the employment of coating technologies on one or both surfaces. The encouragement of appropriate cellular interactions with these surfaces (endothelial cells on the lumen side, fibroblasts on the wall side) might ultimately be achieved by the provision of adhesion peptides that can discriminate among cell types [25], or by the judicious selection of growth factors and co-factors on each surface [14]. An adaptation of endothelial cell seeding or sodding of the luminal surface to increase the likelihood of the rapid development of a luminal antithrombotic surface might prove beneficial[44].

Advancements in this area will face the unique constraints of graft deployment through low profile catheters and the possible alteration by balloon dilation of material characteristics [35].

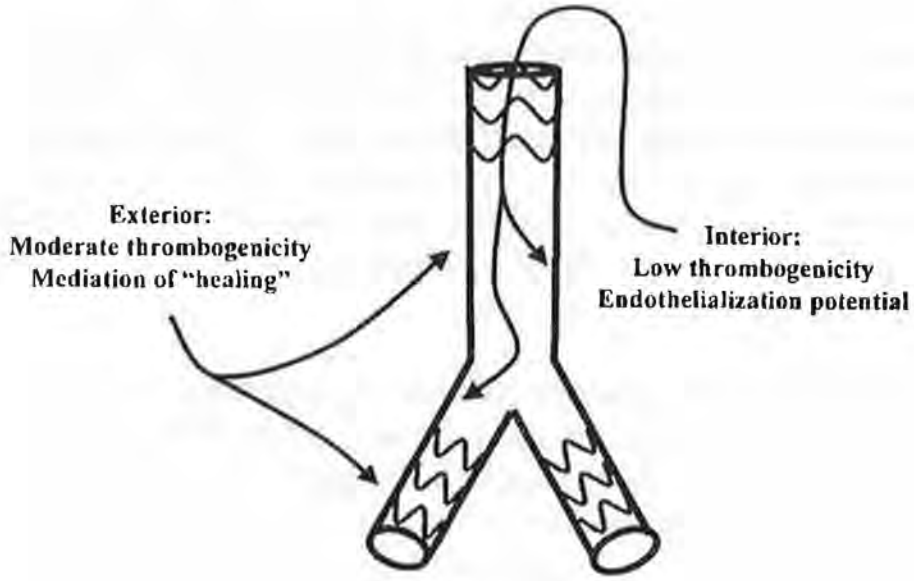

FIGURE 5

The differential surface design considerations are illustrated for the stent graft. Surface coatings or modification strategies may permit such surfaces to be created.

The application of stent graft methodologies to small diameter peripheral sites, as well as to sites with a low tolerance for thromboembolic complications (*eg* carotid placement), will depend upon adequate strategies for preventing the propensity of artificial surfaces to support thrombosis. Virchow's triad provides a framework for studying and ultimately addressing this phenomenon. Investigators must keep in mind the interplay of flow, surface, and blood in defining the constraints of the problem and ultimately in designing solutions.

ACKNOWLEDGEMENTS

This work was partially supported by a grant from the Whitaker Foundation (WRW).

REFERENCES

1. Al-Mondhiry, H, WE Pae, CA Miller, WS Pierce. Platelet and Fibrinogen Survival in Calves Implanted with Artificial Heart and

Ventricular Assist Device: Correlation with Autopsy Findings. Thromb Haemostas 1992; 67:413-416

2. Anderson, JM. Cardiovascular Device Retrieval and Evaluation. Cardiovasc Pathol 1993; 2(Suppl.):199S-208S
3. Bake,r LC, MV Kameneva, MJ Watach, et al. Assessment of Bovine Platelet Life Span with Biotinylation and Flow Cytometry. Artif Organs 1998; 22:799-803
4. Baker, LC, WC Davis, J Autieri, et al. Flow Cytometric Assays to Detect Platelet Activation and Aggregation in Device-implanted Calves. J Biomed Mater Res 1998; 41:312-321
5. Blum, U, G Voshage, J Lammer, et al. Endoluminal Stent-Grafts for Infrarenal Abdominal Aortic Aneurysms. N Engl J Med 1997; 336: 13-20
6. Broeders, IAMJ, JD Blakensteijn, BC Eikelboom. The EndoVascularTechnologies System. In: Hopkinson, B, W Yusuf, S Whitaker, F Veith (Editors). ***Endovascular Surgery for Aortic Aneurysms***. WB Saunders, Philadelphia, 1997, 104-121
7. Chinn, JA, TA Horbett, BD Ratner. Baboon Fibrinogen Adsorption and Platelet Adhesion to Polymeric Materials. Thromb Haemost 1991; 65:608-617
8. Cholakis, CH, W Zingg, MV Sefton. Effect of Heparin-PVA Hydrogel on Platelets in a Chronic Canine Arterio-venous Shunt. J Biomed Mater Res 1989; 23:417-441
9. Chuter, TAM. Chuter-Gianturco Bifurcated Stent-Grafts for Abdominal Aortic Aneurysm Exclusion. In: Hopkinson, B, W Yusuf, S Whitaker, F Veith (Editors). **Endovascular Surgery for Aortic Aneurysms**. WB Saunders, Philadelphia, 1997, 88-103
10. de Leval, MR, G Dubini, F Migliavacca, et al. Use of Computational Fluid Dynamics in the Design of Surgical Procedures: Application to the Study of Competitive Flows in Cavopulmonary Connections. J Thorac Cardiovasc Surg 1996; 111:502-513
11. De Mol Van Otterloo, JC, JH Van Bockel, ED Ponfoort, et al. Systemic Effects of Collagen-impregnated Aortoiliac Dacron Vascular Prostheses on Platelet Activation and Fibrin Formation. J Vasc Surg 1991; 14:59-66
12. Dereume JP, J Ferreira. The Corvita System. In: Hopkinson B, Yusuf W, Whitaker S, Veith F (Editors). **Endovascular Surgery for Aortic Aneurysms.** WB Saunders, Philadelphia, 1997, 122-139
13. Folie, BJ, LV McIntire. Mathematical Analysis of Mural Thrombogenesis: Concentration Profiles of Platelet-Activating Agents and Effects of Viscous Shear Flow. Biophys J 1989; 56: 1121-1141

14. Greisler ,HP, C Gosselin, D Ren, et al. Biointeractive Polymers and Tissue Engineered Blood Vessels. Biomaterials 1996; 17:329-336
15. Grunkemeier, J, C Wan, T Horbett. Changes in Binding Affinity of a Monoclonal Antibody to a Platelet Binding Domain of Fibrinogen Adsorbed to Biomaterials. J Biomater Sci Polym Ed 1996; 8:189-209
16. Harasaki H, K Fukamachi, M Benavides, et al. A Comprehensive Hematologic Study in Calves with Total Artificial Hearts. ASAIO J 1995; 41:M266-M271
17. Harker, LA, SJ Slichter, LR Sauvage. Platelet Consumption by Arterial Prostheses: The Effects of Endothelialization and Pharmacologic Inhibition of Platelet Function. Ann Surg 1977; 186: 594-601
18. Hayoz D, DD Do, F Mahler, et al. Acute Inflammatory Reaction Associated with Endoluminal Bypass Graft. J Endovasc Surg 1997; 4:354-360
19. Hedeman Joosten, PP, HJ Verhagen, GJ Heijnen-Snyder, et al. Thrombogenesis of Different Cell Types Seeded on Vascular Grafts and Studied Under Blood-flow Conditions. J Vasc Surg 1998; 28: 1094-1103
20. Henry M, M Amor, A Cragg, et al. Occlusive and Aneurysmal Peripheral Arterial Disease: Assessment of a Stent-Graft System. Radiology 1996; 201:717-724
21. Hiramatsu, Y, N Gikakis, JH Gorman 3rd, et al. A Baboon Model for Hematologic Studies of Cardiopulmonary Bypass. J Lab Clin Med 1997; 130:412-420
22. Hubbell, JA, LV McIntire. Platelet Active Concentration Profiles Near Growing Thrombi: A Mathematical Consideration. Biophys J 1986; 50:937-945
23. Hubbell JA, LV McIntire. Technique for Visualization and Analysis of Mural Thrombogenesis. Rev Sci Instrum 1986; 57:892-897
24. Hubbell JA, LV McIntire. Visualization and Analysis of Mural Thrombogenesis on Collagen, Polyurethane and Nylon. Biomaterials 1986 7:354-363
25. Hubbell, JA, SP Massia, NP Desai, PD Drumheller. Endothelial Cell-Selective Materials for Tissue Engineering in the Vascular Graft via a New Receptor. Bio/Technology 1991; 9:568-572
26. Kottke-Marchant, K, JM Anderson, Y Umenura, RE Marchant. Effect of Albumin Coating on the *In vitro* Blood Compatibility of Dacron Arterial Prostheses. Biomaterials 1989; 10:147-155
27. Lambert, TL, V Dev, E Rechavia, et al. Localized Arterial Wall Drug Delivery From a Polymer-coated Removable Metallic Stent:

Kinetics, Distribution, and Bioactivity of Forskolin. Circulation 1994; 90:1003-1011

28. Lei, M, JP Archie, C Kleinstreuer. Computational Design of a Bypass Graft that Minimizes Wall Shear Stress Gradients in the Region of the Distal Anastomosis. J Vasc Surg 1997; 25:637-646
29. Meyer, RS, S Deutsch, JC Maymir, et al. Three-component Laser Doppler Velocimetry Measurements in the Regurgitant Flow Region of a Bjork-Shiley Monostrut Mitral Valve. Ann Biomed Eng 1997; 25:1081-1091
30. Miyazoe Y, T Sawairi, K Ito, et al. Computational Fluid Dynamic Analyses to Establish Design Process of Centrifugal Blood Pumps. Artif Organs 1998; 22:381-385
31. Nojiri, C, T Kido, T Sugiyama, et al. Can Heparin Immobilized Surfaces Maintain Nonthrombogenic Activity During In Vivo Long-term Implantation? ASAIO J 1996; 42:M468-M475
32. Parodi, JC, C Schonholz, R LaMura. The Parodi System. In: Hopkinson B, Yusuf W, Whitaker S, Veith F (Editors). ***Endovascular Surgery for Aortic Aneurysms***. WB Saunders, Philadelphia, 1997, 164-179
33. Pieters, H, JP Roodt, PN Badenhorst,et al. Antithrombotic Activity of Bay u3405, a Thromboxane A2-antagonist, in Patients with Dacron Aortic Grafts: A Random Controlled Clinical Trial. Thromb Haemost 1993 70:903-908
34. Ravanat, C, M Freund, F Dol, et al. Cross-reactivity of Human Molecular Markers for Detection of Prethrombotic States in Various Animal Species. Blood Coagul Fibrinolysis 1995; 6:446-455
35. Salzmann, DL, DC Yee, DJ Roach, et al. Healing Response Associated with Balloon-Dilated ePTFE. J Biomed Mater Res 1998; 41:364-370
36. Schafer, AI. Hypercoagulable States: Molecular Genetics to Clinical Practice. Lancet 1994; 344:1739-1742
37. Schneider, PA, HF Kotze, ADP Heyns, SR Hanson. Thromboembolic Potential of Synthetic Vascular Grafts in Baboons. J Vasc Surg 1989; 10:75-82
38. Species Effects in Testing Materials and Cardiovascular Devices in Experimental Animals. In: ***Guidelines for Blood-Material Interactions***. NIH Publication No. 85-2185, National Institutes of Health, Bethesda, MD, 1985, 203-218
39. Stelter, W, T Umscheid, P Ziegler. Three-year Experience with Modular Stent-Graft Devices for Endovascular AAA Treatment. J Endovasc Surg 1997; 4:362-369

40. Suga, K, K Nishigauchi, N Kume, et al. The Effects of New Platelet Inhibitory Drug E-5510 on Platelet Deposition on Aortic Bifurcation Grafts: Assessment by Indium-111-oxime Labeled Platelet Imaging. Clin Nucl Med 1998; 23:365-369
41. Treichler, J, SE Rosenow, G Damm, et al. A Fluid Dynamic Analysis of a Rotary Blood Pump for Design Improvement. Artif Organs 1993; 17:797-808
42. Wakefield, TW, BL Shulkin, EP Fellows, et al. Platelet Reactivity in Human Aortic Grafts: A Prospective, Randomized Midterm Study of Platelet Adherence and Release Products in Dacron and Polytetrafluoroethylene Conduits. J Vasc Surg 1989; 9:234-243
43. Wilhelm, CR, J Ristich, RL Kormos, WR Wagner. Monocyte Tissue Factor Expression and Ongoing Complement Generation in Ventricular Assist Device Patients. Ann Thorac Surg 1998; 65: 1071-1076
44. Williams, SK, DG Rose, BE Jarrell. Microvascular Endothelial Cell Sodding of ePTFE Vascular Grafts: Improved Patency and Stability of the Cellular Lining. J Biomed Mater Res 1994; 28:203-212
45. Woodard, JC, FD Shaffer, RD Schaub, et al. Optimal Management of a Ventricular Assist System: Contribution of Flow Visualization Studies. ASAIO J 1992; 38:M216-M219

Chapter 10

A PATHOLOGIST'S VIEW OF STENTING: BARE STENTS AND STENT GRAFTS

Andrew Farb, MD, Frank D Kolodgie, PhD, Renu Virmani, MD

The relatively high incidence of restenosis following arterial balloon angioplasty and the less frequent, but clinically important complication of abrupt vessel closure have directly lead to the development of intraarterial stents. A stent is a prosthetic intraluminal scaffolding device designed to maintain lumen patency in the setting of an underlying intrinsic or extrinsic disease state. Currently, stent placement is being increasingly utilized for the treatment of atherosclerotic coronary and peripheral vascular disease. In the heart, emergency coronary artery stent placement is used as a bailout procedure for abrupt or threatened artery closure due to arterial dissection following percutaneous transluminal coronary angioplasty (PTCA) and has reduced the need for urgent coronary bypass surgery [27, 33, 58]. The use of stents as primary therapy for atherosclerosis has gained wide acceptance, with reports of reduced restenosis rates in selected coronary lesions compared with PTCA [20, 21, 24, 62].

Keywords: *Stent, stent graft, artery, atherosclerosis, pathology*

Renu Virmani, MD (corresponding author), Department of Cardiovascular Pathology, Armed Forces Institute of Pathology, Washington, DC 20306-6000

The opinions and assertions contained herein are the private views of the authors and are not to be construed as official or reflecting the views of the Department of the Army or the Department of Defense.

Stent Graft Update, Edited by J Vossoughi, N Kipshidze, JW Karanian

In the peripheral circulation, stents have become an accepted treatment for atherosclerosis of the iliofemoral arteries. Recently, stent grafts have been introduced for revascularization of atherosclerotic lesions as well as treatment for aneurysms of the aorta and its major branches, traumatic aneurysms, and arteriovenous fistulas [29]. With the presence of a graft in addition to a stent, it is hoped that there will be a reduction in restenosis that occurs secondary to neointimal growth from the surrounding vessels [17]. In the treatment of peripheral aneurysms, the purpose of the stent graft is to isolate the aneurysmal segment from blood flow thereby reducing the risk of aneurysmal rupture and embolization of atherothrombotic material from the aneurysm sac [17].

While stents reduce restenosis rates in carefully selected lesions [24, 63], in-stent restenosis remains a recognized clinical problem [31] and can be expected to increase in incidence as stenting becomes more frequent and is utilized in less ideal lesions [55]. Despite the tremendous expansion of the use of stents, there has been little published data on the pathology of stents deployed in human atherosclerotic arteries [2, 32, 67]. Most experimental studies of stenting in large animals employ normal, non-atherosclerotic vessels. In these studies, thrombus formation and acute inflammation have been identified early after stenting; smooth muscle cells and scattered chronic inflammatory cells predominate in the intima 2-4 weeks post-deployment [7]. When stents have been used in atherosclerotic models (mostly rabbit aorta and iliac arteries), early thrombus formation followed by smooth muscle cell proliferation has been observed [45, 50, 65]. Studies in normal arteries in experimental models suggest a relationship between the severity of arterial injury and subsequent neointima formation [51, 52, 59].

In this chapter, a general overview of stents and stent grafts will be presented. The pathology of stenting with and without grafts in experimental animals and in human atherosclerotic coronary arteries will be described to highlight stent-vessel wall interaction.

STENTS

The development of stents was pioneered in the experimental work of Dotter (stainless steel and nitinol wire coil) [19], Cragg (nitinol coil stent) [14], Maass (self-expanding stainless steel coil stents) [36], Gianturco (spring-loaded zigzag stainless steel and interdigitating coil stents) [53, 74], and Palmaz (stainless steel slotted tube stent) [43] which was followed by initial stent implants in humans by Sigwart (self-expanding mesh stent) [64].

The metals used in intravascular stents include surgical-grade stainless steel, nickel-titanium alloy (nitinol), titanium, and gold-coated stainless steel alloys [66]. Stainless steel has excellent tensile strength and is resistant to corrosion, but is relatively thrombogenic compared to the other metals. Titanium has high strength per unit density allowing for lighter devices, is corrosion-resistant, and has excellent biocompatibility. The shape memory property of nitinol allows for devices to be highly compressed and resume original shape upon warming. Nitinol exerts a strong radial expanding force and good biocompatibility. Gold coating of stainless steel adds visibility via enhanced radio-opacity and inhibits corrosion and infection. The basic designs of stents currently in use are the coil, slotted tube, mesh, and corrugated ring.

BIOLOGIC RESPONSES TO STENTING

Stent placement elicits the following sequence of local vascular events: thrombus formation and inflammation early after deployment with subsequent neointimal growth. These events are affected by changes in local shear stress, blood flow velocity, stent design, vessel injury, and the presence or absence of underlying pathology in the artery in which the stent is deployed. The biologic responses to stent grafts can be expected to be similar to those found after placement of bare stents.

Thrombosis

Damage to the vessel wall endothelial lining, either by a bare stent or stent graft, induces platelet activation and aggregation accompanied by fibrin deposition resulting in thrombus formation. The stent wires themselves produce turbulence proximal and distal to the strut resulting in focal low shear stress areas which can precipitate increased thrombus formation. Thrombus deposition on stent struts is a uniform finding following device deployment, but thrombus size may be affected by stent design [51]. Tubular slotted stents implanted in normal canine coronary arteries show thrombus composed of platelets, fibrin and trapped erythrocytes with an immature endothelial layer at 1 week [56]. In the porcine restenosis model, thrombus adjacent to mesh stent struts is composed of platelets, fibrin, acute inflammatory cells, and trapped erythrocytes [7]. In human atherosclerotic arteries, stent-associated thrombus is common, particularly early after stenting, consisting of platelets, fibrin, and inflammatory cells (Figure 1) and is seen with all stent designs evaluated (Palmaz-Schatz, Gianturco-Roubin, Gianturco-Roubin II, Multi-Link, and Wiktor) [22].

Inflammation

Stent placement invariably involves injury to the underlying artery by the stent itself, that is embedded in the arterial wall, and by adjunctive PTCA,

which is associated with plaque disruption (in atherosclerotic arteries) and medial dissection or rupture (in normal and atherosclerotic arteries). Plaque compression by stent struts is uniformly seen in experimental studies and in human arteries [2, 22, 45]. In animal models, acute inflammatory cells are observed at 24 hours post-stenting with macrophage infiltration by 7 days [7]. In human atherosclerotic coronary arteries, neutrophils accumulate in the first week after deployment, begin to decline in number by 1 month, and then are no longer seen beyond 30 days [22, 67]. The extent of inflammation increases with greater arterial injury and with the penetration of stent struts into the necrotic core of atherosclerotic plaques (Figure 2). Chronic inflammation (lymphocytes and macrophages) around stent struts is also commonly seen at all time points post-stenting and probably reflects the chronic inflammatory response already commonly seen in atherosclerotic lesions that is further augmented by the presence of the stent acting as a foreign body [22, 30].

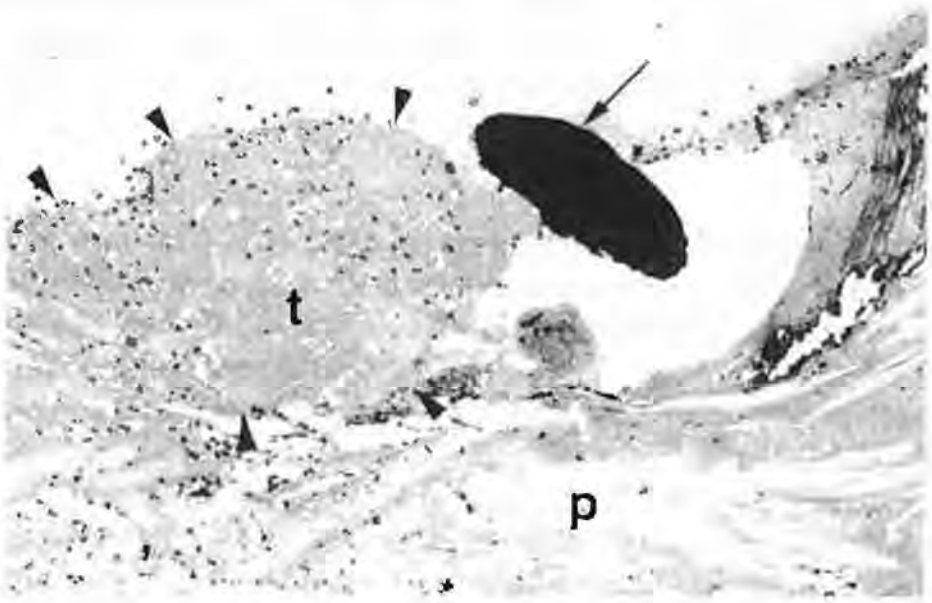

FIGURE 1

A fibrin and platelet-rich thrombus (t, outlined by arrowheads) containing inflammatory cells is present adjacent to an AVE stent strut (arrow) 8 hours post-deployment. A ruptured fibrous cap overlying the plaque (p) necrotic core is present below the strut. (Hematoxylin-eosin stain)

Cellular Proliferation

In the porcine coronary artery restenosis model, Carter et al showed maximal cellular proliferation 7 days after stent placement (18.6 ± 3.5%

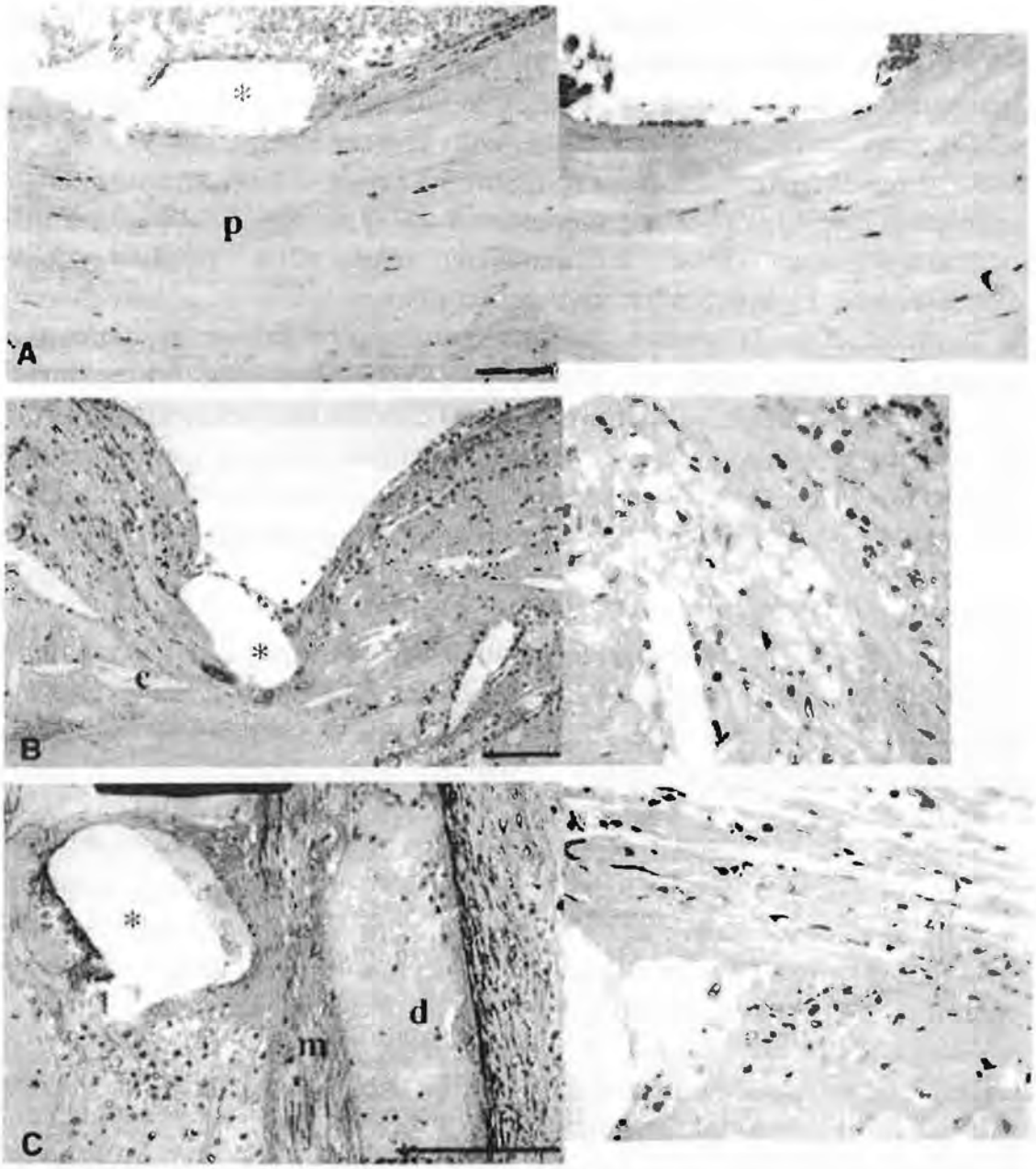

FIGURE 2

Arterial inflammation in coronary arteries with stents placed ≤3 days antemortem. Movat pentachrome stains are presented in the left panels with higher power hematoxylin-eosin from same section shown in the right panels. In A, few inflammatory cells are present adjacent to Palmaz-Schatz strut (*) in contact with fibrous plaque (p). In B, increased numbers of inflammatory cells are associated with a Palmaz Schatz strut (*) that penetrates into a necrotic core (c). In C, a Palmaz Schatz strut (*) is in contact with damaged media (m) with dissection (d) and numerous associated inflammatory cells. (A and B scale bars 0.10 mm; C scale bar 0.14 mm). *Reproduced with permission from reference 22.*